DYNAMICS AND CONTROL OF A CLASS OF GROUND BASED MOBILE FLEXIBLE MANIPULATORS

By

Thomas Charles Ries

B. Sc. (Physics), University of British Columbia, 1976

B. A.Sc. (Mechanical Engineering), University of British Columbia, 1979

A THESIS SUBMITTED IN PARTIAL FULFILLMENT OF

THE REQUIREMENTS FOR THE DEGREE OF

MASTER OF APPLIED SCIENCE

in

THE FACULTY OF GRADUATE STUDIES

MECHANICAL ENGINEERING

We accept this thesis as conforming

to the required standard

THE UNIVERSITY OF BRITISH COLUMBIA

November 1993

In presenting this thesis in partial fulfilment of the requirements for an advanced degree at the University of British Columbia, I agree that the Library shall make it freely available for reference and study. I further agree that permission for extensive copying of this thesis for scholarly purposes may be granted by the head of my department or by his or her representatives. It is understood that copying or publication of this thesis for financial gain shall not be allowed without my written permission.

Mechanical Engineering
The University of British Columbia
6224 Agricultural Road
Vancouver, Canada
V6T 1W5

Date: November 29, 1993

ABSTRACT

The thesis studies dynamics and control of a two-link flexible manipulator, free to undergo planar translational and slewing maneuvers, through numerical simulation. To begin with, kinematics and kinetics of the system are investigeted, for a general N-link system undergoing planar motion, leading to the nonlinear, nonautonomous and coupled equations of motion, obtained using the Lagrangian procedure. A parametric study follows to assess the influence of system variables on the dynamical response and particularly on the positioning error of the payload. A joint based non-collocated algorithm, using the Feedback Linearization Technique (FLT) that accounts for the complete nonlinear dynamics of the system, is proposed for the tip control. The results are useful in the design of the ground based flexible, mobile servicing systems which are gradually appearing on the industrial scene and are likely to be more common in the future.

Table of Contents

List of Figures

LIST OF SYMBOLS

α_i	angle between the reference frames F_{i-1} and F_i
α_{ik}	sum of angles $\alpha_i + \alpha_{i+1} + \cdots + \alpha_k$,
$\vec{a}_i$	position vector to the origin of the frame F_i w.r.t. frame F_{i-1} projected on to the inertial frame
β_1	specified joint angle for link 1
β_2	specified joint angle for link 2
$\beta_{\vec{p}_3}$	specified position vector to the tip (payload) w.r.t. the inertial frame
$\beta_{p_{3x}}$	x-component of $\beta_{\vec{p}_3}$ w.r.t. the inertial frame
$\beta_{p_{3y}}$	y-component of $\beta_{\vec{p}_3}$ w.r.t. the inertial frame
β_{p_x}	x-component of the specified base or joint 1 position vector in the inertial frame
β_{p_y}	y-component of the specified base or joint 1 position vector in the inertial frame
C_i	$\cos(\alpha_i)$
C_{ik}	$\cos(\alpha_i + \alpha_{i+1} + \cdots + \alpha_k)$
δ_{ij}	generalized co-ordinate associated with mode j of link i
m	number of modes used in the simulation
$\mathbf{F_0}$	inertial frame
$\mathbf{F_1}$	base and link 1 local frame at joint 1
$\mathbf{F_2}$	link 2 local frame at joint 2
$\mathbf{F_3}$	payload local frame at its CM
$\vec{f}_D$	K.E. part of the differential equation derived from the time

	derivative segment of the Lagrangian equation but contains only the acceleration terms
$\vec{f}_{TD}$	K.E. part of the differential equation that is derived from the time derivative segment of the Lagrangian equation but does not contain any acceleration terms
$\vec{f}_{T}$	the K.E. part of the differential equation that is not derived from the time derivative segment of the Lagrangian equation and does not contain any acceleration terms
$\vec{f}_{U}$	the P.E. part of the differential equation that is derived from the Lagrangian equation
$\mathbf{J_1}$	joint 1
$\mathbf{J_2}$	joint 2
$\mathbf{H_{a,b}}$	homogeneous transformation matrix between the frames F_b and F_a
k_j	eigenvalue for the mode function ϕ_j
$(kl)_j$	spatial frequency for the mode function ϕ_j
$\mathbf{L_1}$	link 1
$\mathbf{L_2}$	link 2
$\vec{\omega}_{i-1,i}$	angular velocity vector of the frame F_i w.r.t. the frame F_{i-1} projected onto the inertial frame used only in the general formulation
$\vec{p}_3$	position vector to the tip (payload) w.r.t. the inertial frame
p_{3x}	X-component of $\vec{p}_3$
p_{3y}	Y-component of $\vec{p}_3$
ϕ_{ij}	mode function for link i, mode j
Φ_{ijk}	modal integral for the link i with modes j and k
Φ'_{ijk}	normalized modal integral with $l_i = 1$
$\vec{p}_i$	position vector to the origin of the frame F_i w.r.t. the inertial frame
p.o.t.	projected onto

p_x	X-component of the base (joint 1) response in the inertial frame
p_y	Y-component of the base (joint 1) response in the inertial frame
$\mathbf{D}$	time varying system mass matrix
$\ddot{\vec{q}}$	acceleration of the generalized coordinates vector
$\vec{Q}$	generalized control force vector
Q_{p_x}	control force acting on the base at the origin of F_1 in the X_0 direction
Q_{p_y}	control force acting on the base at the origin of F_1 in the Y_0 direction
Q_{θ_1}	control torque acting at joint 1
Q_{θ_2}	control torque acting at joint 2
$\mathbf{R}_{\mathrm{a,b}}$	rotation transformation matrix between frames F_b and F_a
$\vec{\rho}_i$	position vector to the elemental mass dm_i w.r.t. the local frame F_i
$\vec{r}_i$	position vector to the elemental mass dm_i w.r.t. the inertial frame
S_i	$\sin \alpha_i$
S_{ik}	$\sin(\alpha_i + \alpha_{i+1} + \cdots + \alpha_k)$
θ_1	joint angle response for link 1
θ_2	joint angle response for link 2
T_{vs}	total specified excursion time of slew trajectory at a constant velocity
w.r.t.	with respect to
$X_0(i)$	initial specified X-coordinate at the tip during slew maneuver
$X_0(f)$	final specified X-coordinate at the tip during slew maneuver
$\mathbf{X_0}$	X-coordinate axis of the inertial frame
$\mathbf{X_1}$	X-coordinate axis of the frame F_1
$\mathbf{X_2}$	X-coordinate axis of the frame F_2
$\mathbf{x_1}$	X-coordinate of the elemental mass dm_1 of link 1 w.r.t. the frame F_1
$\mathbf{x_2}$	X-coordinate of the elemental mass dm_2 of link 2 w.r.t. the frame F_2
$Y_0(i)$	initial specified Y-coordinate at the tip during slew maneuver
$Y_0(f)$	final specified Y-coordinate at the tip during slew maneuver

$\mathbf{Y_0}$	Y-coordinate axis of the inertial frame
$\mathbf{Y_1}$	Y-coordinate axis of the frame F_1
$\mathbf{Y_2}$	Y-coordinate axis of the frame F_2
$\mathbf{y_1}$	Y-coordinate of the elemental mass dm_1 of link 1 w.r.t. the frame F_1
$\mathbf{y_2}$	Y-coordinate of the elemental mass dm_2 of link 2 w.r.t. the frame F_2
y_{l_1}	deflection of the tip of link 1 w.r.t. to the frame F_1
$\vec{\zeta}_i$	position vector of the flexible elemental mass dm_i w.r.t. the frame F_i used only in the development of the generalized equations of motion
c_x	damping constant of the base in the x-direction
c_y	damping constant of the base in the y-direction
c_1	damping constant of joint 1
c_2	damping constant of joint 2
$(EI)_1$	flexural rigidity of link 1
$(EI)_2$	flexural rigidity of link 2
g	gravitational acceleration
k_x	stiffness of the base in the x-direction
k_y	stiffness of the base in the y-direction
k_1	stiffness of joint 1
k_2	stiffness of joint 2
l_1	lenght of link 1
l_2	lenght of link 2
m_1	mass of link 1
m_2	mass of link 2
m_B	mass of the manipulator base
m_P	mass of the manipulator payload

ACKNOWLEDGEMENT

The author wishes to express his sincere thanks to Prof. V.J. Modi and Dr. F. Karray for their guidance throughout the preparation of this thesis. The project was supported by the Natural Sciences and Engineering Research Council of Canada, Grant No. A-2181, and the Networks of Centers of Excellence Program, Grant No. IRIS/C-8, 5-55380. Special thanks are extended to my wife, Louise, for her patience, encouragement, and tireless assistance.

Chapter 1

INTRODUCTION

1.1 Preliminary Remarks

The continuously evolving technology of robotic joint actuators coupled with the introduction of direct drive systems have led to a rapid increase in speed and payload capacity of ground based manipulators. As a result, the flexibility of previously considered rigid links have become increasingly significant. Due to rigidity requirements, present generation of robotic manipulators [1], [2] are normally restricted in their load carrying capacity to approximately 5-10 % of their own weight. For example, the Cincinatti-Milicron T3R3 robot weighs about 2000 Kg but can carry a payload of only about 20 Kg. If a controller is designed to account for the:

- flexibility of the links;
- flexibility of the joint actuator systems;
- flexibility of the base structure of the manipulator;
- effects of gravity;

then, in principle, it may be possible to increase the payload/robot weight ratio as well as the manipulator speed for a given mass and positioning requirements. There are other obvious advantages in accounting for the manipulator's flexible character:

- Cheaper drive components can be used since less power is required to move the lighter structural components, assuming equivalent accelerations and payload capacity to the rigid link design.

- Safer operation in case of collision, since lighter components are used.

- Added weight reduction due to simpler actuator and structural design. This is a result of the reduced power requirement. Now the direct drive actuators can easily be adapted thereby eliminating the need for gears. This also results in reduced backlash and improved actuator linearity.

- Increased structural compliance due to flexibility in the links. End effector compliance is very important in standard pick and place maneuvers involving delicate assembly operations. Flexible links can provide this compliance in a very simple and cost effective manner.

Suprising as it may seem, interest in the ground based mobile, flexible manipulators. accounting for the gravitational effects, is relatively recent and the associated literature rather scarce. With this as background and the above mentioned benefits as motivation, a reasonably general model of the ground based mobile flexible manipulator is considered for study to gain some insight into its dynamical performance and control.

1.2 A Brief Review of the Relevant Literature

A challenge introduced by the flexibility consideration is so immense that, as pointed out before, research in this area was initiated only in the past decade and the accumulated literature is quite limited, particularly with respect to the ground based systems. This, of course, is understandable as for most industrial applications, links and joints were essentially rigid; hence flexibility was never an issue, at least for the intended objectives.

On the other hand, for space applications, where weight is always a major governing factor, flexible structural members in the forms of solar panels, antennas and beams were introduced relatively earlier. However, now the structures, such as the Canada Arm aboard the Space Shuttle [3], operate in the microgravity environment with an entirely different class of problems. Modi [4], Chan [5] and Mah [6] have reviewed this literature at a considerable length.

Studies aimed at dynamics and control of ground based mobile, flexible, multi-link manipulators, accounting for gravity, are indeed rare. However, there have been some investigations concerning tip control of a single flexible link [7], [8]. Almost all commercial robots use colocated control (the position sensor located at the joint actuator where the generalized force is applied), as then it is easier to maintain stability of the controlled system. With noncolocated position sensing, stable control is extremely difficult to chieve. In that sense Binford and Cannon's contribution is noteworthy [9]. They successfully demonstrated tip-position control of a single flexible link manipulator (fixed at one position, i.e. not mobile) using noncolocated (position sensing at the tip rather than at the joints where generalized forces are applied) control strategy.

Several different procedures have been studied to control single and multi-link manipulators. They include: Linear Quadratic Regulator [LQR, [5]]; variable structure or sliding mode control [10]; model following adaptive techniques [11]; and pole placement, selftuning control [12]. In most cases, their applications are limited to stationary manipulators in general, with two links if rigid and a single link when flexible. Rovner and Franklin [13] incorporated variation of the payload mass in their formulation and applied a selftuning regulator approach to adaptive control of a flexible single link manipulator. Although accurate noncolocated tip control was achieved it was found to be quite sensitive to modeling errors. Modeling and control of robots with rigid links but elastic joints have also received some attention [14].

The thesis takes a small step in this neglected area of dynamics and control of earth-based mobile flexible manipulators accounting for gravitational forces.

1.3 Scope of the Investigation

In general earth-based mobile, flexible, multilink manipulators, with flexible joints and supported by a flexible base, present a formidable problem in dynamics and control. Rapid and accurate control of the payload using non-colocated position sensing add to the challenge. The thesis considers a simplified planar model of such a system to gain insight into the complicated

dynamics involved, effect of parametric changes, and develop an effective control strategy.

To begin with a mobile manipulator, with an arbitrary number of Euler-Bernoulli beam-type links and joints with torsional flexibility, supported by a mobile flexible base is considered. The manipulator carries an arbitrary point payload, and is free to undergo translational as well as slewing maneuvers in the vertical plane. The continuum system deformations, also in the vertical plane, are discretized using admissible functions in conjunction with time dependent generalized coordinates. The governing nonlinear, nonautonomous and coupled equations of motion are obtained using the Lagrangian procedure.

As can be expected, the governing equations are not amenable to any closed-form solution. A special case of two-link manipulator is considered and a numerical code written for its dynamical analysis and control.

A parametric study follows to help appreciate the effects of system variables and slew maneuvers on the dynamical response. It also suggests a need for control under critical combinations of system parameters and initial conditions. Finally, a noncolocated control strategy is developed for the payload trajectory tracking and its effectiveness is assessed over a range of slewing time histories.

The thesis ends with some concluding comments and recommendations for possible extension of the study.

Chapter 2

FORMULATION OF THE PROBLEM

Most general purpose commercial robots, such as the one shown in Figure 2.1, have 4 - 6 degrees of freedom. Normally the base, joints and links are treated as rigid distributed mass structures. In reality, this is an approximation. To make the positioning and tracking of the payload accurate to within a prescribed tolerance, designers are required to considerably over design the structural and drive components to make the end-tip position sufficienly predictable. This results in a prohibitively excessive robot weight combined with meager payload capacity and slow slewing response.

One approach to overcome these undesireable elements would be to reduce, significantly, the total mass of each element but retain its structural integrity through an acceptable factor of safety with respect to mechanical stresses based on maximum loads. This would result in a lighter and faster manipulator. If the control strategies are modified to include the flexibility effects of the links, the base and the joints in the dynamical equations, then the manipulator can be made to position the payload as accurately as before.

With this as background, the development of the formulation starts with a mathematical model for an earth based flexible, mobile, manipulator. The model aims at realistic measures of time and effort, yet remains sufficiently comprehensive to capture essential features of the system. Reference frames and generalised coordinates are selected to describe the state of the system. Deformations of continuous flexible members are presented by discrete modal functions. The kinetic and potential energy expressions are derived and the governing equations of motion obtained using the Lagrangian procedure.

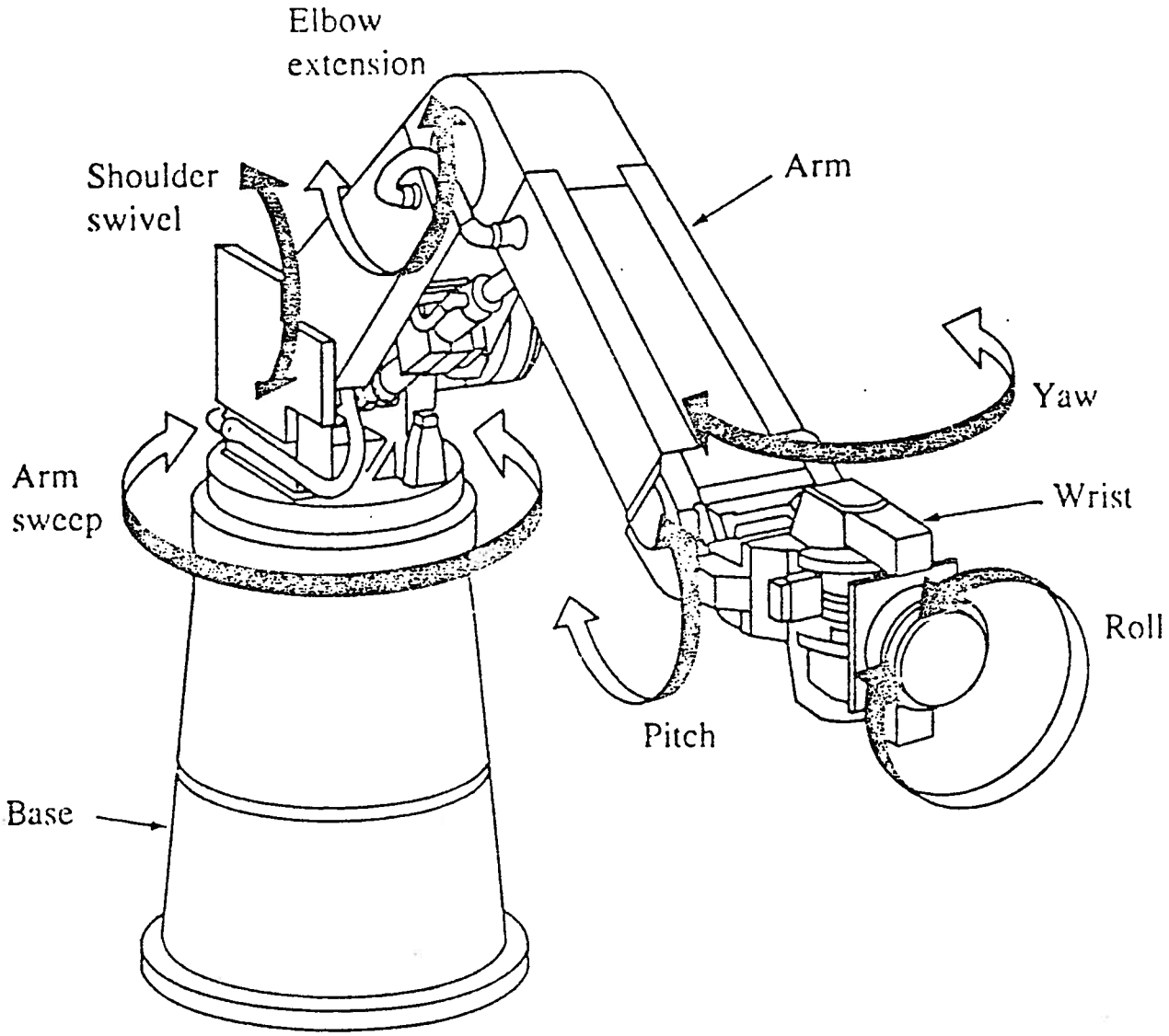

Figure 2.1: A commercial general purpose six degrees of freedom robotic manipulator

2.1 System Model

Consider a mobile manipulator with an arbitrary number of Eulerian beam-type members, interconnected to form an open chain geometry, carrying a point payload m_P. The two-link version of this general configuration is schematically presented in Figure 2.2. The joints J_i are considered to have torsional rigidity as well as damping. Translation motion of the mobile base, treated as a point mass, is also represented realistically through inclusion of the linear stiffness and viscous damping. The system is free to undergo translational and slewing maneuvers as well as link deformations in the vertical plane (plane of the paper).

The model is carefully selected so as to retain essential features of a robotic manipulator, particularly with reference to the elastic character of the base, joints and links. The emphasis is on the flexibility effects on the payload trajectory and its control.

2.2 Reference Frames, Generalized Coordinates and Maneuvers

The manipulator shown in Figure 2.2 is assigned local reference base coordinates and generalized coordinates as described here in more detail.

The elasticity of the base and the mechanisms at the joints will affect the performance and accuracy of the manipulator by permitting oscillations about the nominal specified slew angles. As a result the base support flexibilities are modeled by straight linear springs and velocity (viscous) dampers. The position of the base C.M., and hence joint 1, is located w.r.t. and projected onto the inertial reference frame F_0 by the vector $\vec{p}$ whose x and y components are defined by p_x and p_y.

The joint flexibility is modeled by a linear torsional spring with a velocity damper. Flexible rotations of the links are described by the *joint* angle, θ_i, and the specified rotations designated as, β_i, where i is the link number; α_i, the angle that the local reference frame F_i, associated with the link i, makes with the previous reference frame F_{i-1}, in this case about the Z_{i-1} axis; and β_i is the specified slew at the joint i measured between the link i and the X_{i-1} axis at the

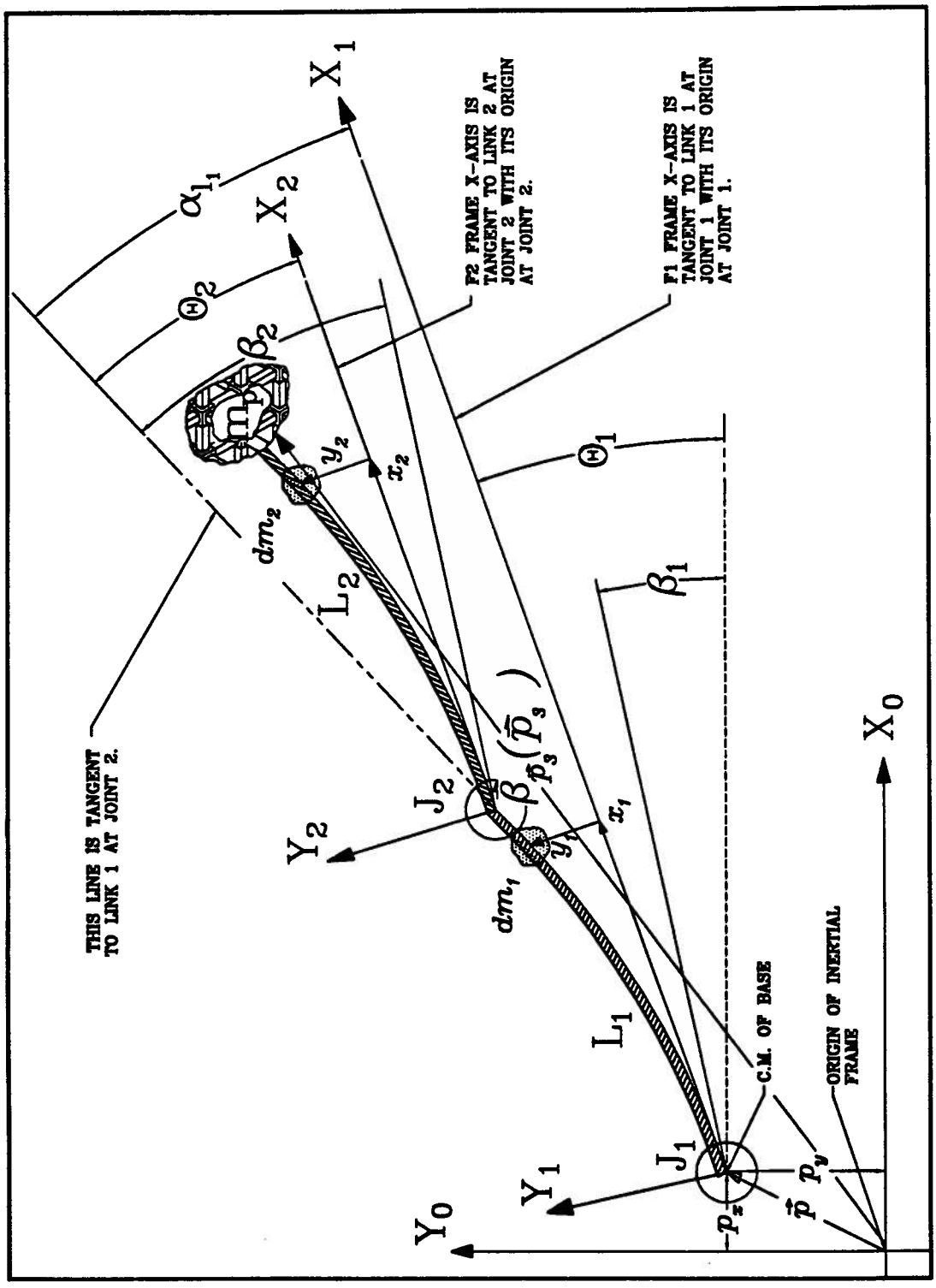

Figure 2.2: A schematic diagram of the mobile, flexible two-link manipulator.

location of the joint i. The actual joint angle at i is θ_i and is measured the same way as the β_i with definitions as follows:

$$\begin{aligned} \alpha_1 &= \theta_1; \\ \alpha_2 &= \theta_2 + \alpha_{l_1}; \end{aligned}$$

where α_{l_1} is the angle of *link* 1 at the tip of *link* 1 measured in the local frame F_1. For the Lagrangian formulation the generalized coordinates are θ_1, θ_2, p_x, and p_y.

The links are assumed to be Euler-Bernoulli beams and their deformations are modeled by spatial modal functions together with time dependent generalized coordinates,

$$y_i(x,t) = \sum_{j=1}^{m} \phi_{ij}(x)\delta_{ij}(t),$$

where ϕ_{ij} represents the j^{th} mode for the i^{th} link while $\delta_{ij}(t)$ is the j^{th} generalized coordinate associated with the i^{th} link. m is the number of modes used in the discretization process. Theoretically, the summation should extend to infinity, however, in practice only a small number of modes are generally used, depending upon the situation. In fact, in the reported literature, most investigators consider the effect of only the first mode since it normally dominates the response.

As can be expected, for rapid convergence to the true response, the selected modal functions $\phi_{ij}(x)$ should satisfy all geometric and natural boundary conditions. This, of course, is often difficult and for complex structures virtually impossible. Fortunately, the modes satisfying the following conditions do present an acceptable set [14], [15], [16], [17] of admissible functions as:

- they are able to describe any link profile;
- they are differentiable over the system domain and to the degree of the differential equations modeling the dynamics;
- they satisfy at least the geometric boundary conditions of the slope and deflection at the ends of the link.

In general, functions that satisfy the above conditions are orthogonal with respect to one another. This property may be used to advantage in deriving the equations of motion. This is illustrated in the following secion.

2.3 Natural Modes of a Bar in Bending Vibration

2.3.1 Modal functions

The translating flexible manipulator under consideration has infinite degrees of freedom. The method of assumed modes effectively transforms the governing partial differential equations into a set of ordinary differential equations. The choice of available modal functions is also large. Modes for beams with various combinations of end conditions are possible candidates. One might consider the use of unconstrained modes incorporating time varying boundary conditions [7]. In this study, to minimize the complexity, cantilever modes of an Eulerian beam are used as admissible functions for the manipulator links. The effects of rotary inertia and shear deformation, which become significant for large deflecions and high frequencies [14], are neglected here. For a cantilever beam with free end (no tip-mass),

$$\frac{\partial^2}{\partial x^2}\left(EI(x)\frac{\partial^2 y(x,t)}{\partial x^2}\right) = -m(x)\frac{\partial^2 y(x,t)}{\partial t^2}$$

where:

$EI(x)$ = flexural ridgidity of the beam;

$m(x)$ = mass per unit length at any point x;

$y(x,t)$ = transverse displacement solution subject to given bounday conditions reflecting the manner in which the ends are supported.

If the beam is assumed uniform, EI is a constant and the governing differential equation reduces to

$$\frac{\partial^2 y}{\partial t^2} + a^2\frac{\partial^4 y}{\partial x^4} = 0\ ,$$

where

$$a^2 = \frac{EI}{m} .$$

For a simple cantilever beam, the boundary conditions are zero displacement and slope at the fixed end and zero shear force and moment at the free end. More specifically:

$$y(0) = 0 ; \qquad \frac{dy}{dx}|_{x=0} = 0 ;$$
$$\frac{d^2y}{dx^2}|_{x=L} = 0 ; \qquad \frac{d^3y}{dx^3}|_{x=L} = 0 .$$

The equation of motion can now be solved by the method of separation of variables. $y = \phi(x) \cdot \delta(t)$, where $\phi(x)$ depends only on the spatial coordinate x and $\delta(t)$ depends only on time. The new set of equations to be solved has the form:

$$\frac{d^4\phi}{dx^4} - \beta^4\phi = 0 ; \quad \text{and} \quad \frac{d^2\delta}{dt^2} + \omega\delta = 0 ;$$

where:

$$\beta^4 = \frac{m\omega^2}{EI} = \frac{\omega^2}{a^2} .$$

The general solution to these equations is given by:

$$\phi(x) = C_1 \sin\beta x + C_2 \cos\beta x + C_3 \sinh\beta x + C_4 \cosh\beta x ;$$
$$\delta(t) = C_5 \sin\omega t + C_6 \cos\omega t .$$

Now the modal function $\phi(x)$ has the form

$$\phi(x) = (\sin\beta x - \sinh\beta x) - \frac{\sin\beta l + \sinh\beta l}{\cos\beta l + \cosh\beta l}(\cos\beta x - \cosh\beta x) ,$$

where

$$\cos\beta l \cosh\beta l = -1 .$$

Here:

$$\beta^4 = \frac{m\omega^2}{EI} = \frac{\omega^2}{a^2};$$

$$
\begin{aligned}
a^2 &= \frac{EI}{m}; \\
EI &= \text{flexural rigidity of the beam ;} \\
m &= \text{mass of the beam per unit length ;} \\
\omega &= \text{circular frequency ;} \\
l &= \text{length of the beam .}
\end{aligned}
$$

The transcendental characteristic equation yields infinite set of eigenvalues β_i. Inserting these values into the equation for $\phi(x)$ gives the desired modes, which are orthogonal and self-adjoint.

The presence of a payload at the tip of the terminal arm would introduce shear boundary condition. The characteristic frequency equation now modifies to

$$\cos\beta l \cosh\beta l + 1 = \frac{m_p}{m}\beta\left(\sin\beta l \cosh\beta l - \cos\beta l \sinh\beta l\right),$$

with the form of the modal function $\phi(x)$ remaining the same as before. The first six roots of the new characteristic equation are summarized in the table below for four payload conditions:

$\frac{m_p}{ml}$	0	1	2	5
$(\beta l)_1$	1.88	1.25	1.08	0.87
$(\beta l)_2$	4.70	4.03	3.98	3.95
$(\beta l)_3$	7.86	7.13	7.10	7.08
$(\beta l)_4$	11.0	10.3	10.2	10.2
$(\beta l)_5$	14.1	13.4	13.4	13.3
$(\beta l)_6$	17.3	16.5	16.5	16.5

2.3.2 Modal integrals

The modal integrals are associated with the kinetic and potential energy evaluation of the system. They represent integration of dynamical quantities over the system domain. As pointed out before, orthogonal character of the modes simplify calculation of the energies and hence derivation of the equations of motion.

The modal integrals are defined as follows:

$$\begin{aligned}
\Phi_{ij} &= \int_{M_i} \phi_{ij}(x)\, dm_i = \int_0^{l_i} \phi_{ij}(x)\, m(x)\, dx; \\
\Phi_{Sij} &= \int_{M_i} \phi_{ij}^2(x)\, dm_i = \int_0^{l_i} \phi_{ij}^2(x)\, m(x)\, dx; \\
\Phi_{Xij} &= \int_{M_i} \phi_{ij}(x)\, x_i dm_i = \int_0^{l_i} x_i m(x)\, dx; \\
\Phi_{Dij} &= \frac{1}{2}(EI)_i \int_0^{l_i} \left(\frac{d^2\phi_i(x)}{dx^2}\right)^2 dx.
\end{aligned}$$

Normalizing with respect to the length of the beam (i.e. length of the manipulator arm) gives:

$$\begin{aligned}
\Phi_{ij} &= M_i \Phi'_{ij}; \\
\Phi_{Sij} &= M_i \Phi'_{Sij}; \\
\Phi_{Xij} &= M_i l_i \Phi'_{Xij}; \\
\Phi_{Dij} &= \frac{(EI)_i}{2l_i^3} \Phi'_{Dij};
\end{aligned}$$

where:

$$\begin{aligned}
i &= \text{link number;} \\
j &= \text{mode number;} \\
x &= lx'; \\
dx &= l dx'; \\
0 \leq\ & x \leq l_i; \\
0 \leq\ & x' \leq 1; \\
m_i(x) &= m_i = \text{uniformly distributed mass of the link } i; \\
M_i &= \text{total mass of the link } i; \\
\Phi'_{Sij} &= \int_0^1 \phi_{ij}(x')\, dx'; \\
\Phi'_{Sij} &= \int_0^1 \phi_{ij}^2(x')\, dx'; \\
\Phi'_{Xij} &= \int_0^1 x' \phi_{ij}(x')\, dx';
\end{aligned}$$

$$\Phi'_{Dij} = -(kl)_j^4 \int_0^1 \left(\left(\sin(kl)_j x' + \sinh(kl)_j x' \right) + C_j \left(\cos(kl)_j x' + \cosh(kl)_j x' \right) \right) dx';$$

$$C_j = \frac{\sin(kl)_j + \sinh(kl)_j}{\cos(kl)_j + \cosh(kl)_j}.$$

These normlized integrals may be evaluated by numerical integration and may be used for a manipulator link with constant flexural rigidity and mass distribution along its length. Values of the integrals as affected by the number of modes used in the discretization process, for $m_p = 0$, are summarized in the table below:

No. of MODES	*MODAL INTEGRALS*			
	Φ'_{ij}	Φ'_{Sij}	Φ'_{Xij}	Φ'_{Dij}
1	0.78299	1.00000	0.568830	12.3620
2	0.43393	1.00000	0.090762	485.510
3	0.25442	1.00000	0.032425	3806.30
4	0.18172	1.00000	0.016450	14606.0
5	0.14147	1.00000	0.009985	39956.0
6	0.11569	1.00000	0.006669	89096.0

Note, the integrals involving products of different modes are not presented here as they vanish due to the orthogonality condition. However, this is not always true for $m_p \neq 0$ because the modal functions for a cantilever beam with tip mass are not necessarily orthogonal.

2.4 Kinematics

To derive the governing equations of motion it is necessary to evaluate the kinetic and potential energies of the system. For this we require the position and velocity vectors for the elemental mass, dm_i, in Link i.

The fundamental kinematic expressions for displacement and velocity are developed in this section. Two approaches are reviewed to aid in choosing a technique best suited for the intended purpose. The first approach utilizes homogeneous transformation matricese [18], [19] to obtain

the position and velocity of dm_i with respect to and projected onto the inertial reference frame. The second approach [5], [6] employs vector methods to arrive at the same end result. By direct experimentation, it became appearant that for simpler systems such as the present two link manipulator, derivation of the equations of motion is considerably easier through the use of homogeneous transformation matrices. This is because the vector method creates a large number of redundant terms which eventually cancel out in the final set of the differential equations. However, it should be noted that the vector method provides a relatively simpler form of the equations of motion for a general system of N flexible links that are mobile and operate under the influence of gravity.

The various reference frames, and generalized coordinates are selected to specify orientation of the system as shown in Figures 2.2 and 2.3. Note, the two diagrams are similar except that the latter is a bit simpler; and while using the homogeneous transformations the local coordinate vector $\vec{\zeta}$ is changed to $\vec{\rho}$. The various reference coordinate systems F_0, F_1, F_2 and F_3 are local frames describing the kinematic specifications of the elemental mass segments of each link *with respect to* (w.r.t.) and projected onto the respective local frame. F_0 is the base or inertial reference frame. F_1 represents the local coordinate frame for link 1 whose origin is coincident with the C.M. of the mobile base as well as the centroid of joint 1, and is fixed to link 1 so that the link is aligned with the X_1-axis of the local frame. F_2 is the local coordinate frame for link 2 with the origin coincident with the centroid of joint 2 and the same conditions apply as for the previous link. F_3 is the local coordinate frame for the payload mass M_p, which is considered to be a point (i.e. negligible rotational inertia). In the local coordinate frame the position vector $\vec{\rho}_i$ locates the mass element dm_i which is defined in terms of its components

$$\vec{\rho} = [x_i, y_i] \ .$$

Note that the choice of reference coordinate frames located at the joints facilitates the use of *cantilever* modal functions. This makes the derivation and computation simpler.

Since the X_i axis is aligned with the rigid body neutral axis of the link, the transverse

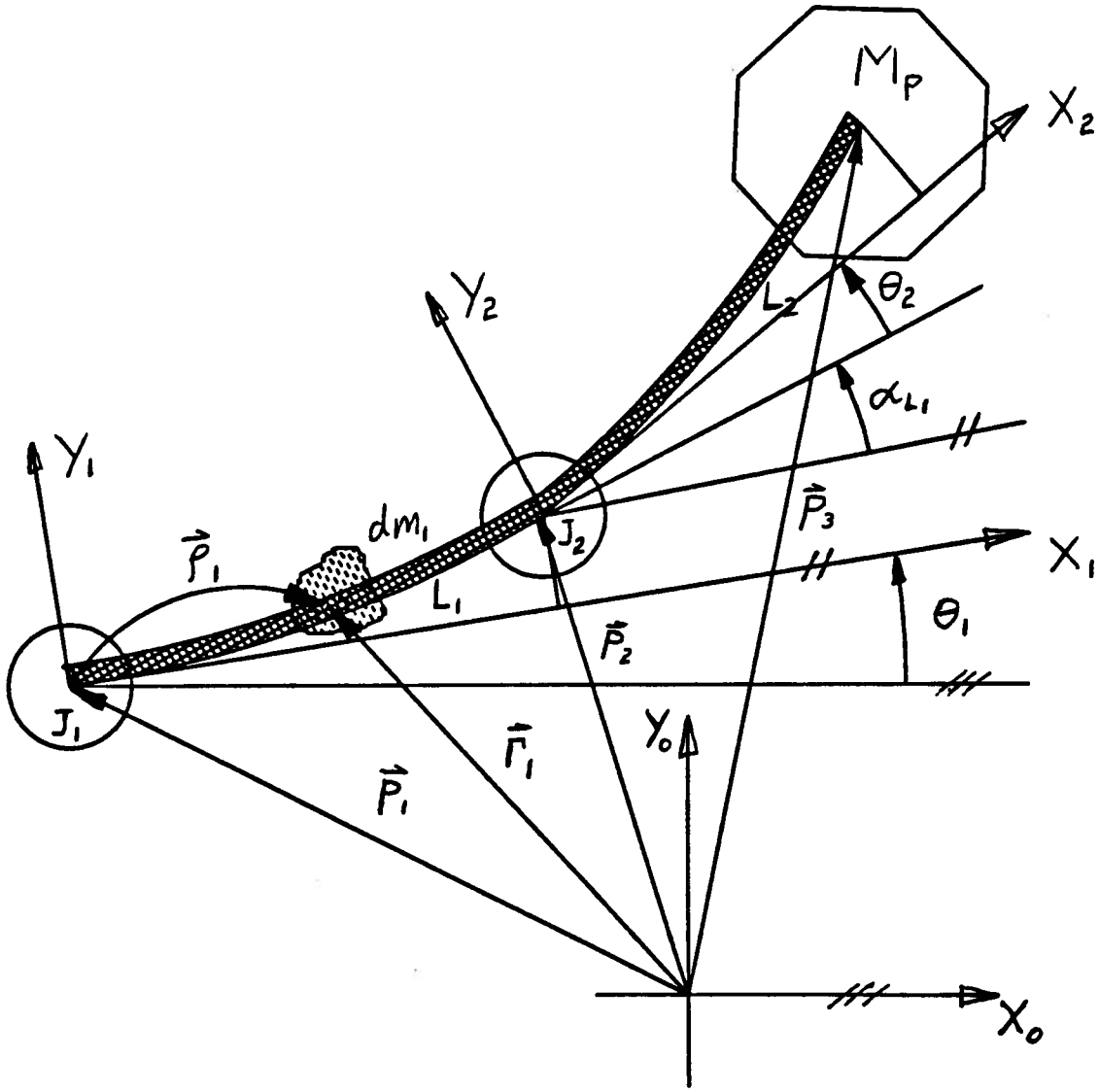

Figure 2.3: Reference frame and generalized coordinates used in the mathematical modeling of the mobile flexible two link manipulator system.

deflection and rotation of a mass element dm_i in the link i are defined as:

$$y_i(x_i,t) = \sum_{j=1}^{m} \phi_{ij}(x)\delta_{ij}(t) \; ;$$

$$\alpha_{l_i}(x_i,t) = \frac{\partial y_i}{\partial x_i} = \sum_{j=1}^{m} \phi'_{ij}(x)\delta_{ij}(t) \; .$$

As an example, joint 2, located at the tip of link 1, is displaced by an amount y_{l_1} and rotated through α_{l_1} w.r.t. the frame F_1.

Before determining the kinetic and potential energies, the displacement and velocity of the elemental mass dm_i must be established w.r.t. the inertial reference frame F_0. The displacement of dm_i is first determined w.r.t. and projected onto the local frame, by the vector $\vec{\rho_i}$. Through a series of homogeneous transformations (i.e. $\mathbf{H_{0,i}}$), it is transferred to the inertial frame. The position vector of the mass element dm_i on the link i with respect to the inertial frame is given by $\vec{r_i}$.

$$\vec{r_i} = \mathbf{H}_{0,i}\vec{\rho_i} \; .$$

where:

$$\mathbf{H}_{0,i} = \left(\begin{array}{ccc|c} & \mathbf{R_{0,i}} & & \vec{\mathbf{p}}_\mathbf{i} \\ \hline 0 & 0 & 0 & 1 \end{array}\right) \; ;$$

$\mathbf{R}_{0,i}$ = rotation matrix (3×3) for the transformation from the local frame F_i to the inertial frame F_i ;

$\vec{\mathbf{p}}_\mathbf{i}$ = position vector to the origin of the local frame F_i w.r.t. the inertial frame.

Determination of the transformation matrix $\mathbf{H}_{0,i}$ is accomplished by postmultiplying the local transformation matrices, $\mathbf{H}_{j-1,j}$, in the consecutive order from the inertial frame to the frame F_i in question. The position vectors to the mass element dm_i are defined as follows:

$$\vec{r_1} = \mathbf{H}_{0,1}\vec{\rho_1} = \left(\begin{array}{ccc|c} C_1 & -S_1 & 0 & p_x \\ S_1 & C_1 & 0 & p_y \\ 0 & 0 & 1 & 0 \\ \hline 0 & 0 & 0 & 1 \end{array}\right) \left(\begin{array}{c} x_1 \\ y_1 \\ 0 \\ 1 \end{array}\right) \; ;$$

$$\vec{r_2} = \mathbf{H}_{0,1}\mathbf{H}_{1,2}\vec{\rho_2} = \left(\begin{array}{ccc|c} C_1 & -S_1 & 0 & p_x \\ S_1 & C_1 & 0 & p_y \\ 0 & 0 & 1 & 0 \\ \hline 0 & 0 & 0 & 1 \end{array}\right)\left(\begin{array}{ccc|c} C_2 & -S_2 & 0 & l_1 \\ S_2 & C_2 & 0 & y_{l_1} \\ 0 & 0 & 1 & 0 \\ \hline 0 & 0 & 0 & 1 \end{array}\right)\left(\begin{array}{c} x_1 \\ y_1 \\ 0 \\ 1 \end{array}\right) \quad ;$$

where:

i = link or reference frame number ;

C_i = $\cos\alpha_i$;

S_i = $\sin\alpha_i$;

l_i = length of link i ;

y_{l_1} = $\sum_{j=1}^{m} \phi_{1j}(x_1 = l_1)\delta_{1j}(t) = \sum_{j=1}^{m} \phi_{l_1 j}\delta_{1j}(t)$;

x_i = distance along the link i (or the X_i-axis) from joint i ;

$y_i(x_i)$ = transverse deflection of link i at position x_i .

Inserting the required variables, differentiating w.r.t. time and multiplying the appropriate matrix elements, the absolute velocities are obtained for the mass elements dm_1, dm_2, as well as m_P:

$$\dot{\vec{r}}_1 = \begin{pmatrix} -x_1\dot{\theta}_1 S_1 - \dot{y}_1 S_1 - y_1\dot{\theta}_1 C_1 + \dot{p}_x \\ x_1\dot{\theta}_1 C_1 + \dot{y}_1 C_1 - y_1\dot{\theta}_1 S_1 + \dot{p}_y \\ 0 \\ 0 \end{pmatrix} \quad ;$$

$$\dot{\vec{r}}_2 = \begin{pmatrix} -x_2\dot{\alpha}_{12}S_{12} - \dot{y}_2 S_{12} - y_2\dot{\alpha}_{12}C_{12} - l_1\dot{\theta}_1 S_1 - \dot{y}_{l_1} S_1 - y_{l_1}\dot{\theta}_1 C_1 + \dot{p}_x \\ x_2\dot{\alpha}_{12}C_{12} + \dot{y}_2 C_{12} - y_2\dot{\alpha}_{12}S_{12} + l_1\dot{\theta}_1 S_1 - \dot{y}_{l_1} C_1 - y_{l_1}\dot{\theta}_1 S_1 + \dot{p}_y \\ 0 \\ 0 \end{pmatrix} \quad ;$$

$$\dot{\vec{r}}_p = \begin{pmatrix} -(l_2\dot{\alpha}_{12} - \dot{y}_{l_2})S_{12} - y_{l_2}\dot{\alpha}_{12}C_{12} - l_1\dot{\theta}_1 S_1 - \dot{y}_{l_1}S_1 - y_{l_1}\dot{\theta}_1 C_1 + \dot{p}_x \\ +(l_2\dot{\alpha}_{12} + \dot{y}_{l_2})C_{12} - y_{l_2}\dot{\alpha}_{12}S_{12} + l_1\dot{\theta}_1 S_1 - \dot{y}_{l_1}C_1 - y_{l_1}\dot{\theta}_1 S_1 + \dot{p}_y \\ 0 \\ 0 \end{pmatrix} .$$

In the next section the use of vector method is demonstrated to identify its strength and weaknesses. Although it is a somewhat complex approach on one hand, it also offers some intuitive insight into the various kinematic terms contributing to the overall system equations. For the present study of the moving two link manipulator, homogeneous transformations are used directly, on a term by term basis, as it is far more efficient.

2.5 Kinetics

Alternatively, in the vector form, the generalized position and velocity of the elemental mass dm_i in an open chain of coordinate systems may be presented as:

$$\begin{aligned} \vec{r}_i &= \vec{p}_i + \vec{\rho}_i \ ; \\ \dot{\vec{r}}_i &= \dot{\vec{p}}_i + (\vec{\omega}_i \times \vec{\rho}_i) + \dot{\vec{\rho}}_i \ . \end{aligned}$$

It should be noted that all the above vector variables must be projected onto the inertial reference frame F_0. This implies that all vectors stated in terms of the local reference frame F_i must be transformed by a series of consecutive rotational transformation matrices. Consider Figure 2.4 for a representation of the open chain of coordinate systems with flexible links. With the position and velocity of each elemental mass dm_i determined, the kinetic energy T and potential energy U of the system can be derived by integrating over the total mass M of the system as a whole.

The kinetic energy [20], [21] for the mobile flexible manipulator can be represented as:

$$\begin{aligned} T &= \frac{1}{2}\int_M \dot{\vec{r}} \cdot \dot{\vec{r}} dM \\ &= \sum_{i=1}^{2} \frac{1}{2}\int_{M_i} \dot{\vec{r}}_i \cdot \dot{\vec{r}}_i dm_i \end{aligned}$$

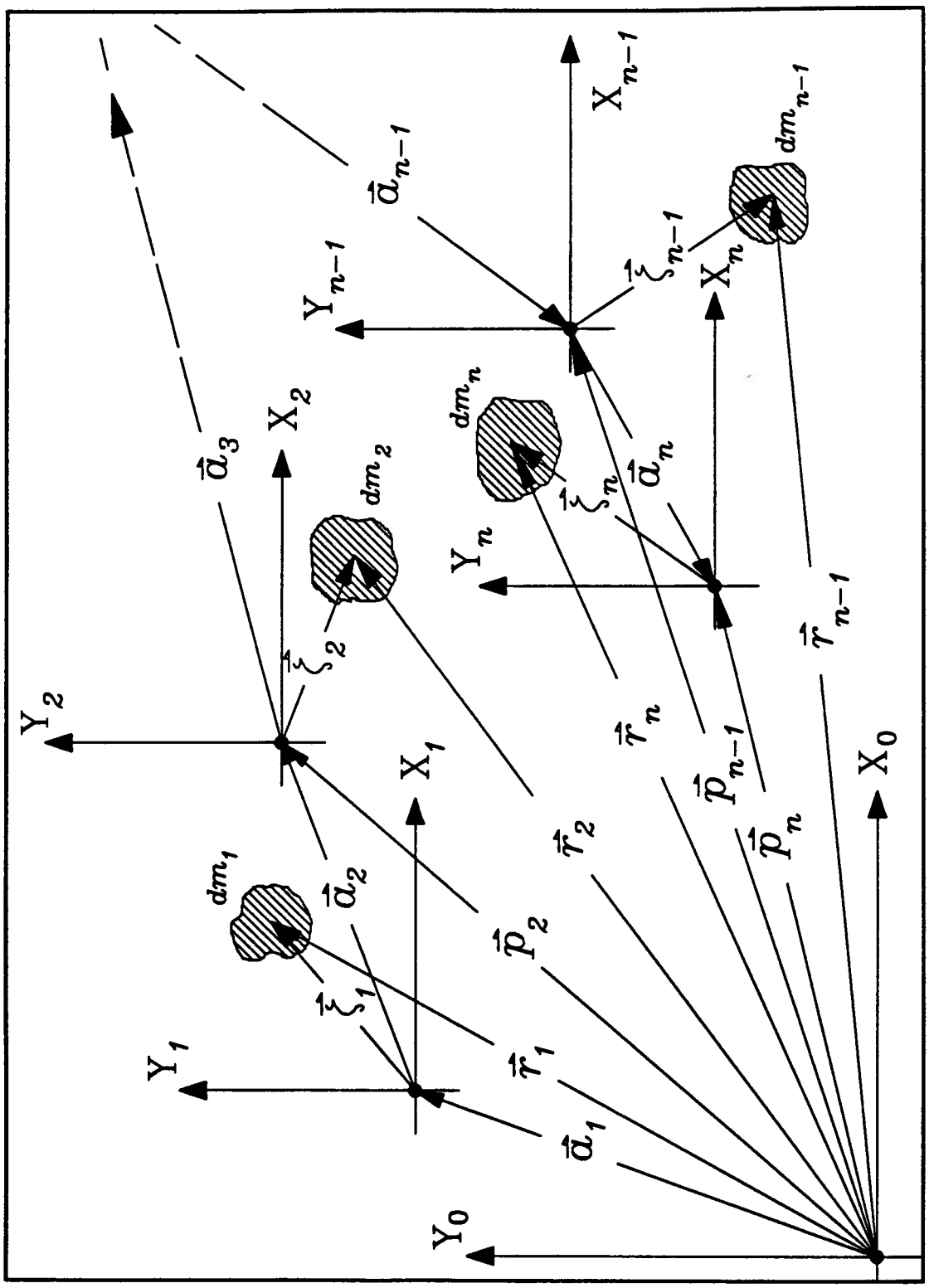

Figure 2.4: Schematic of the open chain of coordinate systems representing infinitessmal flexible mass elements dm_i in the local and the inertial reference coordinate frames

$$
\begin{aligned}
&= \sum_{i=1}^{2} \frac{1}{2} \int_{M_i} (\dot{\vec{p}}_i + (\vec{\omega}_i \times \vec{\rho}_i) + \dot{\vec{\rho}}_i) \cdot (\dot{\vec{p}}_i + (\vec{\omega}_i \times \vec{\rho}_i) + \dot{\vec{\rho}}_i) dm_i \\
&= \sum_{i=1}^{2} \int_{M_i} [\frac{1}{2}((\dot{\vec{p}}_i \cdot \dot{\vec{p}}_i) + (\vec{\omega}_i \times \vec{\rho}_i) \cdot (\vec{\omega}_i \times \vec{\rho}_i) + \dot{\vec{\rho}}_i \cdot \dot{\vec{\rho}}_i) \\
&\quad + (\dot{\vec{p}}_i \cdot (\vec{\omega}_i \times \vec{\rho}_i) \dot{\vec{p}}_i \cdot \dot{\vec{\rho}}_i + (\vec{\omega}_i \times \vec{\rho}_i) \cdot \dot{\vec{\rho}}_i] dm_i \\
&= T_{CMT} + T_{CMR} + T_{MV} + T_{HH}
\end{aligned}
$$

where:

$$
\begin{aligned}
T_{CMT} &= \tfrac{1}{2} \textstyle\sum_{i=1}^{N} \int_{M_i} \dot{\vec{p}}_i \cdot \dot{\vec{p}}_i dm_i \ , \\
&= \text{total translational K.E. of the C.M. of the system;} \\
T_{CMR} &= \tfrac{1}{2} \textstyle\sum_{i=1}^{N} \int_{M_i} (\vec{\omega}_i \times \vec{\rho}_i) \cdot (\vec{\omega}_i \times \vec{\rho}_i) dm_i \ , \\
&= \textstyle\sum_{i=1}^{N} \tfrac{1}{2} \vec{\omega}_i^T \mathbf{I} \vec{\omega}_i \ , \\
&= \text{total rotational K.E. of the C.M. of the system w.r.t. the local frames;} \\
T_{MV} &= \textstyle\sum_{i=1}^{N} \tfrac{1}{2} \int_{M_i} \dot{\vec{\rho}}_i \cdot \dot{\vec{\rho}}_i dm_i \ , \\
&= \text{total K.E. w.r.t. the local frames;} \\
T_{HH} &= \textstyle\sum_{i=1}^{N} \int_{M_i} (\dot{\vec{p}}_i \cdot (\vec{\omega}_i \times \vec{\rho}_i) \dot{\vec{p}}_i \cdot \dot{\vec{\rho}}_i + (\vec{\omega}_i \times \vec{\rho}_i) \cdot \dot{\vec{\rho}}_i) dm_i \ , \\
&= \text{angular momenta terms for the system;} \\
\mathbf{I} &= \text{instantaneous inertia matrix w.r.t. the local frames.}
\end{aligned}
$$

The kinetic energy T_{CMT} describes a nominal value associated with the C.M. of each frame w.r.t. and p.o.t. the inertial frame. The energy T_{CMR} is the rotational kinetic energy associated with the instantaneous inertia measured in each frame. Kinetic energy arising from modal vibration in the flexible links is described by T_{MV}. Energy T_{HH} represents the coupling between the various degrees of freedom within the manipulator system as a whole.

It should be noted that, when evaluating T for the Lagrangian procedure, all vector parameters must ultimately be *projected onto* the inertial frame F_0 through a series of rotational transformations. The vector method offers good intuitive insight into the nature of the various contributors to the total kinetic energy. However, it is more labour intensive compared to the homogeneous transformation procedure. It leads to numerous redundant cross-terms in the

differential equations of motion which ultimately cancel. Hence the homogeneous transform method was used to derive the kinetic energy for the specific case in study (Appendix A). However, in the following sections vector method is used to determine the form of the generalized equations of motion for an open chain of N flexible links.

2.5.1 Kinetic Energy for the N-Link System

The nature of the vector method and its extension to a multi-degree of freedom system of N links is demonstrated in this section. The expression obtained in the previous section for the kinetic energy, T, can be further transformed into a general expression for an N link manipulator system as follows:

$$\begin{aligned}
T &= \frac{1}{2}\int_M \dot{\vec{r}}\cdot\dot{\vec{r}}dM \ ; \\
&= \sum_{i=1}^{N}\frac{1}{2}\int_{M_i}\dot{\vec{r}}_i\cdot\dot{\vec{r}}_i dm_i \ ; \\
&= \sum_{i=1}^{N}\frac{1}{2}\int_{M_i}(\dot{\vec{p}}_i+(\vec{\omega}_i\times\vec{\rho}_i)+\dot{\vec{\rho}}_i)\cdot(\dot{\vec{p}}_i+(\vec{\omega}_i\times\vec{\rho}_i)+\dot{\vec{\rho}}_i)dm_i \ ; \\
&= \sum_{i=1}^{N}\int_{M_i}[\frac{1}{2}((\dot{\vec{p}}_i\cdot\dot{\vec{p}}_i)+(\vec{\omega}_i\times\vec{\rho}_i)\cdot(\vec{\omega}_i\times\vec{\rho}_i)+\dot{\vec{\rho}}_i\cdot\dot{\vec{\rho}}_i) \\
&\quad +(\dot{\vec{p}}_i\cdot(\vec{\omega}_i\times\vec{\rho}_i)\dot{\vec{p}}_i\cdot\dot{\vec{\rho}}_i+(\vec{\omega}_i\times\vec{\rho}_i)\cdot\dot{\vec{\rho}}_i]dm_i \ .
\end{aligned}$$

If the local frame mass element position vector is changed from $\vec{\rho}$ to $\vec{\zeta}$ to indicate that the body being integrated over is a flexible cantilever beam, then the kinetic energy expression takes the following form;

$$\begin{aligned}
T &= \sum_{i=1}^{N}T_i \ ; \\
&= \sum_{i=1}^{N}\left[\frac{1}{2}\left(\dot{\vec{p}}_i\cdot\dot{\vec{p}}_i\right)M_i+\dot{\vec{p}}_i\cdot\left(\vec{\omega}_{0,i}\times\int_{M_i}\vec{\zeta}_i dm_i+\int_{M_i}\dot{\vec{\zeta}}_i dm_i\right)\right. \\
&\quad \left.+\frac{1}{2}\vec{\omega}_{0,i}^{T}\mathbf{I}_i\vec{\omega}_{0,i}+\frac{1}{2}\vec{\omega}_{0,i}\cdot\int_{M_i}\vec{\zeta}_i\times\dot{\vec{\zeta}}_i dm_i+\frac{1}{2}\int_{M_i}\dot{\vec{\zeta}}_i\cdot\dot{\vec{\zeta}}_i dm_i\right] \ .
\end{aligned}$$

This can be rewritten in pure summation form by making the following substitutions:

$$\vec{\omega}_{0,i} = \vec{\omega}_1+\vec{\omega}_2+\cdots+\vec{\omega}_i \ ;$$

$$
\begin{aligned}
&= \mathbf{R}_{0,0}\vec{\omega}_1' + \mathbf{R}_{0,1}\vec{\omega}_2' + \cdots + \mathbf{R}_{0,i-1}\vec{\omega}_i' \ ; \\
\vec{v}_i &= \dot{\vec{a}}_0 + \dot{\vec{a}}_1 + \dot{\vec{a}}_2 + \cdots + \dot{\vec{a}}_{i-1} \ ; \\
&= \mathbf{R}_{0,0}\dot{\vec{a}}_0' + \mathbf{R}_{0,1}\dot{\vec{a}}_1' + \mathbf{R}_{0,2}\dot{\vec{a}}_2' + \cdots + \mathbf{R}_{0,i-1}\dot{\vec{a}}_{i-1}' \ ; \\
&= \sum_{j=1}^{i} \mathbf{R}_{0,j-1}\dot{\vec{a}}_{j-1}' \ ;
\end{aligned}
$$

where:

$\mathbf{R}_{0,0}$ = Identity matrix $\mathbf{I}$;

$\mathbf{R}_{0,i}$ = Rotation transformation matrix from the inertial frame to the local link frame. i ;

$\vec{a}_i'$ = Position vector describing the origin of the frame i w.r.t. and p.o.t. the previous frame $i-1$ in the chain ;

$\vec{a}_i$ = Position vector describing the origin of the frame i w.r.t. the previous frame but p.o.t. the inertial frame ;

$\vec{p}_i$ = Position vector of the origin of frame i w.r.t. and p.o.t. the inertial frame ;

$\vec{\zeta}_i'$ = The position vector of the elemental mass dm_i w.r.t and p.o.t. local frame i ;

$\vec{\zeta}_i$ = The position vector of the elemental mass dm_i w.r.t. and p.o.t. the inertial frame ;

$\vec{\omega}_i'$ = Angular velocity vector of frame i w.r.t. and p.o.t. the previous local frame $i-1$;

$\vec{\omega}_{0,i}$ = Angular velocity vector of frame i w.r.t. and p.o.t. the inertial frame.

The total kinetic energy of the system then becomes:

$$
\begin{aligned}
T &= \sum_{i=1}^{N} T_i = \frac{1}{2}\sum_{i=1}^{N}\left[\sum_{j=1}^{i}\mathbf{R}_{0,j-1}\dot{\vec{a}}_{j-1}\cdot\sum_{j=1}^{i}\mathbf{R}_{0,j-1}\dot{\vec{a}}_{j-1}\right] m_i \\
&\quad + \sum_{i=1}^{N}\left[\sum_{j=1}^{i}\mathbf{R}_{0,j-1}\dot{\vec{a}}_{j-1}\cdot\left(\sum_{j=1}^{i}\mathbf{R}_{0,j-1}\vec{\omega}_i\times\mathbf{R}_{0,i}\int_{M_i}\vec{\zeta}_i dm_i + \mathbf{R}_{0,i}\int_{M_i}\dot{\vec{\zeta}}_i dm_i\right)\right]
\end{aligned}
$$

$$+\frac{1}{2}\sum_{i=1}^{N}\left[\left(\sum_{j=1}^{i}\mathbf{R}_{0,j-1}\vec{\omega}_j\right)^T \mathbf{I}_i\left(\sum_{j=1}^{i}\mathbf{R}_{0,j-1}\vec{\omega}_j\right)\right]$$

$$+\frac{1}{2}\sum_{i=1}^{N}\left[\sum_{j=1}^{i}\mathbf{R}_{0,j-1}\vec{\omega}_j\cdot\mathbf{R}_{0,i}\int_{M_i}\vec{\zeta}_i\times\dot{\vec{\zeta}}_i dm_i\right]+\frac{1}{2}\sum_{i=1}^{N}\int_{M_i}\dot{\vec{\zeta}}_i\cdot\dot{\vec{\zeta}}_i dm_i\ .$$

Carrying out the required algebraic manipulations the generalized kinetic energy equation can be further reduced to the following form:

$$T=\frac{1}{2}\vec{\mathbf{v}}^T\left[\mathbf{M}\vec{\mathbf{v}}+2\vec{\mathbf{\Phi}}_2\right]+\frac{1}{2}\vec{\omega}^T\left[\mathbf{I}\vec{\omega}+2\vec{\mathbf{\Phi}}_1+\vec{\mathbf{\Phi}}_3\right]+\frac{1}{2}\sum_{i=1}^{N}\mathbf{\Phi_{4i}}\ ;$$

where:

$$\mathbf{M} = \begin{bmatrix} \sum_{i=1}^{N} m_i & \sum_{i=2}^{N} m_i & \cdots & m_N \\ \sum_{i=2}^{N} m_i & \sum_{i=2}^{N} m_i & \cdots & m_N \\ \vdots & \vdots & \ddots & \vdots \\ m_N & m_N & \cdots & m_N \end{bmatrix},$$

= Global rigid body mass matrix for the total system;

$$\mathbf{I} = \begin{bmatrix} \sum_{i=1}^{N}\mathbf{I_i} & \sum_{i=2}^{N}\mathbf{I_i} & \cdots & \mathbf{I_n} \\ \sum_{i=2}^{N}\mathbf{I_i} & \sum_{i=2}^{N}\mathbf{I_i} & \cdots & \mathbf{I_n} \\ \vdots & \vdots & \ddots & \vdots \\ \mathbf{I_n} & \mathbf{I_n} & \cdots & \mathbf{I_n} \end{bmatrix},$$

= Global rigid body inertia matrix for the total system ;

$$\vec{\mathbf{\Phi}}_1 = \begin{bmatrix} \sum_{i=1}^{N}\mathbf{R}_{0,i-1}\vec{\mathbf{\Phi}}_{1i}\times\mathbf{R}_{0,0}\dot{\vec{a}}_1+\cdots\cdots+\mathbf{R}_{0,n-1}\vec{\mathbf{\Phi}}_{1n}\times\mathbf{R}_{0,n-1}\dot{\vec{a}}_n \\ \sum_{i=2}^{N}\mathbf{R}_{0,i-1}\vec{\mathbf{\Phi}}_{1i}\times\mathbf{R}_{0,0}\dot{\vec{a}}_1+\cdots\cdots+\mathbf{R}_{0,n-1}\vec{\mathbf{\Phi}}_{1n}\times\mathbf{R}_{0,n-1}\dot{\vec{a}}_n \\ \vdots \\ \mathbf{R}_{0,n-1}\vec{\mathbf{\Phi}}_{1n}\times\mathbf{R}_{0,0}\dot{\vec{a}}_1+\mathbf{R}_{0,n-1}\vec{\mathbf{\Phi}}_{1n}\times\mathbf{R}_{0,n-1}\dot{\vec{a}}_n \end{bmatrix},$$

= A time dependent inertia vector ;

$$\vec{\Phi}_2 = \begin{bmatrix} \sum_{i=1}^{N} \mathbf{R}_{0,i-1}\vec{\Phi}_{2i} \\ \sum_{i=2}^{N} \mathbf{R}_{0,i-1}\vec{\Phi}_{2i} \\ \vdots \\ \mathbf{R}_{0,n-1}\vec{\Phi}_{2n} \end{bmatrix},$$

= Global momentum vector ;

$$\vec{\Phi}_3 = \begin{bmatrix} \sum_{i=1}^{N} \mathbf{R}_{0,i-1}\vec{\Phi}_{3i} \\ \sum_{i=2}^{N} \mathbf{R}_{0,i-1}\vec{\Phi}_{3i} \\ \vdots \\ \mathbf{R}_{0,n-1}\vec{\Phi}_{3n} \end{bmatrix}.$$

= Global angular momentum vector ;

$$\vec{\mathbf{v}} = \begin{bmatrix} \mathbf{R}_{0,0}\dot{\vec{a}}_1 \\ \mathbf{R}_{0,1}\dot{\vec{a}}_2 \\ \vdots \\ \mathbf{R}_{0,n-1}\dot{\vec{a}}_n \end{bmatrix},$$

= Global velocity vector for local reference frames ;

$$\vec{\omega} = \begin{bmatrix} \mathbf{R}_{0,0}\vec{\omega}_1 \\ \mathbf{R}_{0,1}\vec{\omega}_2 \\ \vdots \\ \mathbf{R}_{0,n-1}\vec{\omega}_n \end{bmatrix},$$

= Global angular velocity vector for local reference frames ;

$$\vec{\Phi}_{1i} = \int_{M_i} \vec{\zeta}_i dm_i \ ;$$

$$\vec{\Phi}_{2i} = \int_{M_i} \dot{\vec{\zeta}}_i dm_i \ ;$$

$$\vec{\Phi}_{3i} = \int_{M_i} \vec{\zeta}_i \times \dot{\vec{\zeta}}_i \mathrm{dm_i} \ ;$$

$$\Phi_{4i} = \int_{M_i} \dot{\vec{\zeta}}_i \cdot \dot{\vec{\zeta}}_i dm_i = \int_{M_i} \left| \dot{\vec{\zeta}}_i \right|^2 dm_i \ ;$$

$\mathbf{I_i}$ = Instantaneous inertia matrix of the link subsystem i w.r.t. the local reference frame i .

In the global kinetic energy equation, T, the bracketted part of the first expression contains the *linear momentum* terms. The bracketted part in the second expression contains the *angular momentnum* terms. The third expression contains the kinetic energies as measured in the *local reference frames.*

2.6 Potential Energy

The following three sources are the sole contributors to the potential energy of the mobile flexible two link system:

- gravitational field ;
- strain energy of the flexible links ;
- linear elastic strain energy of the joints ;

resulting in:

$$U = U_G + U_L + U_J \ .$$

The gravitational potential energy for the twolink flexible manipulator is given by

$$U_G = -\sum_{i=1}^{2} \int_{M_i} \vec{\mathbf{g}} \cdot \vec{\mathbf{r}}_i dm_i \ ,$$

where:

$\vec{\mathbf{g}}$ = gravitational acceleration;

$\vec{\mathbf{r}}_i$ = position vector of the element mass dm_i w.r.t. the inertial frame.

The strain energy due to bending is given by

$$U_L = \sum_{i=1}^{2} \frac{1}{2} \int_0^{l_i} (EI)_i (\frac{\partial^2 y_i}{\partial x_i^2})^2 dx_i \ ,$$

where:

$$(EI)_i = \text{bending stiffness of the link } i \ ;$$

$$\partial^2 y_i / \partial x_i^2 = \text{curvature of the link } i \ .$$

The potential energy stored within the flexible joints is

$$U_J = \sum_{i=1}^{2} \frac{1}{2} k_i (\beta_i - \theta_i)^2 \ ,$$

where:

$$k_i = \text{torsional stiffness of the joint } i \ ;$$

$$\beta_i = \text{specified slew angle of the joint } i \ ;$$

$$\theta_i = \text{response angle at joint } i.$$

Details of the potential energy expressions are given in Appendix B.

2.6.1 Potential Energy for the N-Link System

The required potential energy terms U_G, U_L, U_J descibed above can be generalized to N links utilizing the orthogonality properties of the modal functions:

$$\begin{aligned} U_G &= -\sum_{i=1}^{N} \int_{M_i} \vec{\mathbf{g}} \cdot \vec{\mathbf{r}}_i dm_i \ , \\ &= -\vec{\mathbf{g}} \cdot \sum_{i=1}^{N} \mathbf{R}_{0,i-1} \left[\vec{\mathbf{a}}_i \sum_{j=i}^{n} \mathrm{m_j} + \mathbf{R}_{i-1,i} \vec{\mathbf{\Phi}}_{1i} \right] \ ; \end{aligned}$$

$$\begin{aligned} U_L &= \frac{1}{2} \sum_{i=1}^{N} \int_0^{l_i} (EI)_i (\frac{\partial^2 y_i}{\partial x_i^2})^2 dx_i \ , \\ &= \frac{1}{2} \sum_{i=1}^{N} \vec{\delta}_i^T \mathbf{K}_i \vec{\delta}_i \ ; \end{aligned}$$

$$U_J = \frac{1}{2} \sum_{i=1}^{N} k_i (\beta_i - \theta_i)^2 \ ;$$

where:

$$\mathbf{K}_i = \begin{bmatrix} \Phi_{i11} & \Phi_{i12} & \Phi_{i13} & \cdots & \Phi_{i1m} \\ \Phi_{i21} & \Phi_{i22} & \Phi_{i23} & \cdots & \Phi_{i2m} \\ \vdots & \vdots & \vdots & \ddots & \vdots \\ \Phi_{im1} & \Phi_{im2} & \Phi_{im3} & \cdots & \Phi_{imm} \end{bmatrix},$$

$=$ Global stiffness matrix in bending associated with link i ;

$$\vec{\delta}_i = \begin{bmatrix} \delta_{i1} \\ \delta_{i2} \\ \delta_{i3} \\ \vdots \\ \delta_{im} \end{bmatrix},$$

$=$ Global generalized coordinate vector associated with link i ;

$$\Phi_{ijk} = \int_0^{l_i} (EI)_i \, \phi''_{ij}(x) \, \phi''_{ik}(x) \, dx \ ;$$

δ_{ij} = generalized coordinate associated with the jth mode of link i ; $i = 1, ..., m$;

$\phi_{ij}(x)$ = spatial admissible function associated with mode j of link i ;

$$\phi''_{ij}(x) = \frac{\partial^2 \phi_{ij}(x)}{\partial x^2} \ ;$$

$\vec{\mathbf{g}}$ = gravitational acceleration field vector ;

m_j = total mass of link associated with local frame j ;

k_i = torsional spring rate of joint i ;

$(\beta_i - \theta_i)$ = angular deflection between the joint i and link i, and is dependent on joint stiffness.

The remaining parameters were defined in the previous sections.

2.7 Governing Equations of Motion

The nonlinear differential equations of motion for the mobile two-link flexible manipulator were derived using the Lagrange equation,

$$\frac{d}{dt}\left(\frac{\partial T}{\partial \dot{q}_k}\right) - \frac{\partial T}{\partial q_k} + \frac{\partial U}{\partial q_k} = Q_k \ ,$$

where $k = 1,...,n_q$; T and U are the total kinetic and potential energies, respectively q_k and Q_k are the generalized coordinates and the generalized forces, respectively; and n_q is the total number of generalized coordinates.

Specifically, the generalized coordinates are defined as follows:

p_x = x-component of the base position vector $\vec{\mathbf{p}}$;

p_y = y-component of base position vector $\vec{\mathbf{p}}$;

θ_1 = joint angle of link 1 ;

θ_2 = joint angle of link 2 ;

δ_{1j} = generalized coordinate associated with the j^{th} mode of link 1, where $j = 1,...,m$;

δ_{2j} = generalized coordinate associated with the j^{th} mode of link 2, where $j = 1,...,m$.

The specified time varying slewing coordinates are:

$$\begin{aligned} \vec{\beta}_p &= \text{mobile base translation vector ;} \\ \beta_1 &= \text{slew angle at joint 1 ;} \\ \beta_2 &= \text{slew angle at joint 2.} \end{aligned}$$

The governing equations of motion may be written as:

$$\frac{d}{dt}\left(\frac{\partial T}{\partial \dot{q}_k}\right) - \frac{\partial T}{\partial q_k} + \frac{\partial U}{\partial q_k} = Q_k \ ;$$

$$\begin{aligned} \vec{f}_D + \vec{f}_{TD} - \vec{f}_T + \vec{f}_U &= \vec{Q} \ ; \\ \mathbf{D}\ddot{\vec{q}} + \vec{f}_{TD} - \vec{f}_T + \vec{f}_U &= \vec{Q} \ ; \\ \mathbf{D}(\vec{q}, t)\ddot{\vec{q}} + \vec{\mathbf{F}}(\dot{\vec{q}}, \vec{q}, t) &= \vec{\mathbf{Q}} \ . \end{aligned}$$

Here $\mathbf{D}$ is the symmetric positive definite time varying inertia matrix for the system; and $\vec{\mathbf{F}}$ represents the non-linear vector containing all the cross influence force terms that are generally associated with centripetal and coriolis accelerations. They are functions of velocity and not acceleration of the generalized coordinate vector $\vec{q}$. $\vec{\mathbf{Q}}$ denotes the generalized force vector containing the input *joint control torque* values. For the generalized modal coordinates the associated generalized forces in the vector $\vec{\mathbf{Q}}$ must be equal to zero since it is assumed that the individual modes of each link cannot be controlled externally. A summary of the nonlinear differential equations is presented in Appendix C.

2.7.1 Equations of Motion for the N-Link System

The kinetic and potential energy expressions for a general system with N flexible links were presented earlier:

$$T = \frac{1}{2}\vec{\mathbf{v}}^T\left[\mathbf{M}\vec{\mathbf{v}} + 2\vec{\mathbf{\Phi}}_2\right] + \frac{1}{2}\vec{\omega}^T\left[\mathbf{I}\vec{\omega} + 2\vec{\mathbf{\Phi}}_1 + \vec{\mathbf{\Phi}}_3\right] + \frac{1}{2}\sum_{i=1}^{N}\mathbf{\Phi_{4i}} \ ;$$

$$U = -\vec{\mathbf{g}}\cdot\sum_{i=1}^{N}\mathbf{R}_{0,i-1}\left[\vec{\mathbf{a}}_i\sum_{j=i}^{n}\mathrm{m_j} + \mathbf{R}_{i-1,i}\vec{\mathbf{\Phi}}_{1i}\right] + \frac{1}{2}\sum_{i=1}^{N}\vec{\delta}_i^{\mathrm{T}}\mathbf{K}_i\vec{\delta}_i + \frac{1}{2}\sum_{i=1}^{N}\mathrm{k_i}(\beta_i - \theta_i)^2 \ .$$

Using the Lagrangian procedure, the governing equations of motion can be obtained, as shown before, from the following equation:

$$\frac{d}{dt}\left(\frac{\partial T}{\partial \dot{q}_k}\right) - \frac{\partial T}{\partial q_k} + \frac{\partial U}{\partial q_k} = Q_k$$

where T and U are the global kinetic and potential energies of the system; with q_k and Q_k as the generalized coordinates (i.e. joint angles, flexural modes) and the associated generalized forces (i.e. forces, torques). Making a substitution for the bracketted expressions to simplify the equations gives:

$$T = \frac{1}{2}\vec{v}^T\vec{b}_1 + \frac{1}{2}\vec{\omega}^T\vec{b}_2 + \frac{1}{2}\sum_{i=1}^{N}\Phi_{4i} \ ,$$

where:

$$\vec{b}_1 = \mathbf{M}\vec{v} + 2\vec{\Phi}_2 \ ;$$

$$\vec{b}_2 = \mathbf{I}\vec{\omega} + 2\vec{\Phi}_1 + \vec{\Phi}_3 \ .$$

Performing the required algebra leads to the generalized equations of motion for the flexible N-link system:

$$\begin{aligned} Q_k = \frac{1}{2}\Bigg[& \left(\frac{d}{dt}\left(\frac{\partial \vec{v}^T}{\partial \dot{q}_k}\right) - \frac{\partial \vec{v}^T}{\partial q_k}\right)\vec{b}_1 + \vec{v}^T\left(\frac{d}{dt}\left(\frac{\partial \vec{b}_1}{\partial \dot{q}_k}\right) - \frac{\partial \vec{b}_1}{\partial q_k}\right) \\ & + \left(\frac{d}{dt}\left(\frac{\partial \vec{\omega}^T}{\partial \dot{q}_k}\right) - \frac{\partial \vec{\omega}^T}{\partial q_k}\right)\vec{b}_2 + \vec{\omega}^T\left(\frac{d}{dt}\left(\frac{\partial \vec{b}_2}{\partial \dot{q}_k}\right) - \frac{\partial \vec{b}_2}{\partial q_k}\right) \\ & + \frac{\partial \vec{v}^T}{\partial \dot{q}_k}\dot{\vec{b}}_1 + \frac{\partial \vec{\omega}^T}{\partial \dot{q}_k}\dot{\vec{b}}_2 + \dot{\vec{v}}^T\frac{\partial \vec{b}_1}{\partial \dot{q}_k} + \dot{\vec{\omega}}^T\frac{\partial \vec{b}_2}{\partial \dot{q}_k} \end{aligned}$$

$$+\sum_{i=1}^{N}\left(\frac{d}{dt}\left(\frac{\partial\Phi_{4i}}{\partial\dot{q}_k}\right)-\frac{\partial\Phi_{4i}}{\partial q_k}\right)\Bigg]+\frac{1}{2}\sum_{i=1}^{N}\left(\frac{\partial\vec{\delta}_i^T}{\partial q_k}\mathbf{K}_i\vec{\delta}_i\right.$$

$$\left.+\vec{\delta}_i^T\mathbf{K}_i\frac{\partial\vec{\delta}_i}{\partial q_k}\right)-\vec{\mathbf{g}}\cdot\left[\frac{\partial\mathbf{R}_{0,i-1}}{\partial q_k}\left(\vec{a}_i\sum_{k=i}^{n}m_k+\vec{\Phi}_{1i}\right)\right.$$

$$\left.+\mathbf{R}_{0,i-1}\left(\frac{\partial\vec{\mathbf{a}}_i}{\partial\mathrm{q_k}}\sum_{\mathrm{k=i}}^{\mathrm{n}}\mathrm{m_k}+\frac{\partial\vec{\Phi}_{4i}}{\partial\mathrm{q_k}}\right)\right]+\frac{1}{2}\sum_{i=1}^{N}k_i\frac{\partial\left(\beta_i-\theta_i\right)^2}{\partial q_k}\ .$$

This can be further expanded and then simplified into the more recognizable form. For the present, it is sufficient to say that since all the terms are clearly defined, an algebraic algorithm may be formulated for the N-link, flexible, mobile manipulator. This algorithm may then be integrated with a symbolic algebraic manipulation software, such as MATHCAD or MATHEMATICA [22], to automatically produce the complete system of differential equations, which can be numerically solved with graphical output through a single command operation.

Chapter 3

DYNAMICAL RESPONSE

The dynamic equations of motion derived in the previous chapter are nonlinear, nonautonomous, and coupled. They are not amenable to any known closed form solutions without considerable simplification. To retain the subtleties of the response characteristics, the equations are integrated numerically over a range of system parameters and prescribed maneuvers.

3.1 The Numerical Approach

The numerical code is in VS FORTAN77 language and is so written as to isolate the effects of various system parameters such as the number of modes used, inertia and flexibility properties of the links, end-tip trajectory tracking, maneuvers, etc. The numerical solution is obtained using the IMSL Version.10 [37] differential equation solver subroutine called DIVPAG and the MTSG system subroutine GEARB. Both subroutines utilize Gear's method [36] to solve initial value problems of ordinary differential equations with greatly varying time constants (i.e. stiff systems). DIVPAG appears to be a relatively slower program with limited capability. On the other hand, the GEARB routine is more versatile and can tackle more difficult situations while giving reliable results. For the mobile flexible two-link manipulator under study, the structural frequencies are in the range of 0.5-100 Hz depending upon the link and joint parameters as well as the number of modes used.

A flow chart for the translating flexible two-link manipulator simulation code is presented in Figure 3.5.

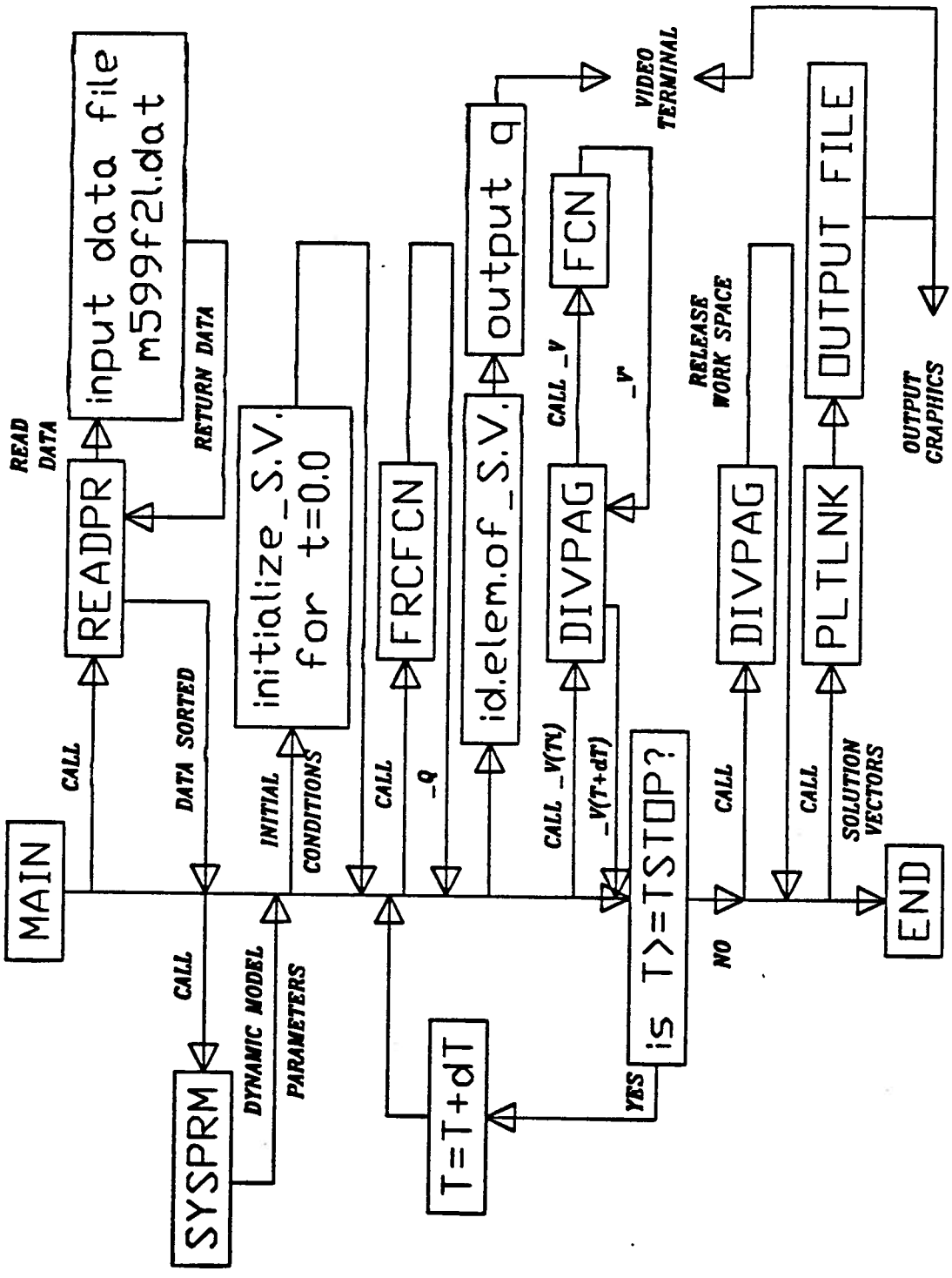

Figure 3.5: Flowchart for the earth based translating flexible twolink manipulator dynamics simulation program.

3.2 Definition of the Program Variables

The following is a summary of the program state variables, output data variables, and their corresponding symbolic notations. This list should be referred to in conjunction with the simulation plots that follow:

BETA1 = β_1 = specified joint angle for link 1

THETA1 = θ_1 = joint angle response for link 1

BETA2 = β_2 = specified joint angle for link 2

THETA2 = θ_2 = joint angle response for link 2

BP3 = $\beta_{\vec{p}_3}$ = specified position vector for the manipulator tip or payload w.r.t. the inertial frame

P3 = $\vec{p}_3$ = position vector to the manipulator tip (payload) w.r.t. the inertial frame

BP3X = $\beta_{p_{3x}}$ = X-component of $\beta_{\vec{p}_3}$

P3X = p_{3x} = X-component of $\vec{p}_3$

BP3Y = $\beta_{p_{3y}}$ = Y-component of $\beta_{\vec{p}_3}$

P3Y = p_{3y} = Y-component of $\vec{p}_3$

BPX = β_{p_x} = X-component of the specified base (joint 1) position vector in the inertial frame

PX = p_x = X-component of the base (joint 1) position vector response in the inertial frame

BPY = β_{p_y} = Y-component of the specified base (joint 1) position vector in the inertial frame

PY = p_y = Y-component of the base (joint 1) position vector response in the inertial frame

DL$i(j)$ = δ_{ij} = generalized co-ordinate associated with the mode j of the link i.

3.3 Numerical Data used in the Simulation

As a first step many simulation runs were carried out with different parameters and under varying slewing conditions until an average parametric configuration was established about which certain parameters can be varied so that the differences in the resultant response characteristics may be observed.

In the following simulation, the physical system that is modelled is constructed from $0.05m \times 0.05m \times 5.0m$ long square aluminum links. When not specified explicitly, the link cross-section and mass distribution are considered uniform, with the joints assumed massless. The payload is considered as a point mass.

The following parameter values represent the nominal configuration mentioned above:

$(EI)_1 = 3.0 \times 10^4$ $[N \cdot m^2]$ = flexural stiffness of link 1

$(EI)_2 = 3.0 \times 10^4$ $[N \cdot m^2]$ = flexural stiffness of link 2

$m_1 = 20.0$ $[Kg]$ = total mass of link 1

$m_2 = 20.0$ $[Kg]$ = total mass of link 2

$l_1 = 5.0$ $[m]$ = total lenght of link 1

$l_2 = 5.0$ $[m]$ = total lenght of link 2

$m_B = 00.0$ $[Kg]$ = total mass of the manipulator base

$m_L = 00.0$ $[Kg]$ = total mass of the manipulator payload

$k_x = 1.0 \times 10^4$ $\left[\frac{N}{m}\right]$ = stiffness of the base in the x-direction

$k_y = 1.0 \times 10^4$ $\left[\frac{N}{m}\right]$ = stiffness of the base in the y-direction

$K_1 = 1.0 \times 10^4$ $\left[\frac{N \cdot m}{rad}\right]$ = stiffness of joint 1

$k_2 = 1.0 \times 10^4$ $\left[\frac{N \cdot m}{rad}\right]$ = stiffness of joint 2

$c_x = 1.0$ $\left[\frac{N}{m/s}\right]$ = damping constant in the x-direction

$c_y = 1.0$ $\left[\frac{N}{m/s}\right]$ = damping constant in the y-direction

$c_1 = 1.0 \times 10^4$ $\left[\frac{N \cdot m}{rad/s}\right]$ = damping constant of joint 1

$c_2 = 1.0 \times 10^4$ $\left[\frac{N \cdot m}{rad/s}\right]$ = damping constant of joint 2 .

g = 0.0 $\left[\frac{m}{s^2}\right]$ = gravitational acceleration.

$X_0(i)$ = starting specified inertial X-coordinate of slew trajectory at the manipulator tip, 6.9m

$Y_0(i)$ = starting specified inertial Y-coordinate of slew trajectory at the manipulator tip, 6.9m

$X_0(f)$= final specified inertial X-coordinate of slew trajectory at the manipulator tip, 6.9m

$Y_0(f)$ = final specified inertial Y-coordinate of slew trajectory at the manipulator tip, 6.9m

T_{vs} = total specified excursion time of slew trajectory at a constant velocity

N_m = number of modes used in the simulation to estimate flexural dynamics of the links, 2

In the initial simulation runs, most of these values were kept constant. The parameters with different values are identified in the captions under the plots.

3.4 Simulation Results and Analysis: Tip Trajectory Tracking

For a planned system simulation with a wide variation in parameter values and initial conditions would result in, literally, enormous amount of information. Therefore, a more concise yet rational approach is adopted. Only the typical results useful in establishing trends are presented here.

The following group of simulation response plots are intended to establish characteristics of the time dependent variables in terms of the manipulator tip and joint trajectory tracking for the basic parametric configuration mentioned above. Information concerning the effect of the number of modes used in the simulation model is also explored.

In the following example, the manipulator payload, i.e. the end effector (tip of link 2), is required to follow a prescribed trajectory. The trajectory is taken to be a straight line and the payload as well as the base mass are considered zero. The tip starts at the global coordinate $[\, X_0(i), Y_0(i), 0\,]$ and is required to follow a straight line at a constant velocity to reach the global coordinates $[\, X_0(f), Y_0(f), 0\,]$ in precisely T_{vs} seconds. The manipulator base is required to be stationary at the origin.

Kinematically, the global slewing coordinates of the manipulator are calculated in prescribed increments of the distance, at each time-step, along the slew trajectory, in global coordinates. Using the *inverse kinematic* equations of the manipulator, the joint angles are calculated at each time-step and are used to provide the joint control torques, Q_{p_x}, Q_{p_y}, Q_{θ_1} and Q_{θ_2}, via the following PD type control equations:

$$
\begin{aligned}
Q_{p_x} &= (\beta_x - p_x)\, k_x + \left(\dot{\beta}_x - \dot{p}_x\right) c_x \; ; \\
Q_{p_y} &= (\beta_y - p_y)\, k_y + \left(\dot{\beta}_y - \dot{p}_y\right) c_y \; ; \\
Q_{\theta_1} &= (\beta_1 - \theta_1)\, k_1 + \left(\dot{\beta}_1 - \dot{\theta}_1\right) c_1 \; ; \\
Q_{\theta_2} &= (\beta_2 - \theta_2)\, k_2 + \left(\dot{\beta}_2 - \dot{\theta}_2\right) c_2 \; .
\end{aligned}
$$

The torques are then used to drive the system equations which, when solved numerically, yield generalized coordinate solutions for the time interval in question. For each simulation run, there are 4 frames within each group, and they are identified by the suffix letters (A), (B), (C) and (D).

The data used in the first simulation run are specified in Figures 3.6, 3.7, 3.8. Figure numbers with suffix letter (A) represent time strobed figures of the manipulator at specific time intervals (Figure 3.6). The slew trajectory is shown as the solid line while the actual path of the end tip is indicated by the dashed line. The simulation time interval T_{vs} is set to 4 seconds so that the lead or lag of the tip relative to the desired trajectory can be clearly observed.

Figure numbers with suffix letter (B) represent the slew trajectory superimposed onto the actual end-tip path vs time, but separated into the X and Y components in global coordinates as shown in Figure 3.7.

Figure numbers with suffix (C) represent the slew joint angles superimposed onto the actual joint angle trajectories vs time, plotted for each joint. The slew angles are calculated from the inverse kinematic relations mentioned before which in turn are based on the required slew trajectory of the manipulator tip in global coordinates.

The top two plots of figure numbers with suffix (D) represent the slew trajectory superimposed onto the actual path or motion of the base but separated into the X and Y components in global coordinates as indicated on the plots (Figure 3.9). The bottom two plots of the same figure represents the generalised modal coordinates vs time. Each graph represents the superposition of the same modal coordinate from each link, so that the dynamic coupling may be easier to observe.

This first run can be perceived as basic test of the dynamic response of the flexible 2 link manipulator without payload. The traverse time from start to finish, from [6.9, 6.9, 0.0] to [1.0, 1.0, 0.0] is 4 seconds at a constant velocity. There is no ramping of speed at either ends leading to lag at the start and overshoot at the end (Figure 3.6). This is mostly due to the phase mismatching between the two joint angles. Note, the maximum deviation of the tip occurs at the start of the slew maneuver. This is due to the fact that the joint 2 slew rate is twice that of joint 1. Link 2 also has an advantage of greater effective *inertial leverage* over link 1. The manipulator tip then settles into the slew trajectory with progressively smaller oscillations about the norm. This is due to the viscous damping at the joints and the base. Since the slew rate is relatively small, the overshoot and excursion at the end are essentially negligible. The starting excursion of the tip can be more clearly seen in Figure 3.7.

Figure 3.8 shows that eventhough the manipulator tip may deviate from the required trajectory, the joint angles follow the commanded profile quite closely. This is the first hint of the problem involved in controlling the tip by judicious application of the joint torques.

In the next two sets of simulation runs all conditions are maintained the same as before but the traverse period is reduced to 2 and 1 second respectively (Figures 3.10, 3.11, 3.12, 3.13 and Figures 3.14, 3.15, 3.16, 3.17). As expected, an increase in the slew velocity by two fold increases the tip excursions significantly.

With the 1 second traverse period the tip excursions become very large. Even the joint angles are starting to show significant departure from the calculated slewing angles. Obviously, a sophisticated control strategy would be required to maintain the desired trajectory.

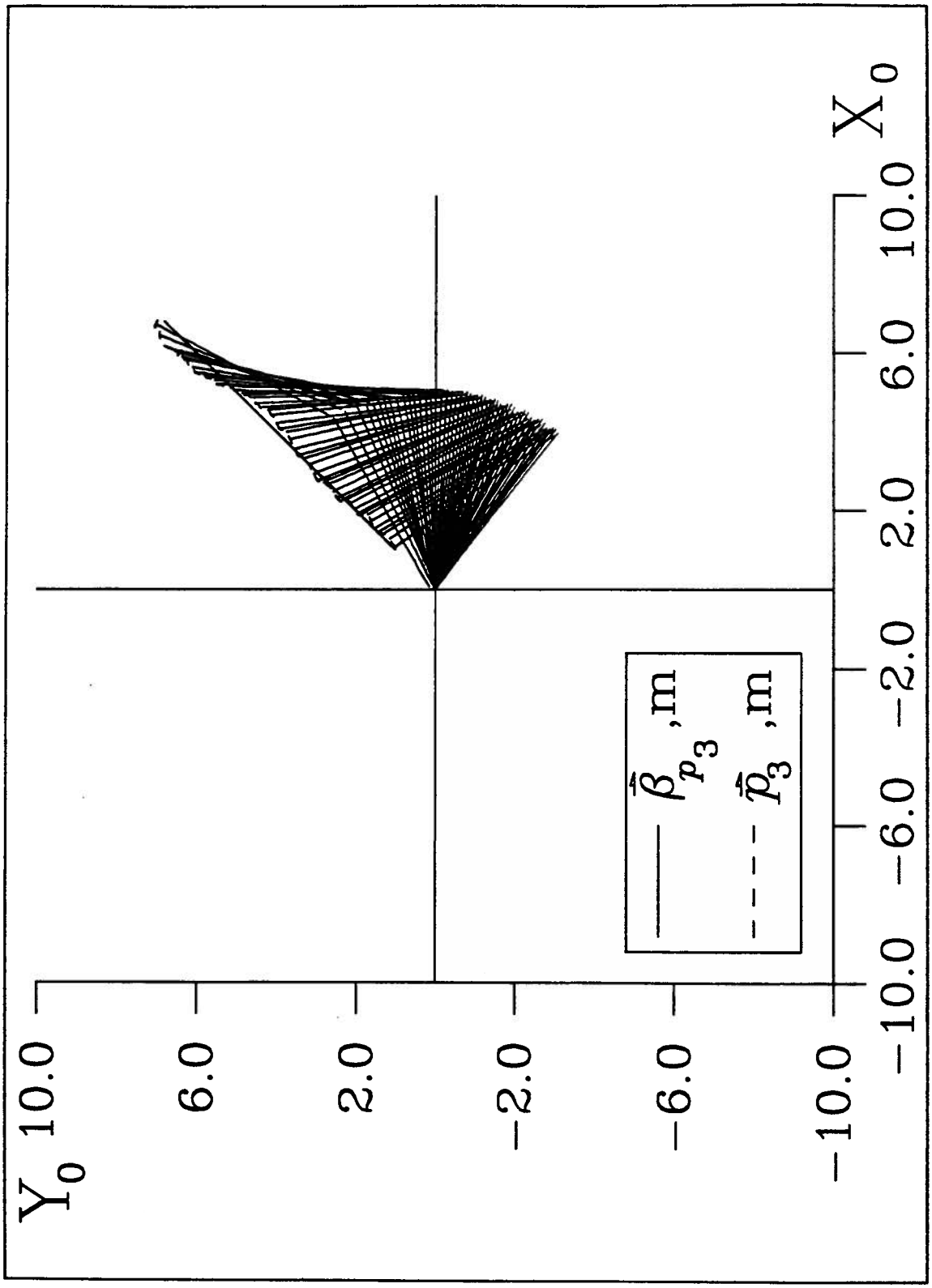

Figure 3.6: (A): Time strobe position plot of 2 link flexible manipulator with stationary base, using two modes for each link, during a straightline tip maneuver from the inertial coordinate (6.9, 6.9, 0)m to (1, 1, 0)m in 4s.

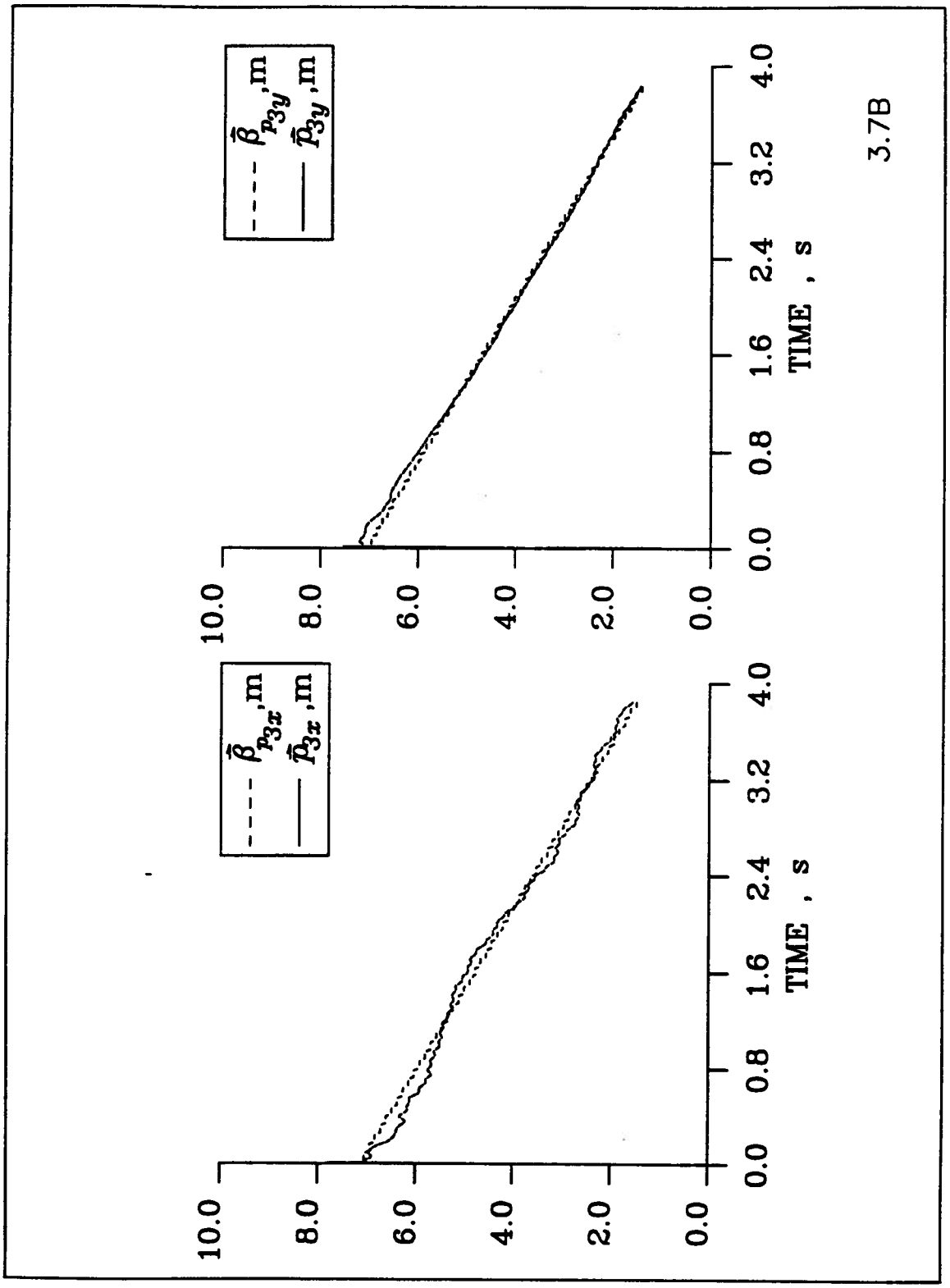

Figure 3.7: (B): Comparison between specified ($\beta_{p_{3x}}$ and $\beta_{p_{3y}}$) and actual (p_{3_x} and p_{3_y}) position of the manipulator tip during a straightline tip maneuver from the inertial coordinate (6.9, 6.9, 0)m to (1, 1, 0)m in 4s.

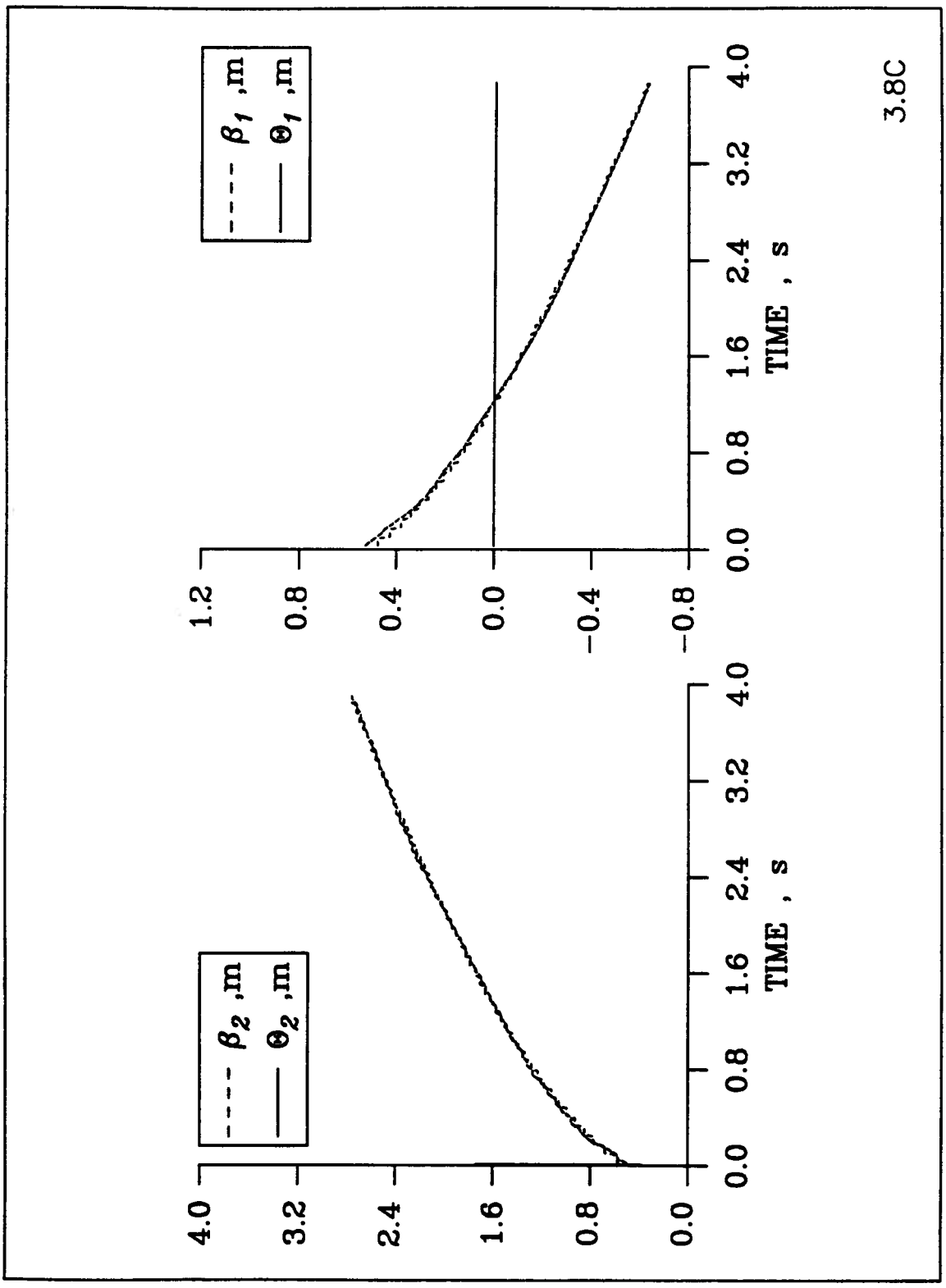

Figure 3.8: (C): Comparison between specified (β_1 and β_2) and actual (θ_1 and θ_2) position of the joint angles during a straightline tip maneuver from the inertial coordinate (6.9, 6.9, 0)m to (1, 1, 0)m in 4s.

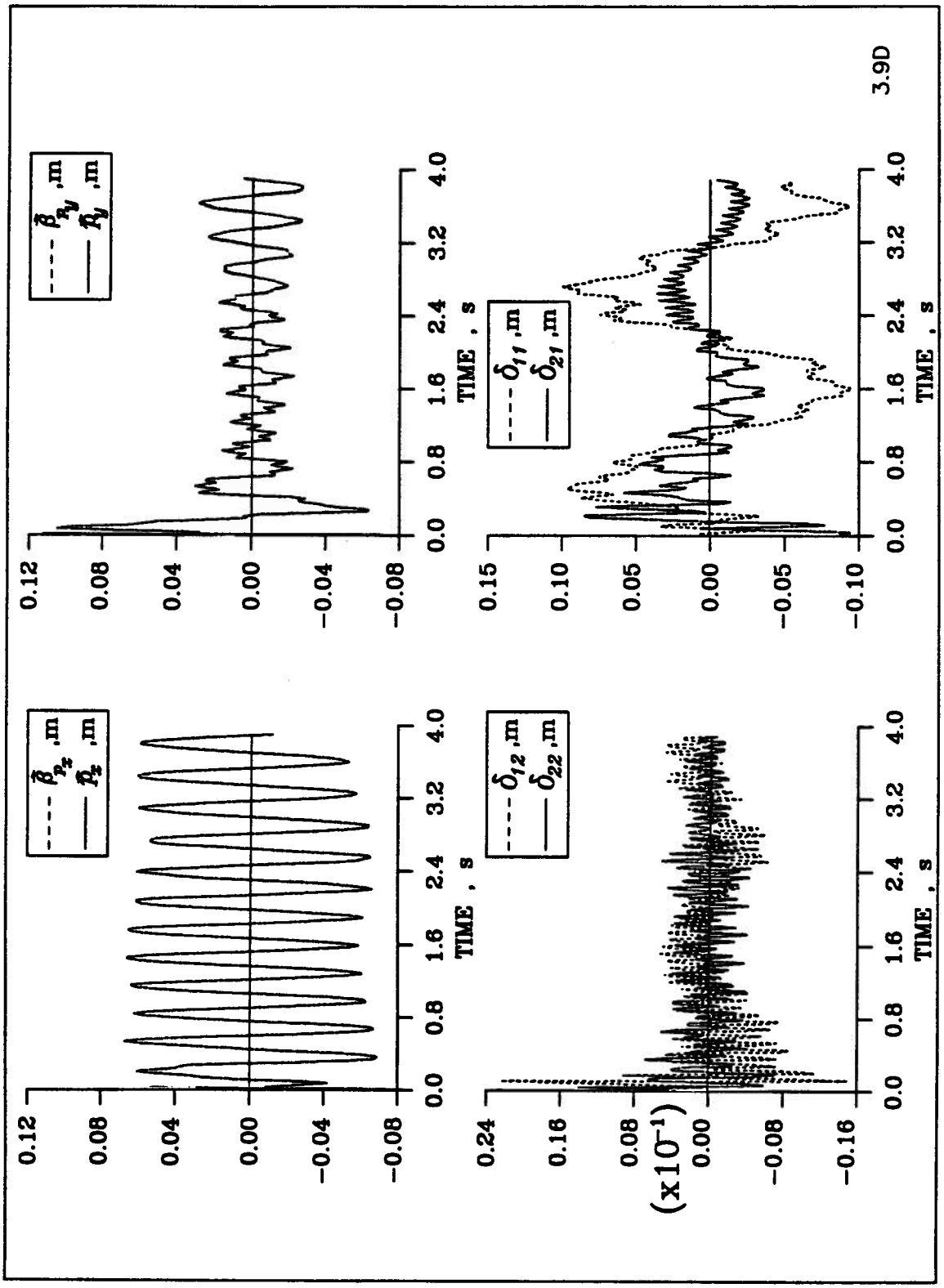

Figure 3.9: (D): Comparison between specified (β_{p_x} and β_{p_y}) and actual (p_x and p_y) position of the joint angles as well as the flexible generalized coordinated during a straightline tip maneuver from the inertial coordinate (6.9, 6.9, 0)m to (1, 1, 0)m in 4s.

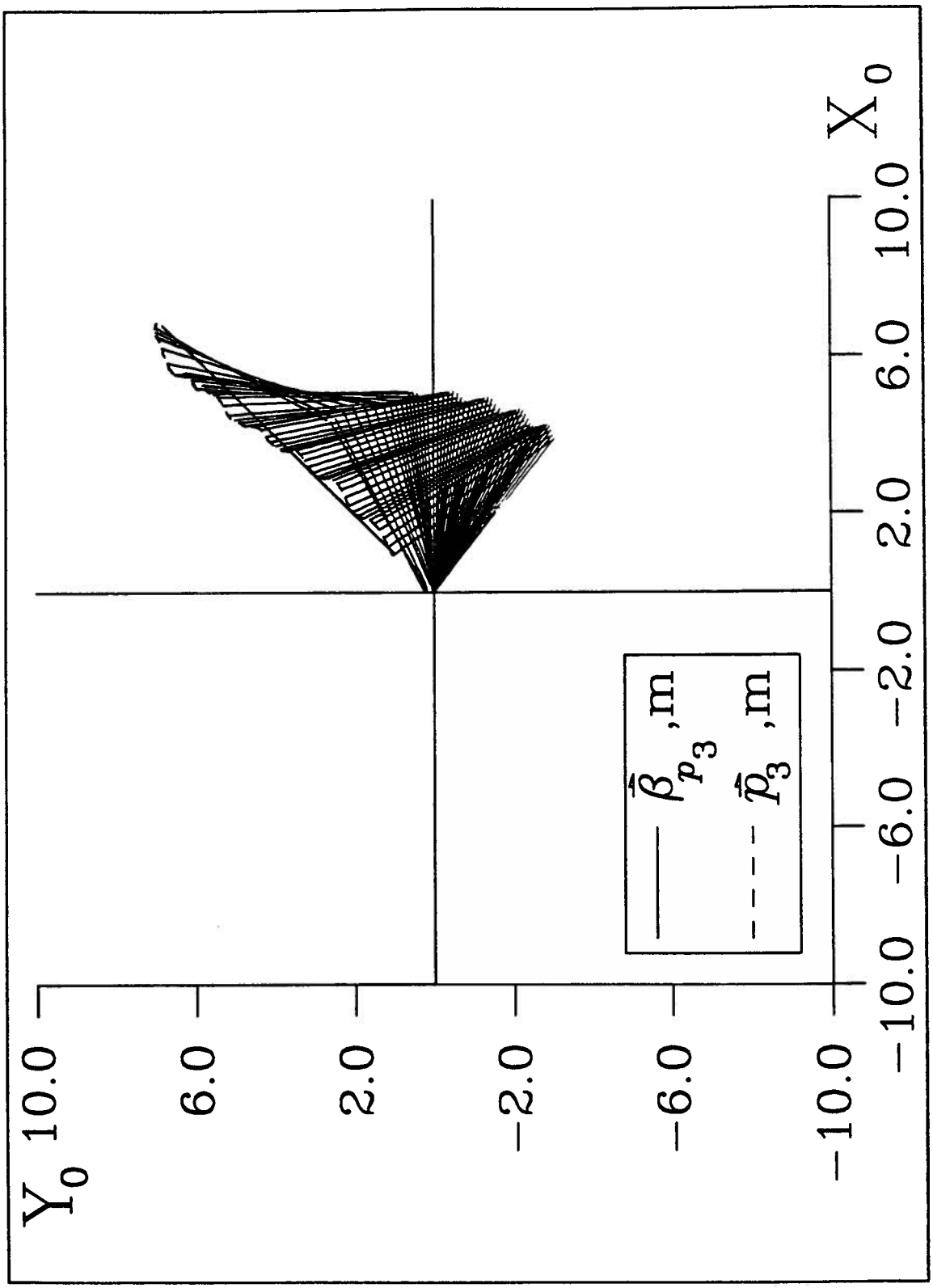

Figure 3.10: (A): Time strobe position plot of 2 link flexible manipulator with stationary base, using two modes for each link, during a straightline tip maneuver from the inertial coordinate (6.9, 6.9, 0)m to (1, 1, 0)m in 2s.

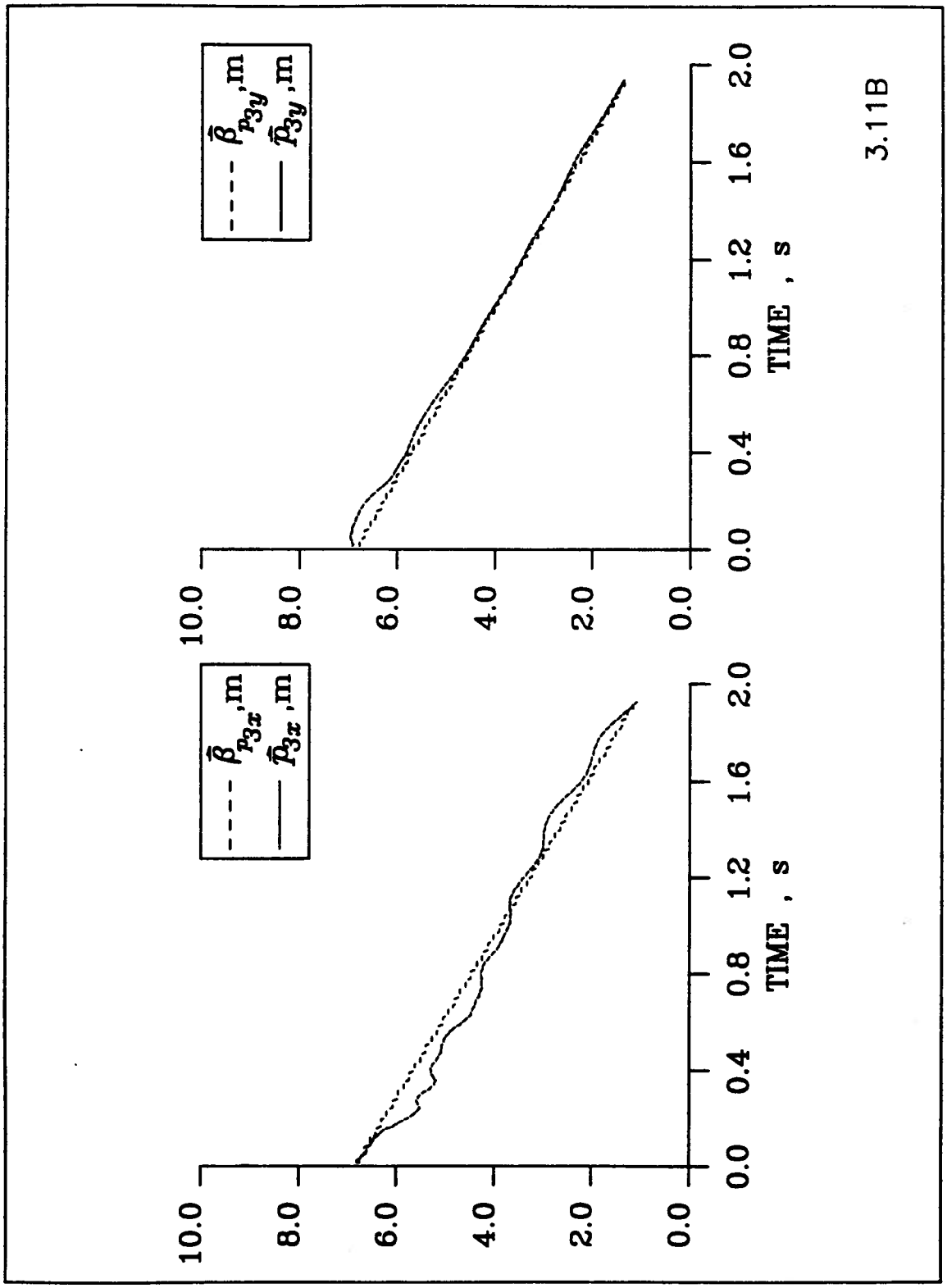

Figure 3.11: (B): Comparison between specified ($\beta_{p_{3x}}$ and $\beta_{p_{3y}}$) and actual (p_{3_x} and p_{3_y}) position of the manipulator tip during a straightline tip maneuver from the inertial coordinate (6.9, 6.9, 0)m to (1, 1, 0)m in 2s.

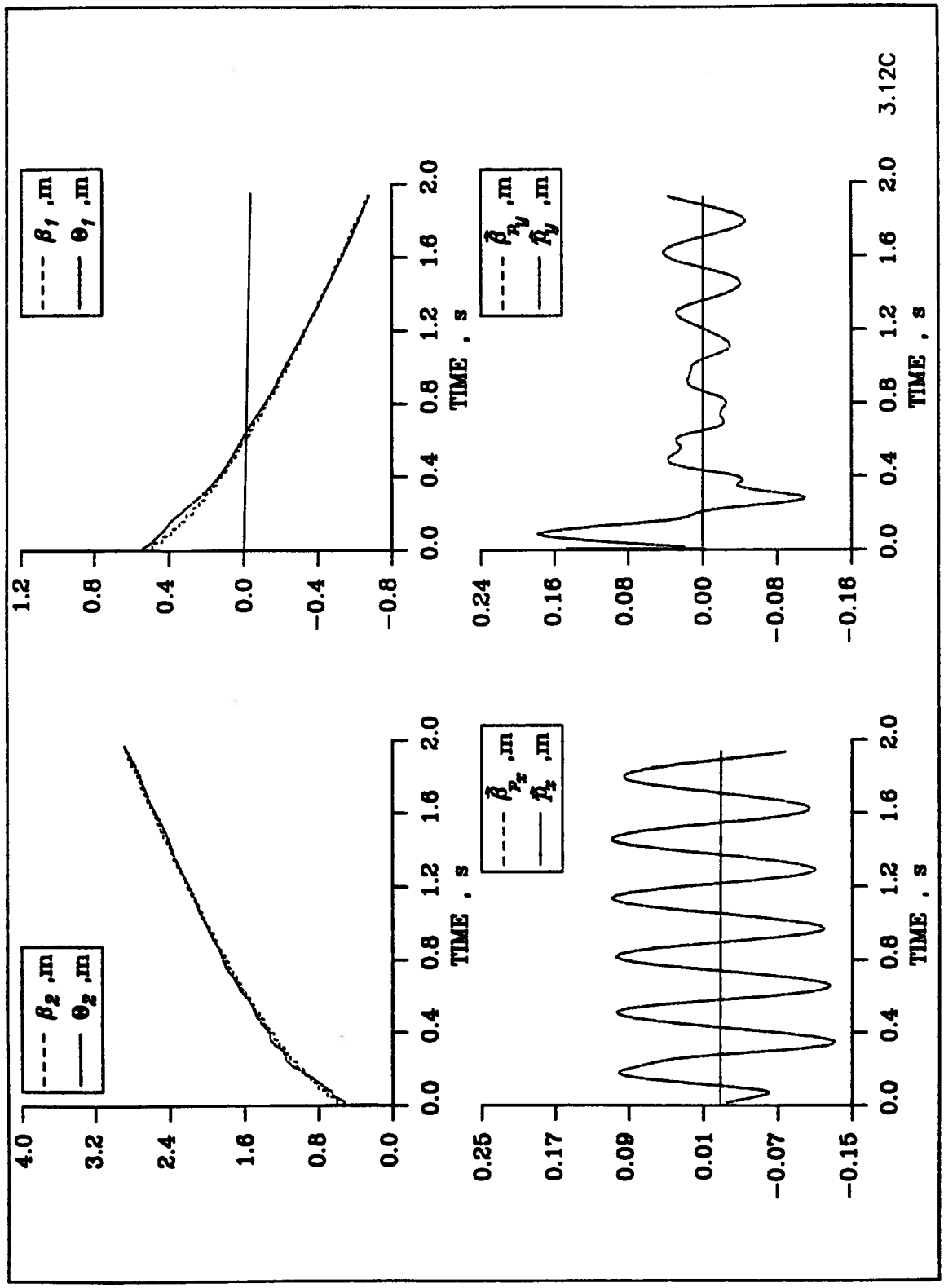

Figure 3.12: (C): Comparison between specified (β_1, β_2, β_{p_x}, and β_{p_y}) and actual (θ_1, θ_2, p_x and p_y) position of the base and joint angles during a straightline tip maneuver from the inertial coordinate (6.9, 6.9, 0)m to (1, 1, 0)m in 2s.

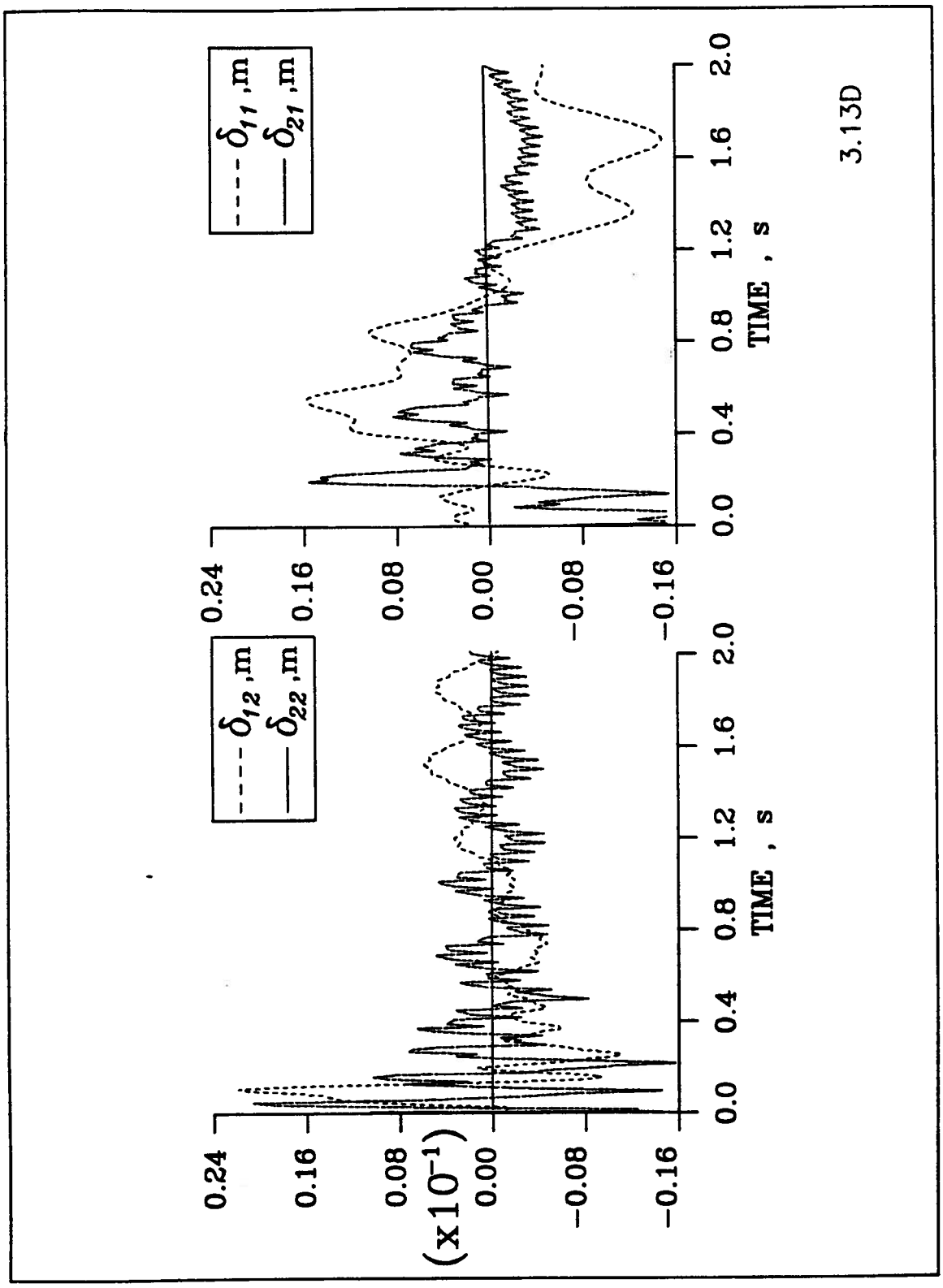

Figure 3.13: (D): Comparison between the flexible generalized coordinates δ_{ij} for each link during a straightline tip maneuver from the inertial coordinate (6.9, 6.9, 0)m to (1, 1, 0)m in 2s.

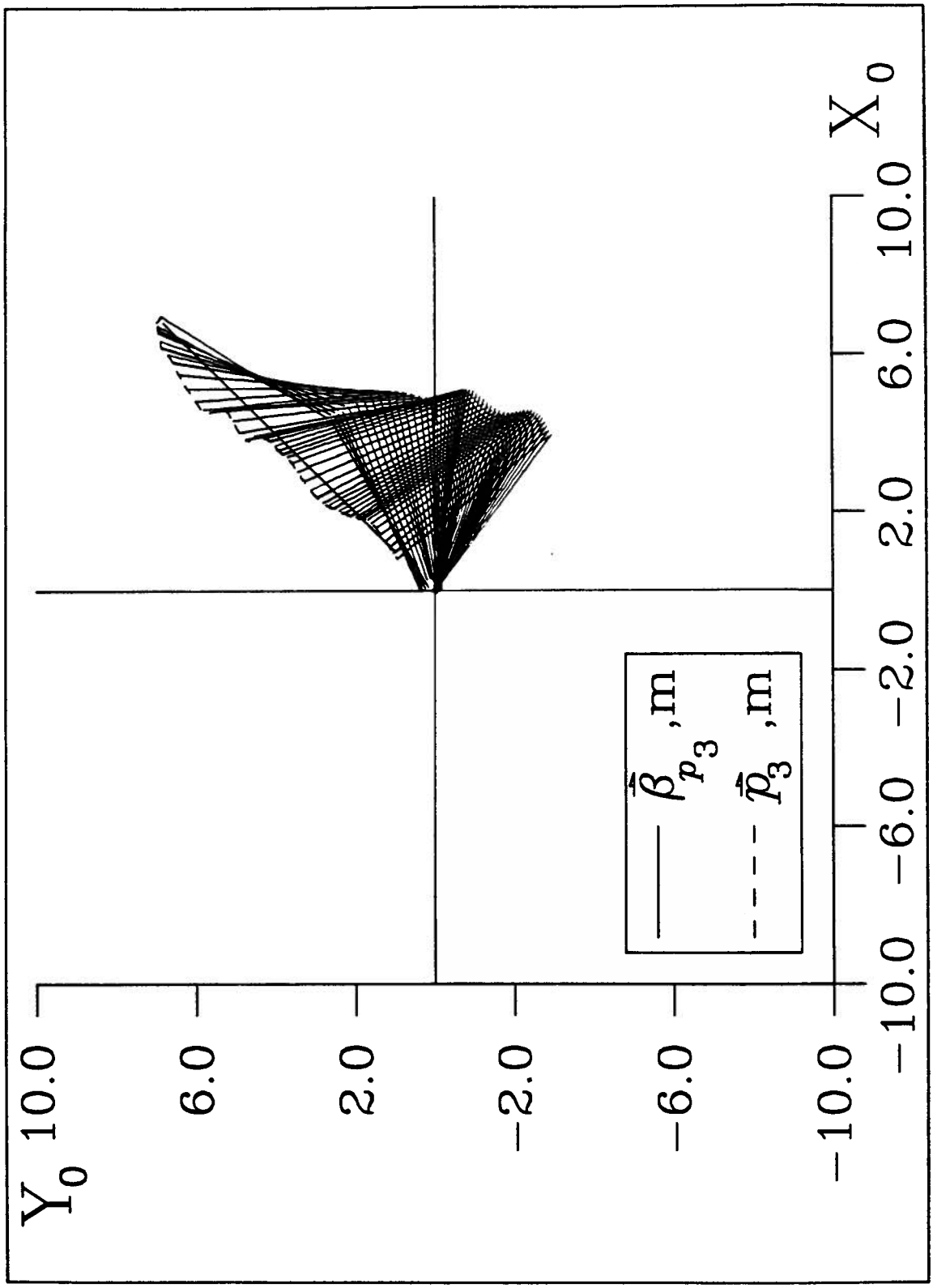

Figure 3.14: (A): Time strobe position plot of 2 link flexible manipulator with stationary base, using two modes for each link, during a straightline tip maneuver from the inertial coordinate (6.9, 6.9, 0)m to (1, 1, 0)m in 1s.

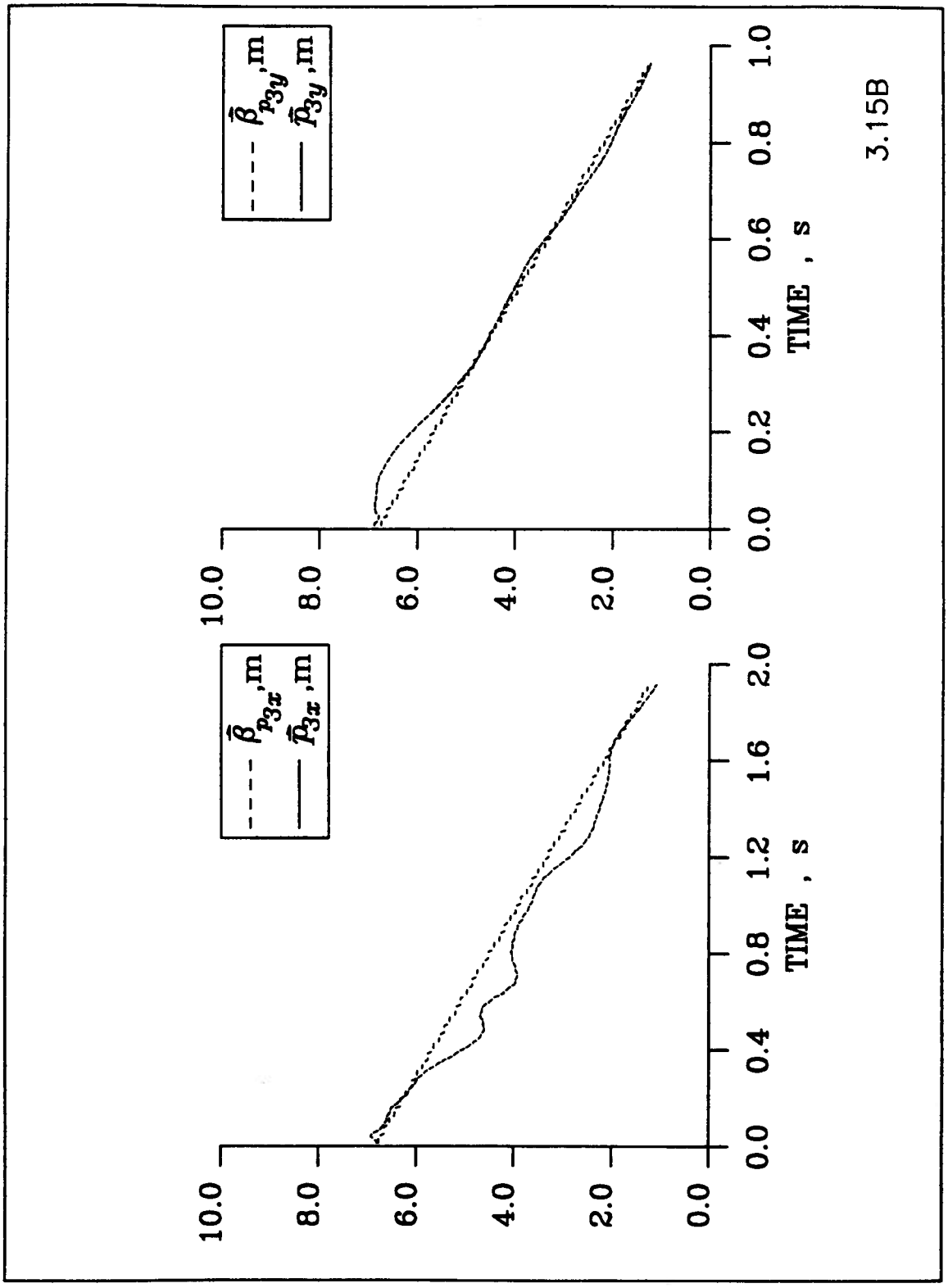

Figure 3.15: (B): Comparison between specified ($\beta_{p_{3x}}$ and $\beta_{p_{3y}}$) and actual (p_{3_x} and p_{3_y}) position of the manipulator tip during a straightline tip maneuver from the inertial coordinate (6.9, 6.9, 0)m to (1, 1, 0)m in 1s.

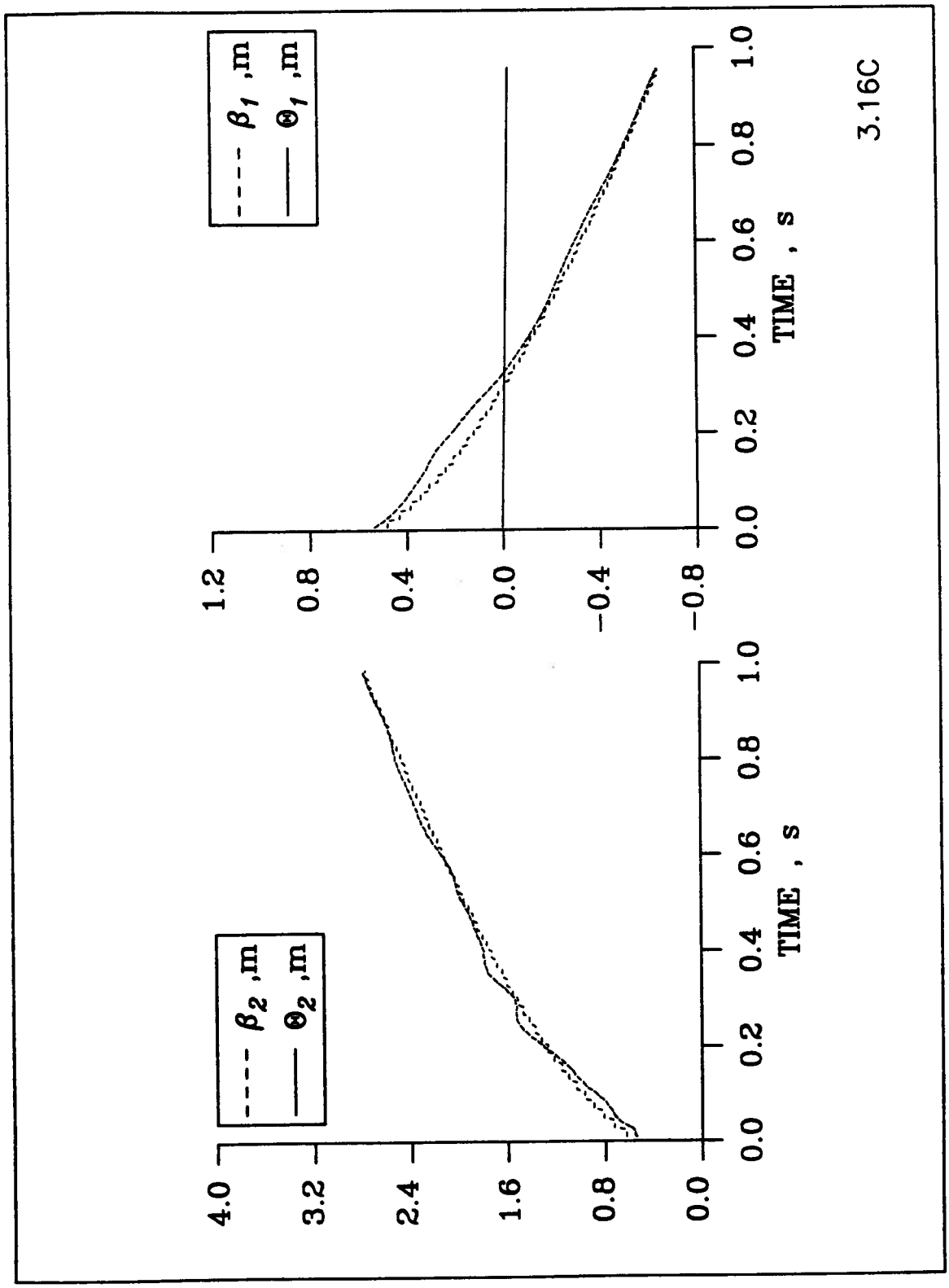

Figure 3.16: (C): Comparison between specified (β_1 and β_2) and actual (θ_1 and θ_2) position of the joint angles during a straightline tip maneuver from the inertial coordinate (6.9, 6.9, 0)m to (1, 1, 0)m in 1s.

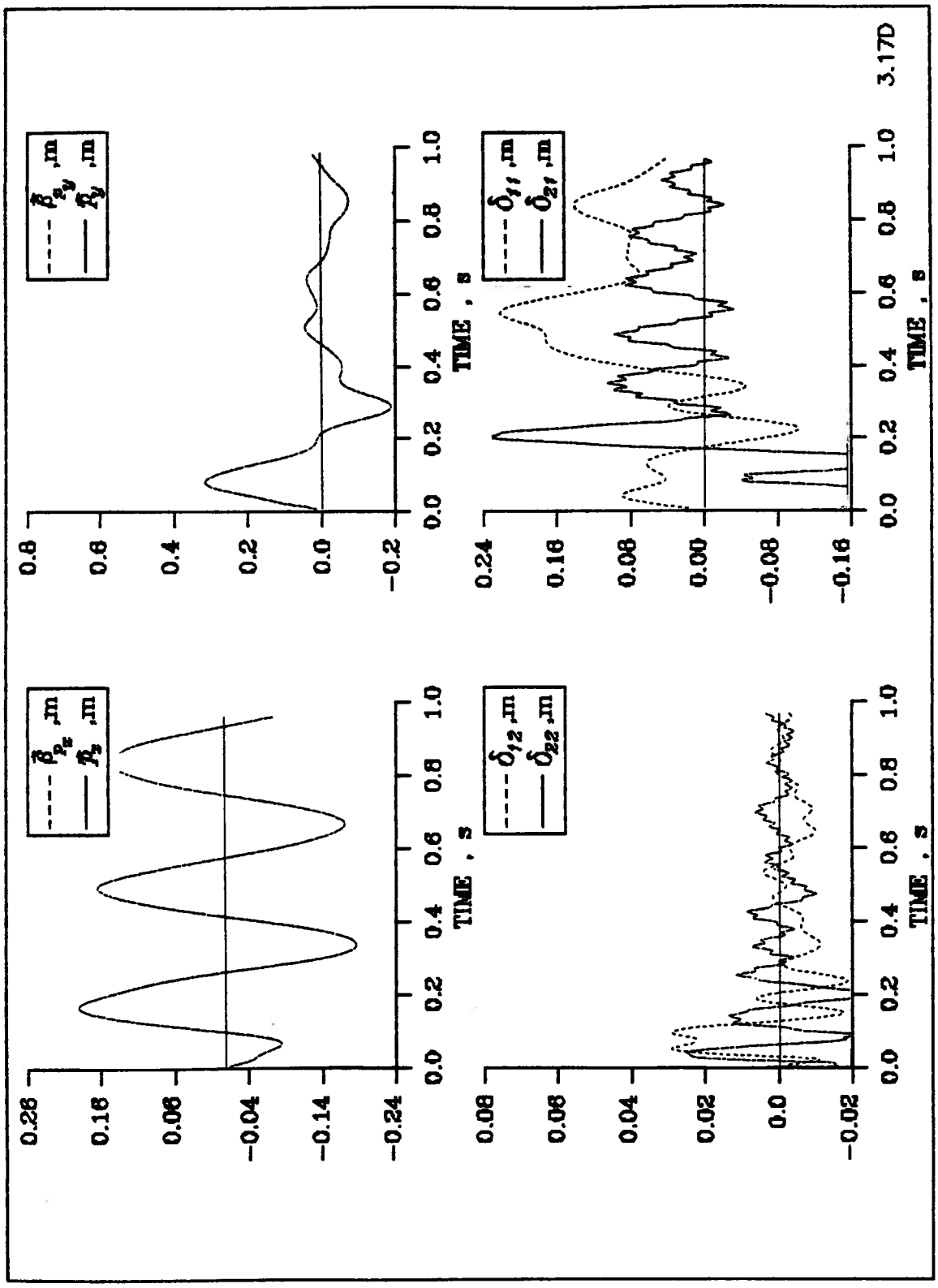

Figure 3.17: (D): Comparison between specified (β_{p_x} and β_{p_y}) and actual (p_x and p_y) position of the joint angles as well as the flexible generalized coordinated during a straightline tip maneuver from the inertial coordinate (6.9, 6.9, 0)m to (1, 1, 0)m in 1s.

Keeping all the parameters constant, the above simulations were repeated but with the direction of the translational maneuver reversed: the manipulator tip moving from $(1.0, 1.0)$ to $(6.9, 6.9)$m. The traverse time is 4 seconds. Note, the manipulator tip trajectory signature is quite different (Figures 3.18, 3.19, 3.20, and 3.21). The main feature appears to be the dominance of low frequency excursions which are further emphasized in Figures 3.23, 3.24, and 3.25 where the maneuver time is reduced to 2s. Again it is evident that a more sophisticated control strategy is required to achieve the desired performance.

Response results were also obtained by systematically varying the trajectory length, orientation, speed and direction. In general, they showed similar trends with the main conclusion as above. With an increasing speed of maneuvers, a sophisticated control procedure will be required to track the trajectory precisely.

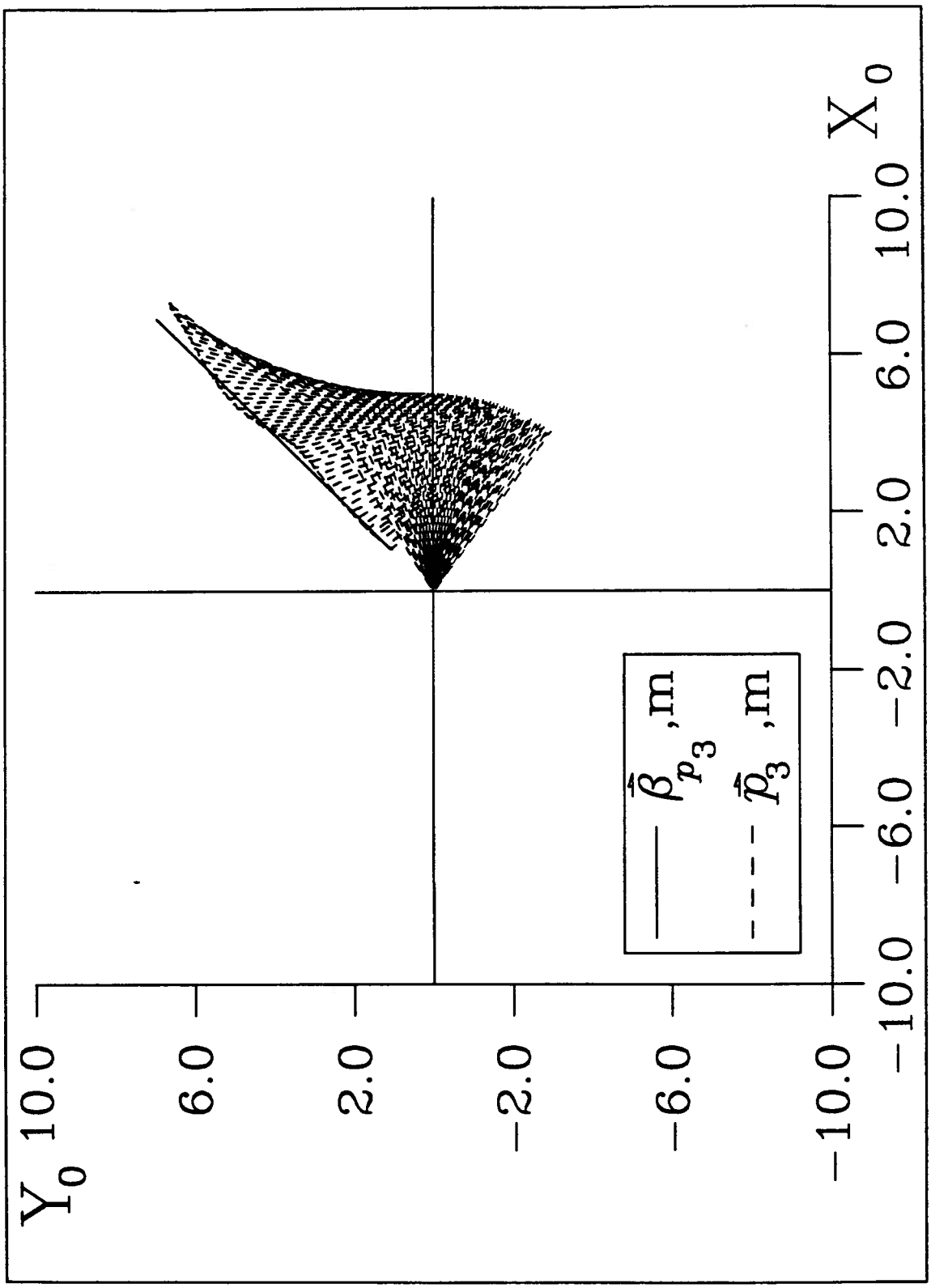

Figure 3.18: (A): Time strobe position plot of 2 link flexible manipulator with stationary base, using two modes for each link, during a straightline tip maneuver from the inertial coordinate (1, 1, 0)m to (6.9, 6.9, 0)m in 4s.

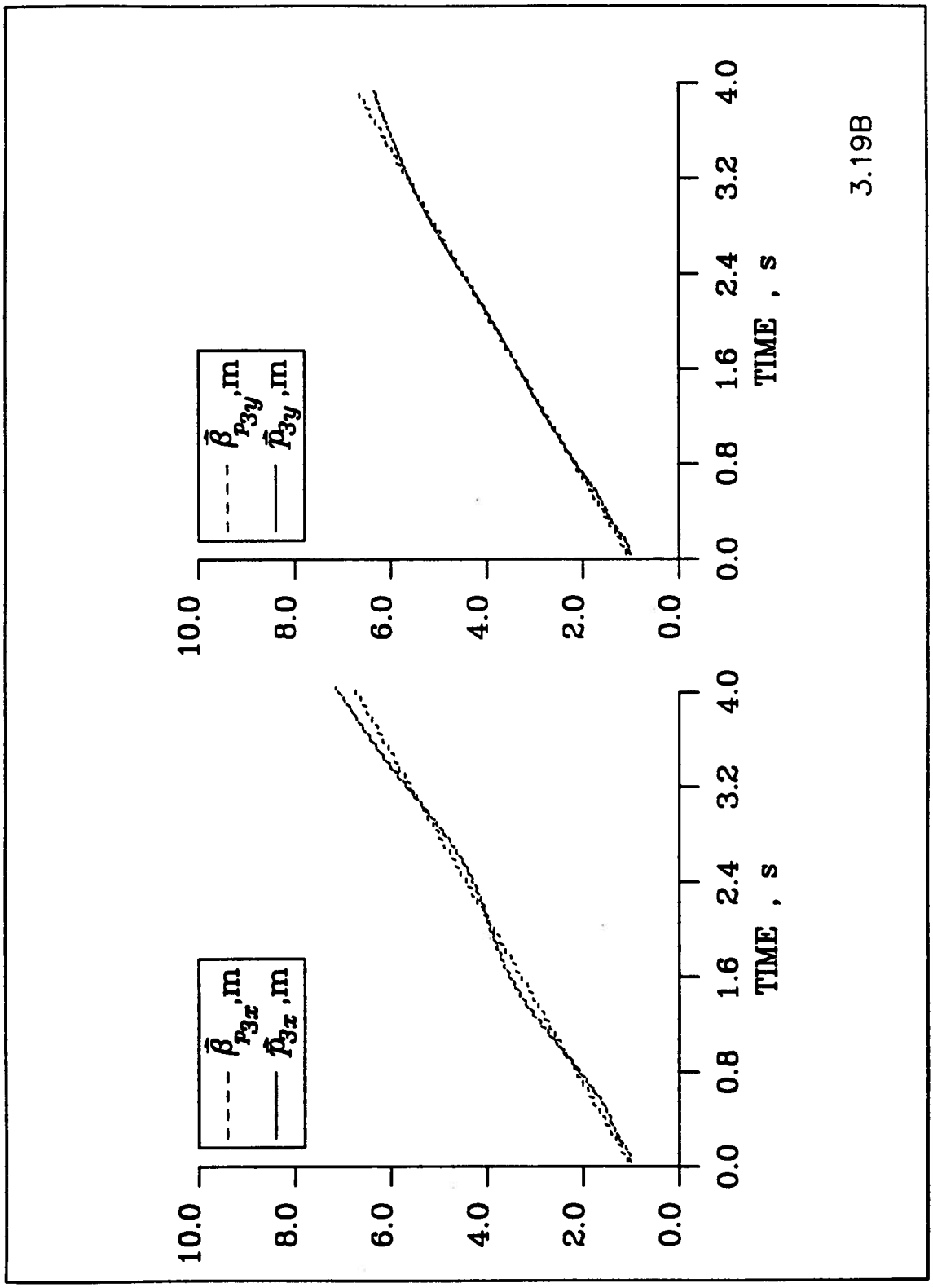

Figure 3.19: (B): Comparison between specified ($\beta_{p_{3x}}$ and $\beta_{p_{3y}}$) and actual (p_{3_x} and p_{3_y}) position of the manipulator tip during a straightline tip maneuver from the inertial coordinate (1, 1, 0)m to (6.9, 6.9, 0)m in 4s.

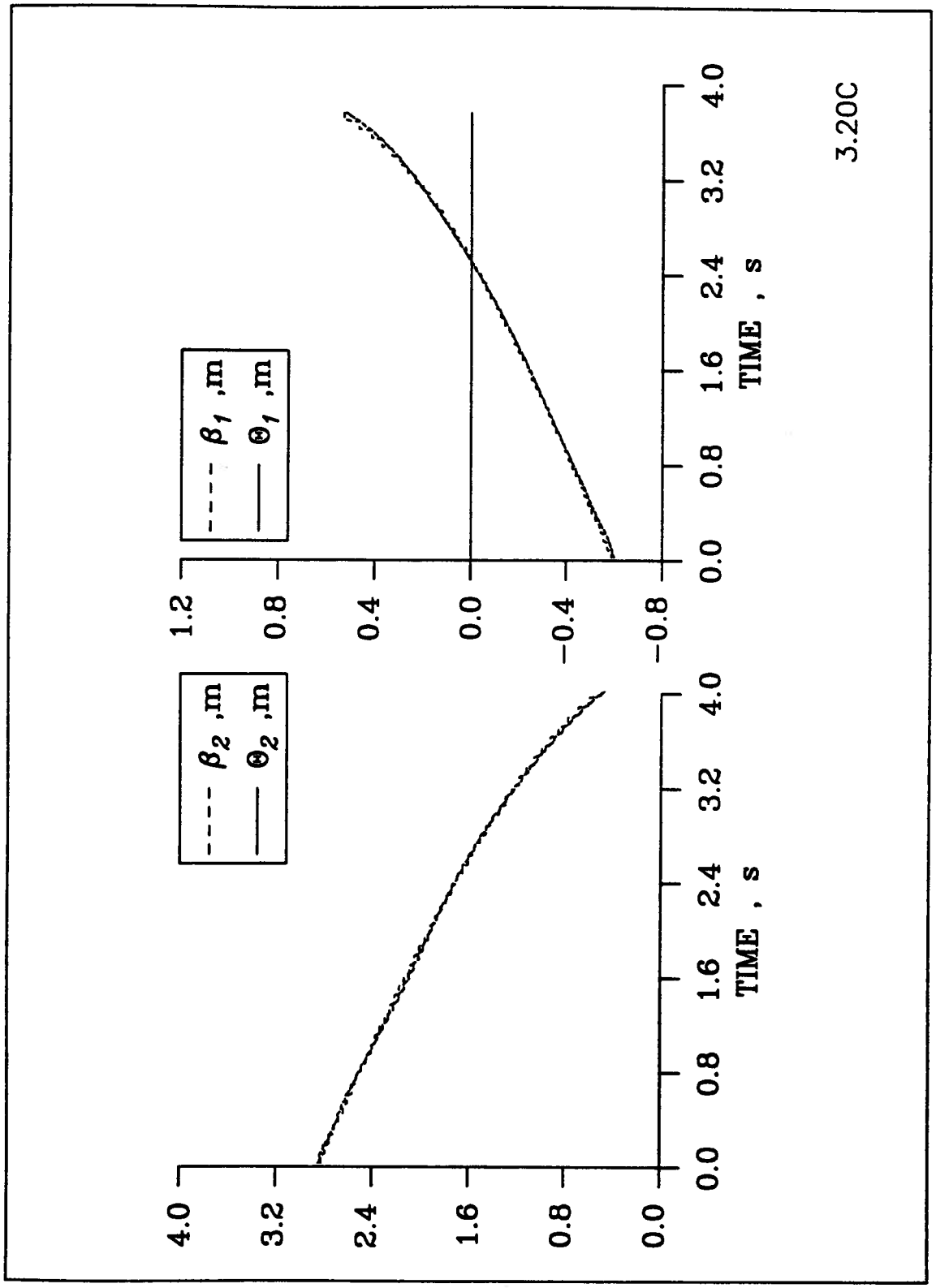

Figure 3.20: (C): Comparison between specified (β_1 and β_2) and actual (θ_1 and θ_2) position of the joint angles during a straightline tip maneuver from the inertial coordinate (1, 1, 0)m to (6.9, 6.9, 0)m in 4s.

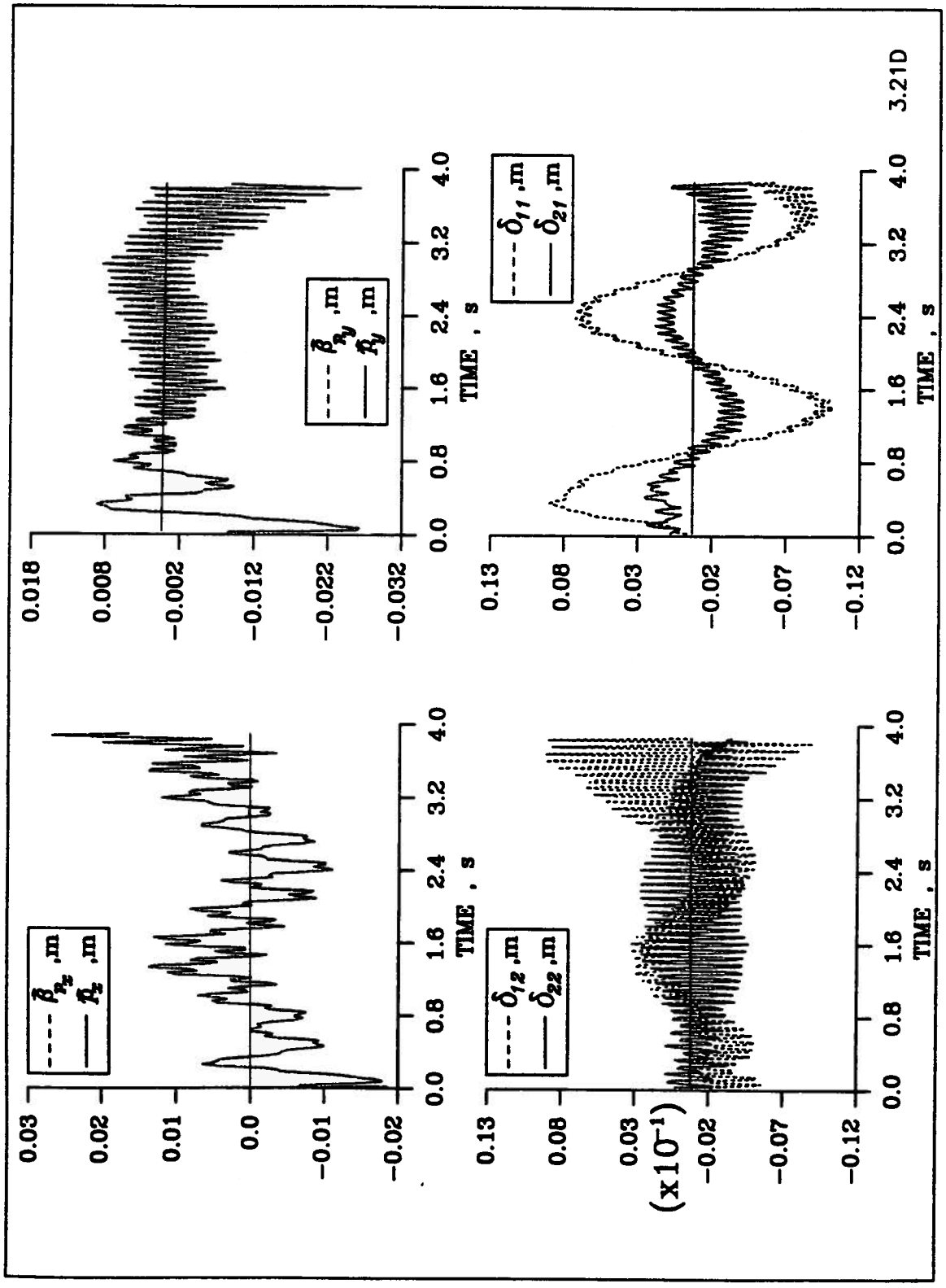

Figure 3.21: (D): Comparison between specified (β_{p_x} and β_{p_y}) and actual (p_x and p_y) position of the joint angles as well as the flexible generalized coordinated during a straightline tip maneuver from the inertial coordinate (1, 1, 0)m to (6.9, 6.9, 0)m in 4s.

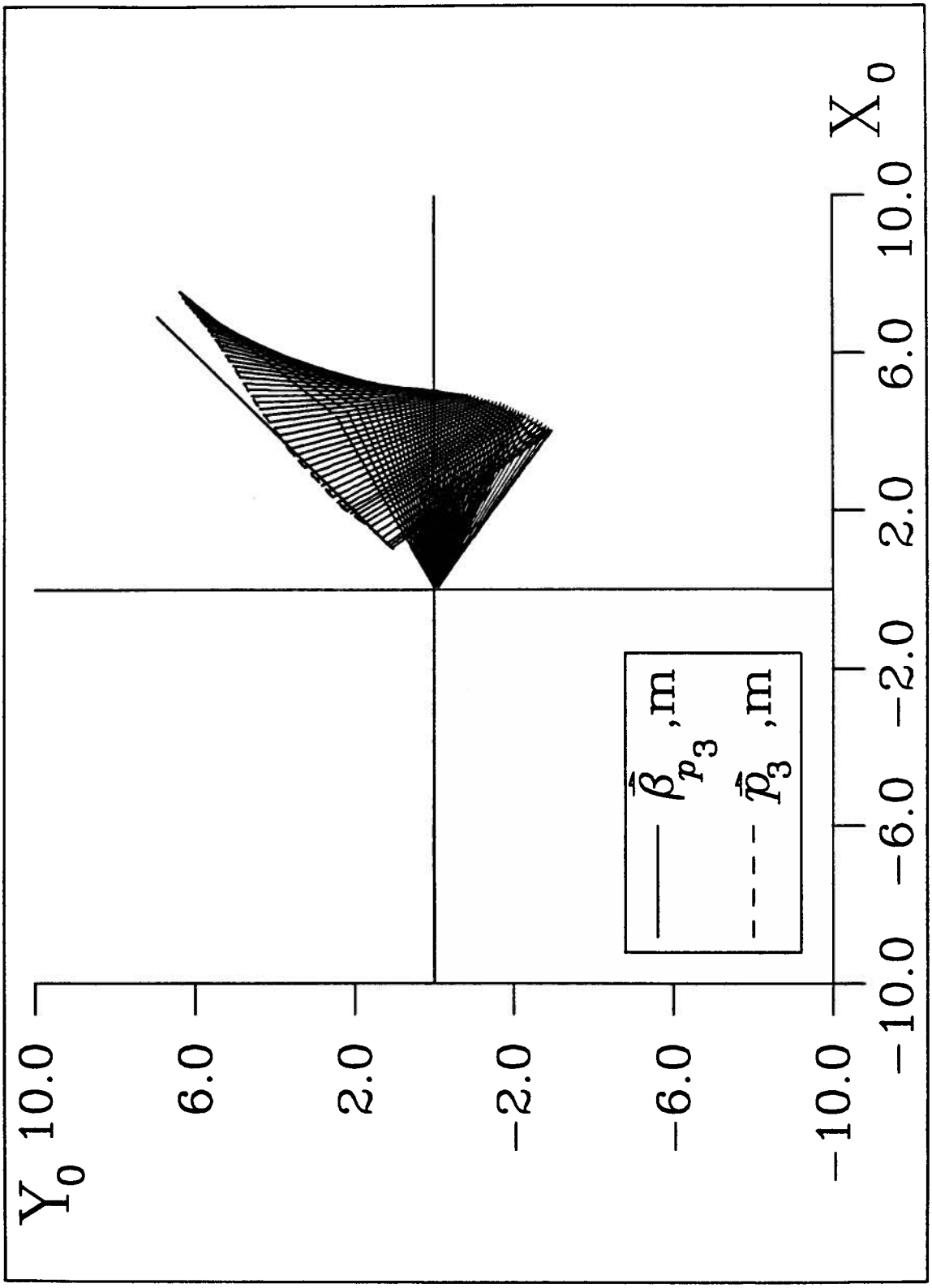

Figure 3.22: (A): Time strobe position plot of 2 link flexible manipulator with stationary base, using two modes for each link, during a straightline tip maneuver from the inertial coordinate (1, 1, 0)m to (6.9, 6.9, 0)m in 2s.

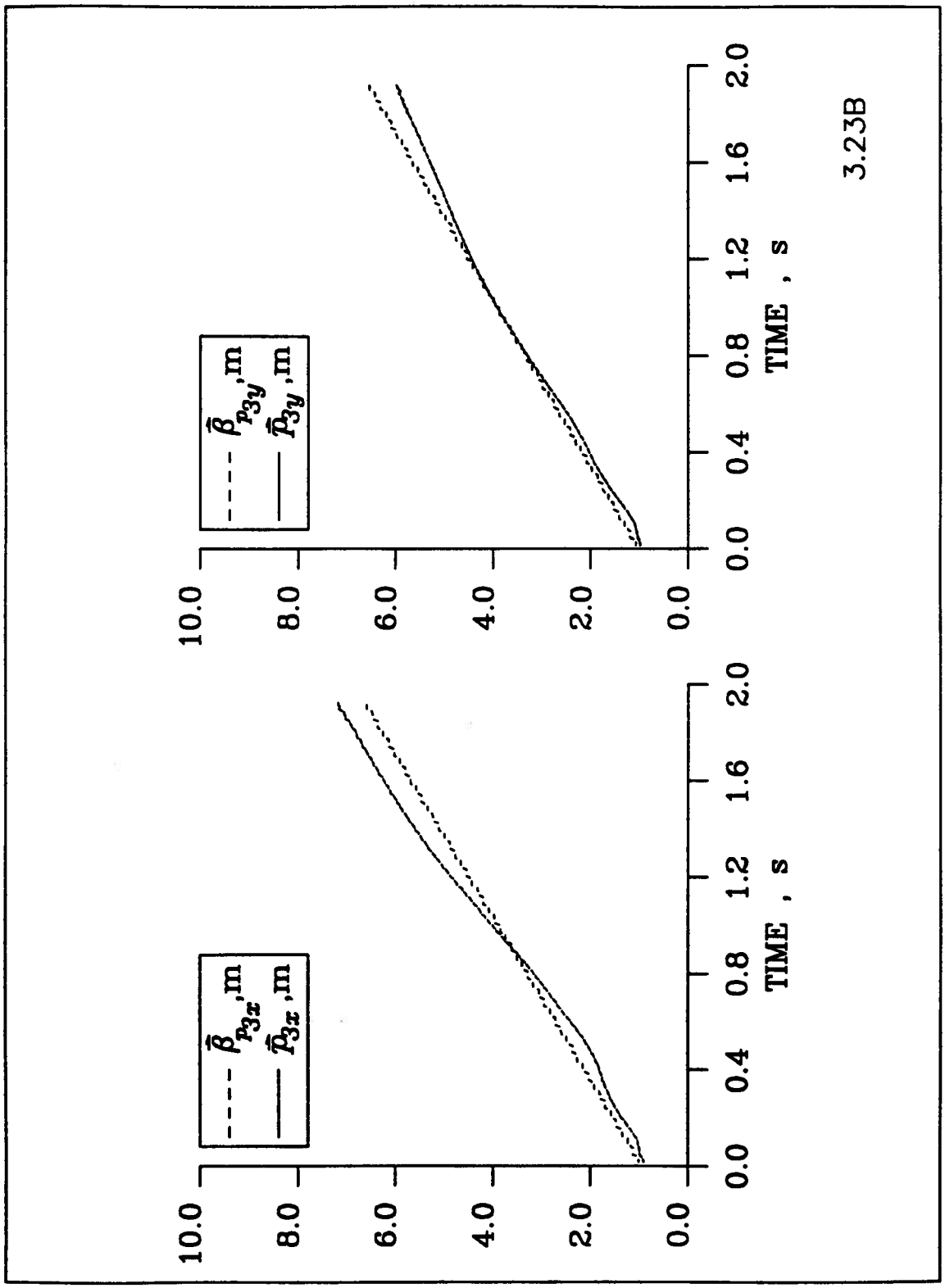

Figure 3.23: (B): Comparison between specified ($\beta_{p_{3x}}$ and $\beta_{p_{3y}}$) and actual (p_{3_x} and p_{3_y}) position of the manipulator tip during a straightline tip maneuver from the inertial coordinate (1, 1, 0)m to (6.9, 6.9, 0)m in 2s.

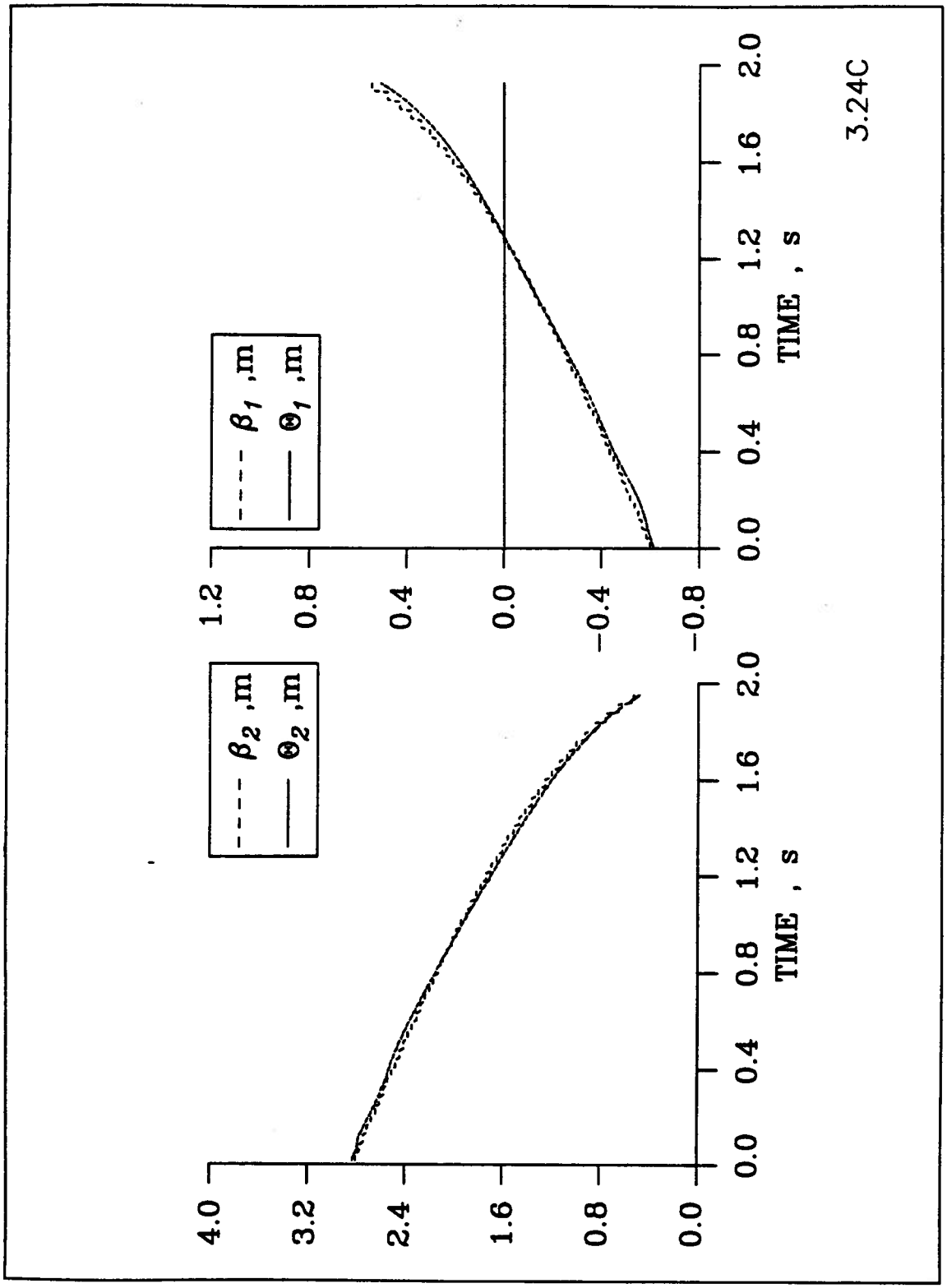

Figure 3.24: (C): Comparison between specified (β_1 and β_2) and actual (θ_1 and θ_2) position of the joint angles during a straightline tip maneuver from the inertial coordinate (1, 1, 0)m to (6.9, 6.9, 0)m in 2s.

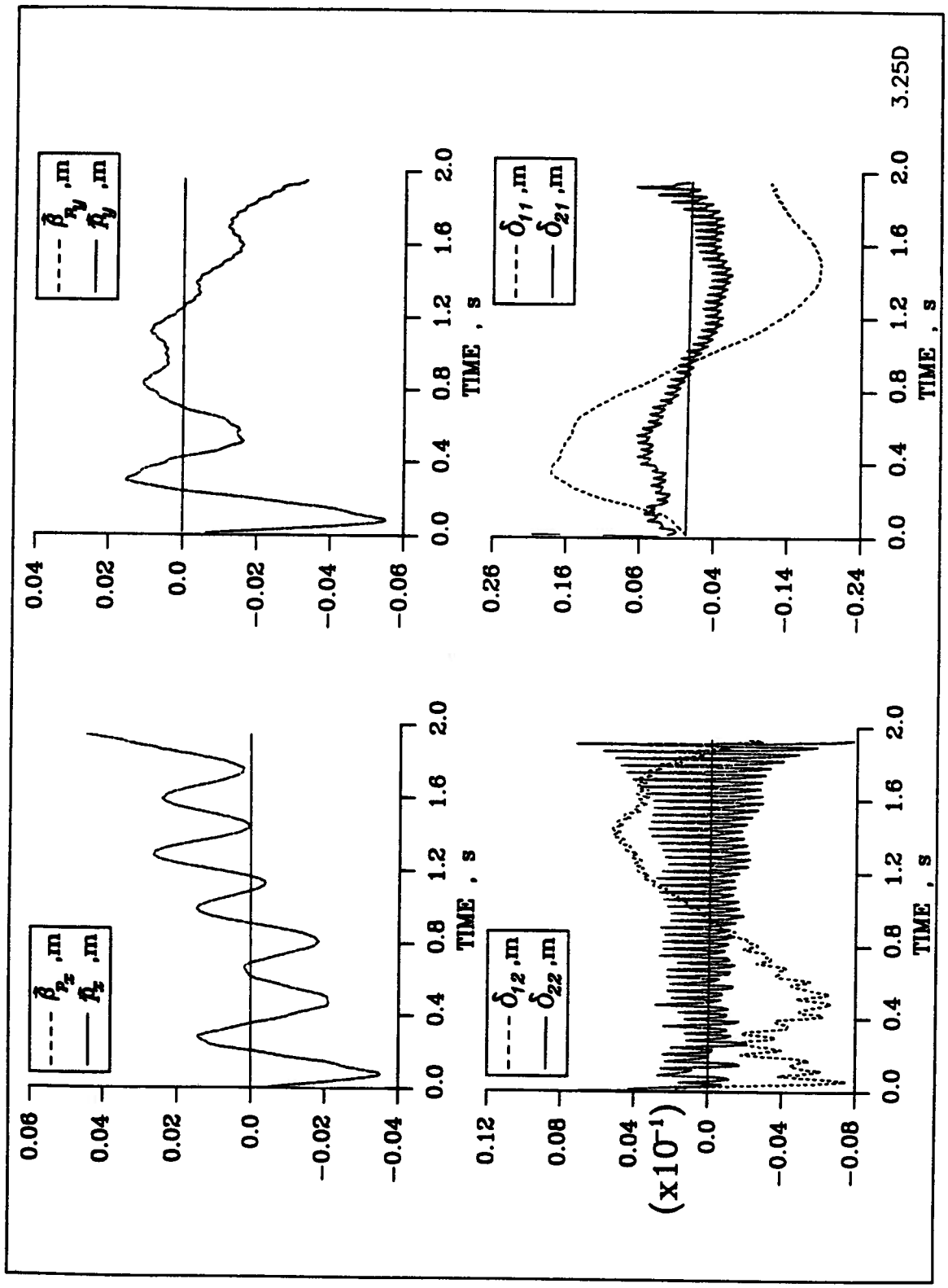

Figure 3.25: (D): Comparison between specified (β_{p_x} and β_{p_y}) and actual (p_x and p_y) position of the joint angles as well as the flexible generalized coordinated during a straightline tip maneuver from the inertial coordinate (1, 1, 0)m to (6.9, 6.9, 0)m in 2s.

Chapter 4

CONTROLLED DYNAMICAL RESPONSE

4.1 Preliminary Remarks

A relatively general formulation for studying the behaviour of a mobile two link manipulator was presented earlier in Chapter 2. Its dynamical response characteristics were studied during tracking of a straight line trajectory at predetermined speeds using the classical colocated proportional-derivative (PD) linear feedback technique applied to the rigid body generalized coordinates. The results suggested a need for a more effective control procedure that would account for the system nonlinearity and coupling better. The next logical step would be to implement a nonlinear control on the system.

One approach to the problem would be application of the sliding mode proceedure [23] . If the right hand side of a differential equation is discontinuous around a hypersurface and if the trajectory of the solution points toward the discontinuity, then it is reasonable that the trajectory eventually slides along the hypersurface. Control laws can be derived that will force the manipulator to follow a specified trajectory defined by these surfaces. This is accomplished by an optimal choice of sliding surfaces. A major problem with this approach pertains to unmodelled dynamics which usually results in high frequency oscillations of the manipulator as it slides along the surface. This is a direct consequence of the switching nature of the controller. Furthermore, the manipulator joints are subjected to high reversing torque impulses which are required for this method to work properly. This is not always practical with many electro-mechanical actuators. Some researchers have improved the controller performance using a filtering process with a high bandwidth for the sliding variable [24] [25]. In an alternate approach, the sliding mode approach is incorporated into an adaptive PD feedback controller

leading to the zero velocity error. The sliding mode controller elliminates the nonzero position errors.

Of course, as is often done, one may proceed to linearize the governing equations.This is accomplished by considering an incremental deviation of the state vector from its operating point at each sampled instant of time. The equations of motion are modified to reflect this change. Re-arranging, one has two sets of equations:

- The first group resembles the original set of non-linear equations describing the large motion of the manipulator.
- The second group of equations describe the incremental deviation of the state vector from the large motion at each sampled point in time.

From the second group we get a linearized model by neglecting the second and higher degree terms of the delta state vector. This can be rearranged to form a set of state equations thereby obtaining the linearized system state matrix about a given operating point [39], [40]. However, for flexible manipulators, control strategy based on linearized system models has often proved to be inadequate. Actual dynamics of the robot arms often deviated significantly from that predicted by a linearized approach.

A solution, proposed by Freund [27], uses the state feedback to decouple the nonlinear system in such a way as to make arbitrary pole placement possible. However, this method is difficult to apply to systems with more than three degrees of freedom. In a subsequent modification, by first simplifying the equations of motion and then strategically partitioning them, Freund [28] showed that the method could be extended to systems with more than three degrees of freedom.

A promising technique that may provide adequate control for both rigid as well as flexible manipulators is a form of inverse method based on the Feedback Linearizations Technique (FLT). It was first investigated by Beijczy [30]. Singh and Schy [31] as well as Spong and Vidyasagar [32] [33] used the FLT to formulate robust control proceedures for rigid manipulators. The method was later applied to the control of robots with flexible joints by Spong [29].

Modi and Karray [34] [35] extended the FLT to include structural flexibility and applied it to the proposed space station based mobile manipulator modeled by Chan [5].

The FLT is sometimes referred to as the computed torque technique, which in effect is a special case of the FLT. This is because the technique feeds back the rigid body state vector to calculate the foreward rigid body dynamics of the system and uses the resultant generalized forces to drive the manipulator according to the required trajectory. The effect of this is to linearize the system such that only a linear compensator is required to obtain the required system output. There are certain advantages to this approach: the control algorithm is quite simple and the linear compensator is easy to implement. The proceedure is schematically described through a block diagram in Figure 4.26.

As can be expected, the method has some limitations just as other control proceedures. It relies on the accurate knowledge of the system model and structural parameters for robustness in the rigid degrees of freedom. Furthermore, another disadvantage is, knowledge of the flexible generalized coordinates is necessary for determination of the control torques and forces. In practice, the problem can be readily overcome by introducing strain gauges to gain information concerning the first few modes.

4.2 Feedback Linearization

The Feedback Linearization Technique (FLT), as applied to a nonlinear rigid body system, is reviewed here. Consider a system governed by

$$\mathbf{D}\left(\vec{q}_r, t\right)\ddot{\vec{q}}_r + \vec{F}\left(\dot{\vec{q}}_r, \vec{q}_r, t\right) = \vec{Q}\left(\dot{\vec{q}}_r, \vec{q}_r, t\right), \tag{4.1}$$

where $\vec{q}_r$ represents the generalized coordinate vector for the rigid system and $\vec{Q}\left(\dot{\vec{q}}_r, \vec{q}_r, t\right)$ is the nonlinear generalized force/torque control vector. Taking the control torque time history as:

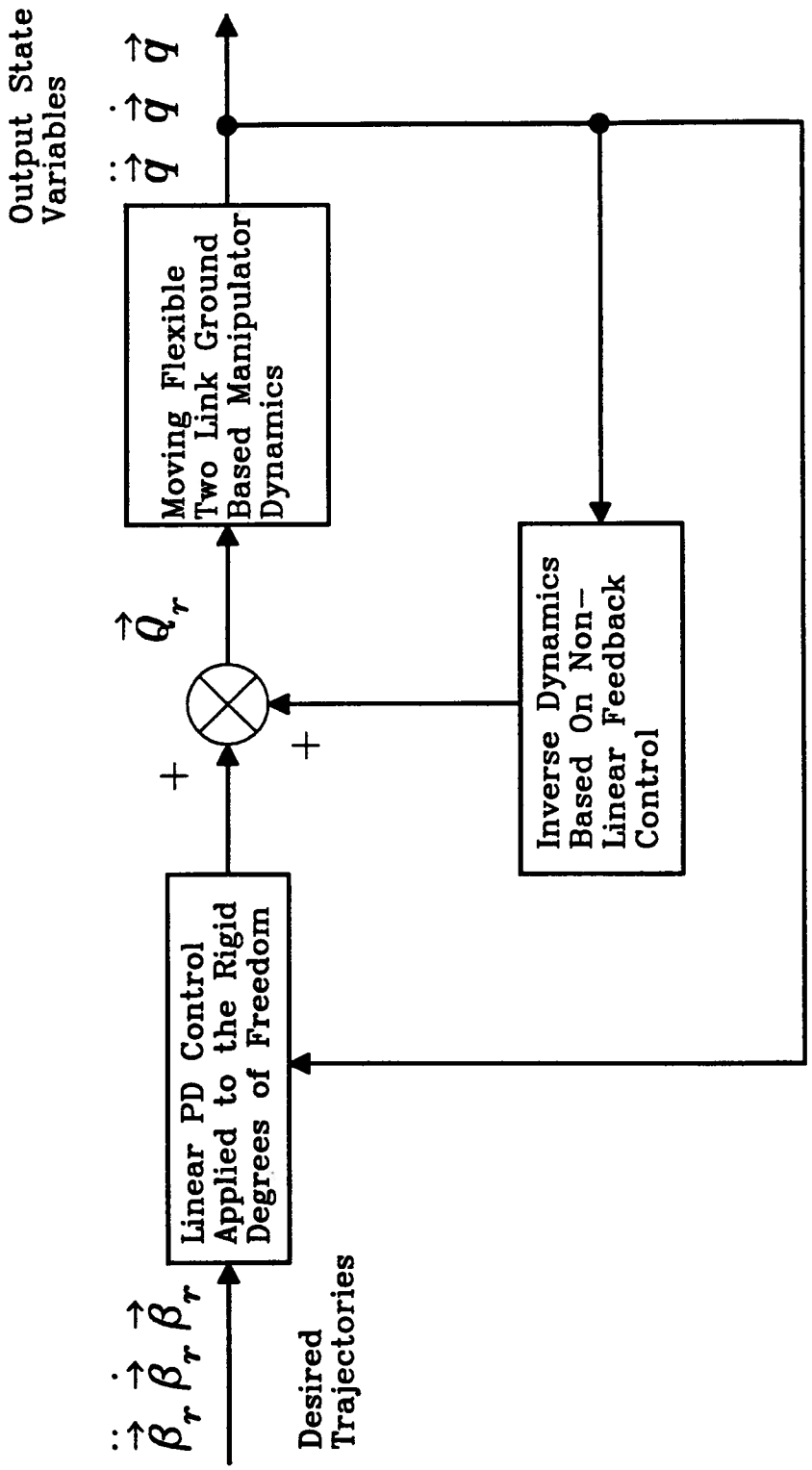

Figure 4.26: A block diagram explaining control through the Feedback Linearization Technique as applied to the mobile, flexible, twolink, ground based manipulator.

$$\vec{Q}\left(\dot{\vec{q}}_r, \vec{q}_r, t\right) = \mathbf{D}(\vec{q}_r, t)\,\vec{\mathbf{v}} + \vec{\mathbf{F}}\left(\dot{\vec{q}}_r, \vec{q}_r, t\right) ; \tag{4.2}$$

$$\vec{\mathbf{v}} = \ddot{\vec{\beta}}_r + \mathbf{K}_v\left(\dot{\vec{\beta}}_r - \dot{\vec{q}}_r\right) + \mathbf{K}_p\left(\vec{\beta}_r - \vec{q}_r\right) ; \tag{4.3}$$

where $\ddot{\vec{\beta}}_r$, $\dot{\vec{\beta}}_r$, and $\vec{\beta}_r$ denote the trajectory related desired acceleration, velocity and displacement, respectively, leads to the linear closed loop control equation as

$$\ddot{\vec{q}}_r = \vec{\mathbf{v}} = \ddot{\vec{\beta}}_r + \mathbf{K}_v\left(\dot{\vec{\beta}}_r - \dot{\vec{q}}_r\right) + \mathbf{K}_p\left(\vec{\beta}_r - \vec{q}_r\right) . \tag{4.4}$$

This can be rewritten as

$$\ddot{\vec{e}} + \mathbf{K}_v\dot{\vec{e}} + \mathbf{K}_p\vec{e} = 0, \tag{4.5}$$

where $\ddot{\vec{e}} = \ddot{\vec{\beta}}_r - \ddot{\vec{q}}_r$, $\dot{\vec{e}} = \dot{\vec{\beta}}_r - \dot{\vec{q}}_r$, and $\vec{e} = \vec{\beta}_r - \vec{q}_r$ are the acceleration, velocity, and displacement errors, respectively. Note, the error is driven towards zero in an asymptotic manner given the correct choices for the position and velocity gain matrices.

If we choose to decouple the system such that each individual degree of freedom can be tuned separately then a suitable choice would a diagonal matrix. The feedback gain matrix $\mathbf{K}_p$ will have diagonal elements equal to ω_j^2. This is directly proportional to the speed of response and will thus determine the response time of the generalized coordinate q_j. Similarly, the feedback gain matrix $\mathbf{K}_v$ may have diagonal elements equal to $2\omega_j$, which will make the jth generalized coordinate response critically damped. In general, therefore, the larger the value of ω_j the more robust will be the response.

4.3 Control Implementation

Implementation of the FLT begins with the appropriately partitioned system mass matrix **D**. The equations of motion are arranged into the groups of rigid and flexible degrees of freedom,

the former related to p_x, p_y, θ_1, θ_2 generalized coordinates while the latter to the flexible coordinates $\delta_{ij}(x_i, t)$. Rearranging these into a matrix format gives

$$\begin{bmatrix} \mathbf{D_{rr}} & \vdots & \mathbf{D_{ff}} \\ \cdots & \cdots & \cdots \\ \mathbf{D_{fr}} & \vdots & \mathbf{D_{ff}} \end{bmatrix} \begin{bmatrix} \ddot{\vec{q}}_r \\ \cdots \\ \ddot{\vec{q}}_f \end{bmatrix} + \begin{bmatrix} \vec{F}_r \\ \cdots \\ \vec{F}_f \end{bmatrix} = \begin{bmatrix} \vec{Q}_r \\ \cdots \\ \vec{Q}_f \end{bmatrix} , \tag{4.6}$$

where: $Drr(\vec{q}_r)$ is the 4 x 4 system mass submatrix representing base translational and joint rotational degrees of freedom; $\mathbf{D_{rf}}(\vec{\mathrm{q}}_\mathrm{r}, \vec{\mathrm{q}}_\mathrm{f})$ is a 4 x 2m submatrix that represents the coupling between the rigid and the flexible generalized coordinates; $\mathbf{D_{fr}} = \mathbf{D_{rf}^T}$ is a 2m x 4 submatrix; and $\mathbf{D_{ff}}(\vec{\mathrm{q}}_\mathrm{f})$ is a 2m x 2m submatrix that represents only the flexible degrees of freedom. Here m is the number of modes used to represent the link deflections. $\vec{F}_r\left(\dot{\vec{q}}_r, \dot{\vec{q}}_f, \vec{q}_r, \vec{q}_f\right)$ and $\vec{F}_f\left(\dot{\vec{q}}_r, \dot{\vec{q}}_f, \vec{q}_r, \vec{q}_f\right)$ are 4 x 1 and 2m x 1 vectors representing the remaining coupled nonlinear forcing terms. $\vec{Q}_r$ and $\vec{Q}_f$ are the control forces supplied by the actuators. In general it would be impractical to control the modal degrees of freedom associated with the manipulator links. In that case $\vec{Q}_f$ is set to zero. Thus $\vec{Q}_r$ is required to control the rigid degrees of freedom directly and the flexible degrees of freedom indirectly.

To design the controller, the next step is to rewrite the submatrices in equation (4.6) in such a way as to determine $\vec{Q}_r$ and to linearize the closed-loop system. This can be accomplished quite readily as follows. Putting $\vec{Q}_f = 0$, equation (4.6) becomes:

$$\mathbf{D_{rr}}\ddot{\vec{\mathrm{q}}}_\mathrm{r} + \mathbf{D_{rf}}\ddot{\vec{\mathrm{q}}}_\mathrm{f} + \vec{\mathrm{F}}_\mathrm{r} = \vec{Q}_r \; ; \tag{4.7}$$

$$\mathbf{D_{fr}}\ddot{\vec{\mathrm{q}}}_\mathrm{r} + \mathbf{D_{ff}}\ddot{\vec{\mathrm{q}}}_\mathrm{f} + \vec{\mathrm{F}}_\mathrm{f} = \vec{Q}_f = 0 \; . \tag{4.8}$$

From Eq. (4.8),

$$\ddot{\vec{q}}_f = -\mathbf{D_{ff}^{-1}}\mathbf{D_{fr}}\ddot{\vec{\mathrm{q}}}_\mathrm{r} - \mathbf{D_{ff}^{-1}}\vec{\mathrm{F}}_\mathrm{f} \; . \tag{4.9}$$

Substituting from Eq. (4.9) into Eq. (4.7) gives

$$\mathbf{D}_{rr}\ddot{\vec{q}}_r + \mathbf{D}_{rf}\left(-\mathbf{D}_{ff}^{-1}\mathbf{D}_{fr}\ddot{\vec{q}}_r - \mathbf{D}_{ff}^{-1}\vec{\mathrm{F}}_f\right) + \vec{\mathrm{F}}_r = \vec{\mathrm{Q}}_r \ ,$$

$$\left(\mathbf{D}_{rr} - \mathbf{D}_{rf}\mathbf{D}_{ff}^{-1}\mathbf{D}_{fr}\right)\ddot{\vec{q}}_r + \left(\vec{F}_r - \mathbf{D}_{rf}\mathbf{D}_{ff}^{-1}\vec{\mathrm{F}}_f\right) = \vec{Q}_r \ . \tag{4.10}$$

Putting:

$$\tilde{\mathbf{D}} = \mathbf{D}_{rr} - \mathbf{D}_{rf}\mathbf{D}_{ff}^{-1}\mathbf{D}_{fr} \ ; \tag{4.11}$$

$$\tilde{\vec{\mathrm{F}}} = \vec{F}_r - \mathbf{D}_{rf}\mathbf{D}_{ff}^{-1}\vec{\mathrm{F}}_f \ ; \tag{4.12}$$

gives

$$\tilde{\mathbf{D}}\ \ddot{\vec{q}}_r + \tilde{\vec{\mathrm{F}}} = \vec{Q}_r \ . \tag{4.13}$$

This represents the rigid body generalized force vector similar to the original differential equations of motion and is a function of all the generalized coordinates. Since it is a *complete* equation, it includes the effects of all the generalized coordinates. Applying the FLT Eq. (4.13) gives the control effort as

$$\vec{Q}_r(\dot{\vec{q}}_r, \dot{\vec{q}}_f, \vec{q}_r, \vec{q}_f, t) = \tilde{\mathbf{D}}\,(\vec{q}_r, \vec{q}_f, t)\vec{\mathrm{v}} + \tilde{\vec{\mathrm{F}}}\,(\dot{\vec{q}}_r, \dot{\vec{q}}_f, \vec{q}_r, \vec{q}_f, t) \ , \tag{4.14}$$

where:

$$\ddot{\vec{q}}_r = \vec{\mathrm{v}} \ ; \tag{4.15}$$

$$\vec{\mathrm{v}} = \ddot{\vec{\beta}}_r + \mathbf{K}_v(\dot{\vec{\beta}}_r - \dot{\vec{q}}_r) + \mathbf{K}_p(\vec{\beta}_r - \vec{q}_r) \ ; \tag{4.16}$$

$$\ddot{\vec{q}}_f = -\mathbf{D}_{ff}^{-1}\mathbf{D}_{fr}\vec{\mathrm{v}} - \mathbf{D}_{ff}^{-1}\vec{\mathrm{F}}_f \ ; \tag{4.17}$$

$$\dot{\vec{e}}_r = \dot{\vec{\beta}}_r - \dot{\vec{q}}_r \ ; \tag{4.18}$$

$$\vec{e}_r = \vec{\beta}_r - \vec{q}_r \ . \tag{4.19}$$

The control effort thus becomes

$$\vec{Q}_r = \tilde{\mathbf{D}}\,\ddot{\vec{\beta}}_r + \tilde{\vec{\mathbf{F}}} + \tilde{\mathbf{D}}\,(\mathbf{K}_v\dot{\vec{e}}_r + \mathbf{K}_p\vec{e}_r)\,. \tag{4.20}$$

Note, the control effort consists of two components:

$$\vec{Q}_{r,nl} = \tilde{\mathbf{D}}\,\ddot{\vec{\beta}}_r + \tilde{\vec{\mathbf{F}}}\;; \tag{4.21}$$

$$\vec{Q}_{r,pd} = \tilde{\mathbf{D}}\,(\mathbf{K}_v\dot{\vec{e}}_r + \mathbf{K}_p\vec{e}_r)\,. \tag{4.22}$$

The first one is the *nonlinear feedback component* $\vec{Q}_{r,nl}$. It cancels the effects of the nonlinear torque/force disturbances on the joint and base actuators resulting from the system dynamics. The effectiveness of this part of the controller is strictly dependent on the closeness of the dynamical equations to the actual manipulator dynamics being modeled. The second one is the *linear proportional/derivative feedback component* $\vec{Q}_{r,pd}$. It ensures robust behaviour with respect to the errors $\vec{e}_r$ and $\dot{\vec{e}}_r$ which may arise as a result of imprecise modeling of the actual manipulator dynamics. Of course, in practice this is always the case and the linear controller is therefore always included to improve performance.

In order to determine the control effort, evaluation of the FLT variable arrays $\tilde{\mathbf{D}}$ and $\tilde{\vec{\mathbf{F}}}$ is necessary, which in turn requires the knowledge of $\vec{q}_f$ and $\dot{\vec{q}}_f$. With this in mind, two different proceedures, Quasi-Open Loop Control (QOLC) and Quasi-Closed Loop Control (QCLC), are suggested by Modi et al. [34].

4.3.1 Quasi-Open Loop Control

If the situation is such that most or all of the generalized variables are not amenable to direct measurement, then these variables must be determined using the nearest approximation to the real system being controlled. In this scheme, the central idea is to evaluate the generalized modal coordinates in an off-line parallel integration procedure, i.e. the dynamics of $\vec{q}_f$ is computed

without the use of $\vec{q}_r$. However, $\vec{q}_f$ is governed by the specified trajectory, $\vec{\beta}_r$, $\dot{\vec{\beta}}_r$, $\ddot{\vec{\beta}}_r$ and the dynamics may be obtained from Eq. (4.17):

$$\ddot{\vec{q}}_r = \ddot{\vec{\beta}}_r \; ; \tag{4.23}$$

$$\ddot{\vec{q}}_f(\vec{q}_f) = -\mathbf{D}_{\mathrm{ff}}^{-1}(\vec{\beta}_{\mathrm{r}}, \vec{\mathrm{q}}_{\mathrm{f}})\mathbf{D}_{\mathrm{fr}}(\vec{\beta}_{\mathrm{r}}, \vec{\mathrm{q}}_{\mathrm{f}})\vec{\mathbf{v}} - \mathbf{D}_{\mathrm{ff}}^{-1}(\vec{\beta}_{\mathrm{r}}, \vec{\mathrm{q}}_{\mathrm{f}})\vec{\mathrm{F}}_{\mathrm{f}}(\vec{\beta}_{\mathrm{r}}, \dot{\vec{\beta}}_{\mathrm{r}}, \vec{\mathrm{q}}_{\mathrm{f}}, \dot{\vec{\mathrm{q}}}_{\mathrm{f}}) \; . \tag{4.24}$$

Solution to Eq. (4.24) results in two rewards. Firstly, it allows the observation of the *approximated* behaviour of the modal coordinates and its derivatives, i.e. $\vec{q}_f$, $\dot{\vec{q}}_f$, and $\ddot{\vec{q}}_f$, off-line without the need for direct measurement. Furthermore, it allows for the off-line computation of the control effort $\vec{Q}_r$ for the rigid degrees of freedom. Figure 4.27 presents a block diagram for the Quasi-Open Loop Control scheme. The procedure would demand considerable amount of computational effort to solve the equations. Also, the method does not fully linearize the control system since it utilizes estimated values.

4.3.2 Quasi-Closed Loop Control

On the other hand. if the situation is such that most of the generalized coordinates are available for measurement than this approach is probably a better one. Here, the rigid and flexible degrees of freedom are both utilized and calculated simultaneously at each control interval, as shown by the following equations:

$$\ddot{\vec{q}}_r = \vec{\mathbf{v}} \; ; \tag{4.25}$$

$$\ddot{\vec{q}}_f(\vec{q}_f) = -\mathbf{D}_{\mathrm{ff}}^{-1}(\vec{\mathrm{q}}_{\mathrm{r}}, \vec{\mathrm{q}}_{\mathrm{f}})\mathbf{D}_{\mathrm{fr}}(\vec{\mathrm{q}}_{\mathrm{r}}, \vec{\mathrm{q}}_{\mathrm{f}})\vec{\mathbf{v}} - \mathbf{D}_{\mathrm{ff}}^{-1}(\vec{\mathrm{q}}_{\mathrm{r}}, \vec{\mathrm{q}}_{\mathrm{f}})\vec{\mathrm{F}}_{\mathrm{f}}(\vec{\mathrm{q}}_{\mathrm{r}}, \dot{\vec{\mathrm{q}}}_{\mathrm{r}}, \vec{\mathrm{q}}_{\mathrm{f}}, \dot{\vec{\mathrm{q}}}_{\mathrm{f}}) \; . \tag{4.26}$$

Note, $\vec{F}_f$ is now a function of $\vec{q}_r$ and $\dot{\vec{q}}_r$ rather than $\vec{\beta}_r$ and $\dot{\vec{\beta}}_r$, and that the control action of the PD controller is now on a *linearized system.* This is true if the system model is *exact* but in practice this is never the case. Robust behaviour, about the desired trajectoy, of the contolled output is mostly dependent on the linear controller part of Eq. (4.16) and the arrays $\mathbf{K}_{\mathrm{v}}$ and $\mathbf{K}_{\mathrm{p}}$. This approach is represented in a block diagram form in Figure 4.28. A bit more

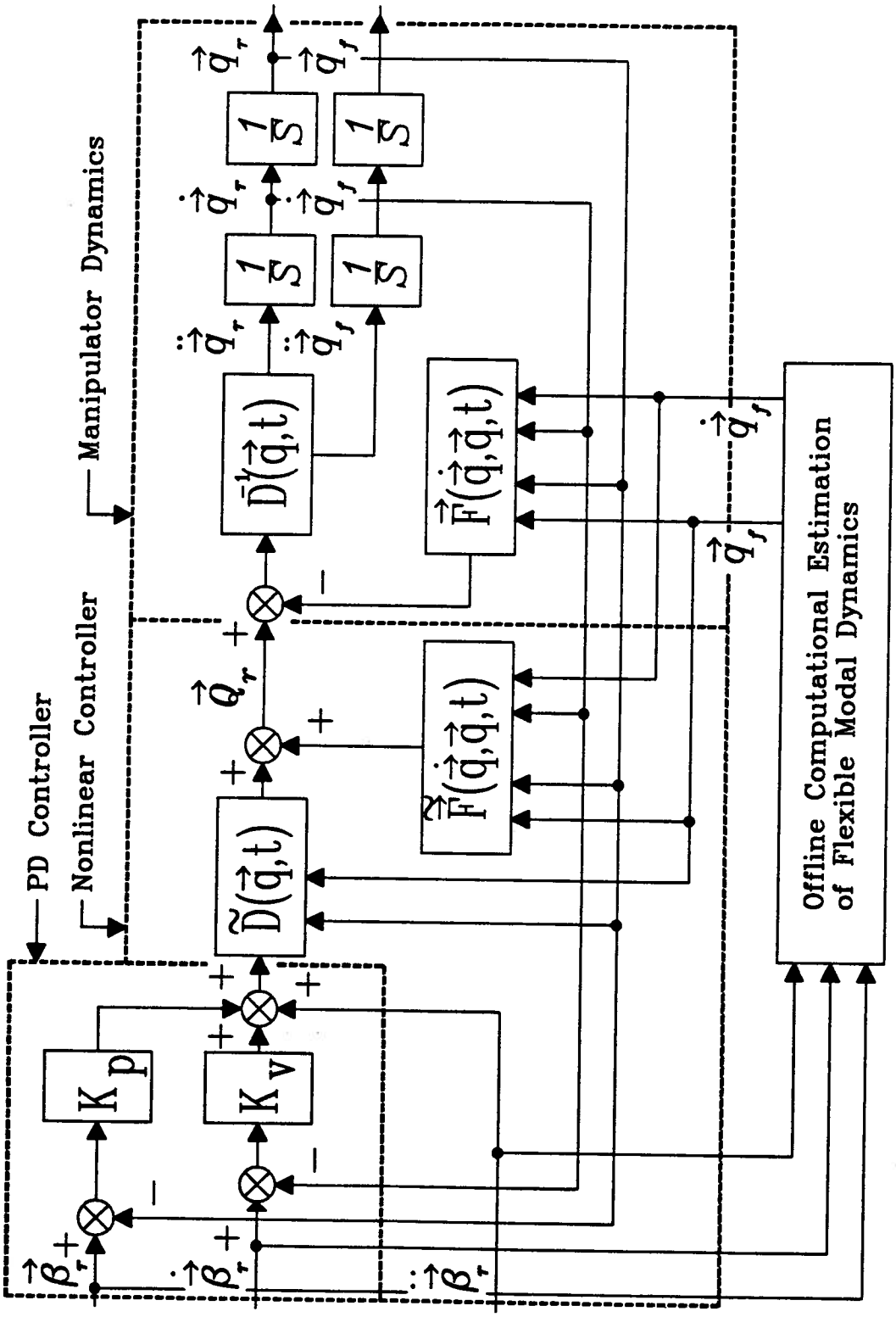

Figure 4.27: Block diagram for the quasi-open loop control of the two-link flexible manipulator.

computation is involved here than in the previous scheme but this disadvantage is more than offset by the increased precision and robustness in the controlled degrees of freedom. Also the QCLC is less sensitive to system uncertainties than the QOLC.

4.4 Application of the Quasi-Closed Loop Control to the Mobile Flexible Two-link Manipulator

The implementation of the QOLC as opposed to the QCLC using the existing program is radically different. The QOLC requires major modifications to the program since it involves a secondary double integration scheme. On the other hand, the QCLC involves minimal additions and revisions. Now the program remains much the same as before but with the addition of a modified control subroutine called FRCFC2, which calculates the required control effort based on the desired trajectory generated by the subroutine INVKB2. The main purpose of FRCFC2 is to rearrange and then partition the mass matrix $\mathbf{D}$, to evaluate $\tilde{\mathbf{D}}$ and $\tilde{\tilde{\mathbf{F}}}$, and then calculate the control effort $\vec{Q}_r$. Since the rigid degrees of freedom can be made to follow the desired trajectories *precisely*, the main interest now is to track the flexible degrees of freedom trajectory with accuracy. The present study is limited to the QCLC of a moving, ground based, flexible, two-link manipulator.

4.4.1 Stationary Manipulator in Zero Gravity Field Without Payload

All the physical parameters and dynamic constants of the manipulator are kept essentially the same as in the earlier study to facilitate a meaningful comparison between the two control schemes. The joint stiffnesses are purposely reduced here by an order of magnitude to illustrate the effects of a highly flexible joint drive system. The duration of the maneuver is in the range 1.0 - 2.0 seconds. Numerical values used in the simulation are listed below:

c_x = 1000 N/m/s

c_y = 1000 N/m/s

c_1 = 1000 N-m/rad/s

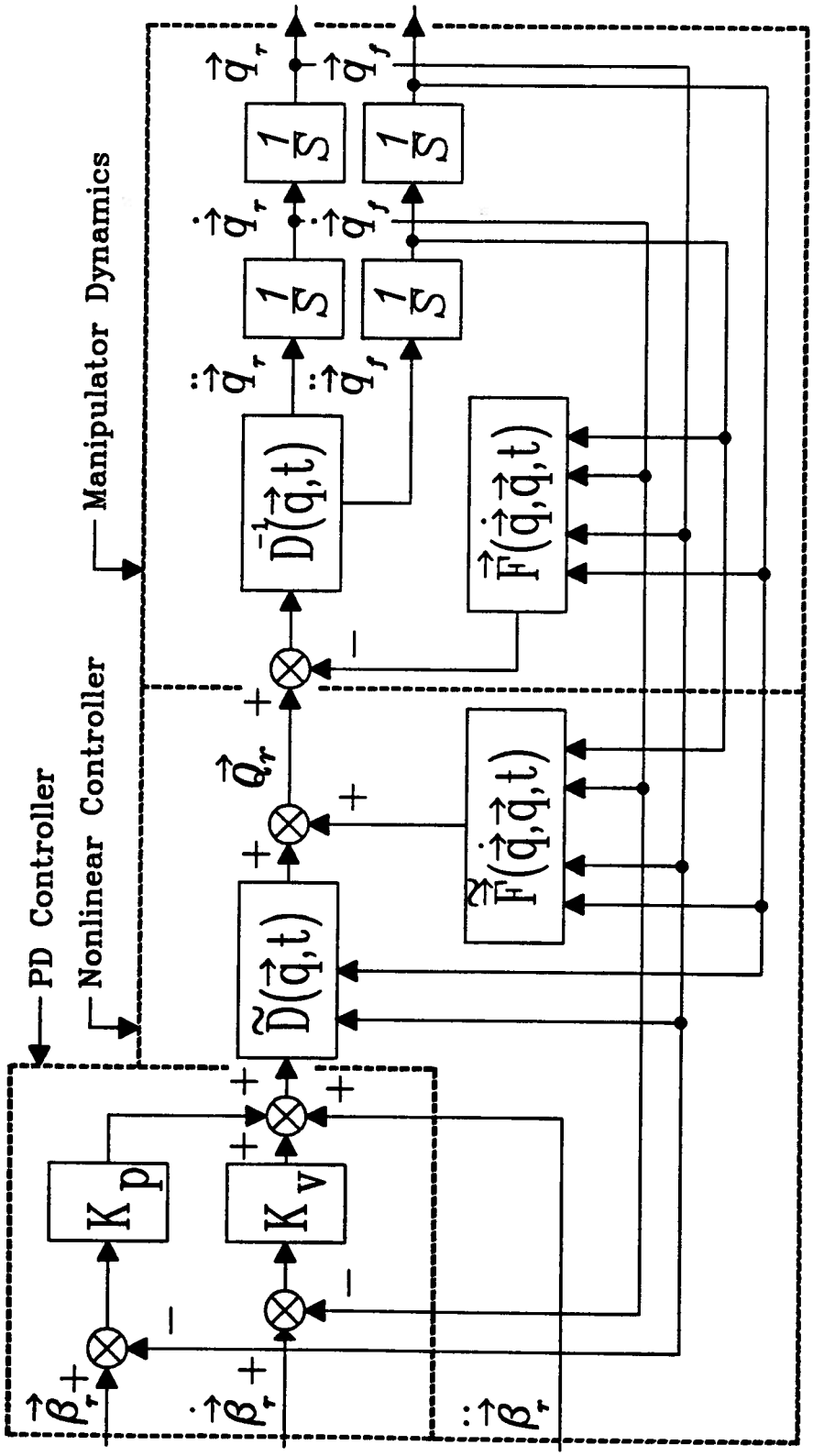

Figure 4.28: Block diagram for the quasi-closed loop control of the mobile manipulator under study.

c_2 = 1000 N-m/rad/s

$(EI)_1$ = 30000 N-m^2

$(EI)_2$ = 30000 N-m^2

k_x = 1000 N/m

k_y = 1000 N/m

k_1 = 1000 N-m/rad

k_2 = 1000 N-m/rad

l_1 = 5 m

l_2 = 5 m

m_1 = 20 Kg

m_2 = 20 Kg

m_B = 0

m_P = 0

Note, the gravitational field is purposely set to zero initially to observe the system dynamics without any outside influence. The joint, base, and link flexural stiffnesses are set fairly low in order to emphasize their effects. In a practical system, the above parameters may correspond to a manipulator constructed from standard .05m x .05m x 5m square solid aluminum bar sections. Only the first two cantilever modes are used to save simulation time and cost. A preliminary study showed that the use of additional modes does not appreciably change the payload tracking characteristics.

In this set of simulations results (Figures 4.29, 4.30, and 4.31), the base is held stationary and the payload is required to follow a rather complex trajectory described by the solid line curve in Figure 4.29. The actual trajectory traced by the payload is indicated by the dash line. The frozen positions of the links at successive time-steps are also included (time-strobe overlays). As shown in Figure 4.29, the manipulator starts the trajectory from the positive X-axis. It is appearant that the PD control is rather inadequate. The tracking errors are indeed quite large. This can be seen, more clearly, from Figures 4.30 and 4.31 where p_{3x}, p_{3y}, θ_1, and

θ_2 are plotted against their desired trajectory counterpart. There is as much as 6 meters of following error between p_{3x} and $\beta_{p_{3x}}$; 4 meters between p_{3y} and p_{3y}; 0.5 radians between β_1 and θ_1; and 0.3 radians between β_2 and θ_2. The combined effect of these leads to a large phase lag between the desired and actual payload load positions as observed in Figure 4.29.

Having observed the dynamic response of the manipulator to sinusoidal trajectory tracking in the presence of the PD control, the next step was to assess effectiveness of the FLT. This is shown in Figures 4.32, 4.33, and 4.34. Note, there is a major improvement in the tracking behaviour of the manipulator tip. The maximum deviation from the desired trajectory is about 0.5 meter. It occurs at the beginning and at the end of the travel where the peak acceleration takes place. Of course, these perturbations are primarily due to the flexible character of the *cantilever* links. This can be verified by analyzing Figures 4.33 and 4.34. Plots of θ_1, θ_2, p_x, and p_y vs time clearly show that there is no detectable deviation from the desired trajectories, suggesting that the only source of the discrepancy must be the flexible degrees of freedom over which there is no direct control at this level.

4.4.2 Mobile Manipulator in Zero Gravity Field Without Payload

Figures 4.35, 4.36, and 4.37 show the tracking characteristics of the manipulator under the PD control with the base now free to move. All other parameters have the same values as before.

The base is made to follow a sinusoidal desired trajectory of amplitude 5 meters in both the -X and +Y directions at a driving frequency of 1.0 radians/second. The first thing to note is that the tracking error is not as great as when the base was stationary under the same control scheme. Furthermore, the tip phase lag is considerably less. This suggests that the nature of the base motion will have considerable effect on the tip tracking efficiency.

Figures 4.38, 4.39, and 4.40 show the tracking characteristics of the mobile manipulator under the FLT control.

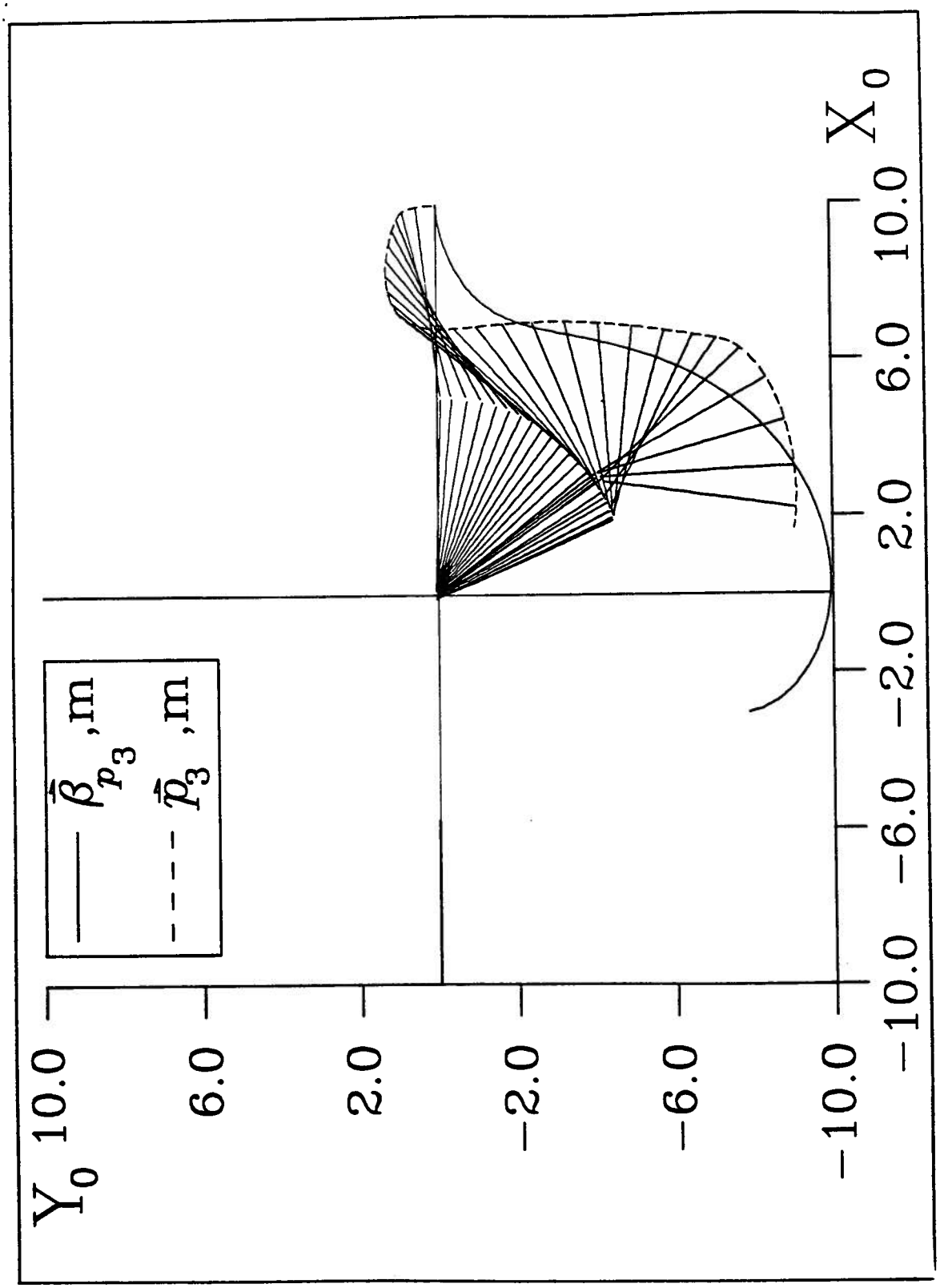

Figure 4.29: (A) Time history response of the manipulator showing the tip and the link postions in the presence of PD control with the base held fixed

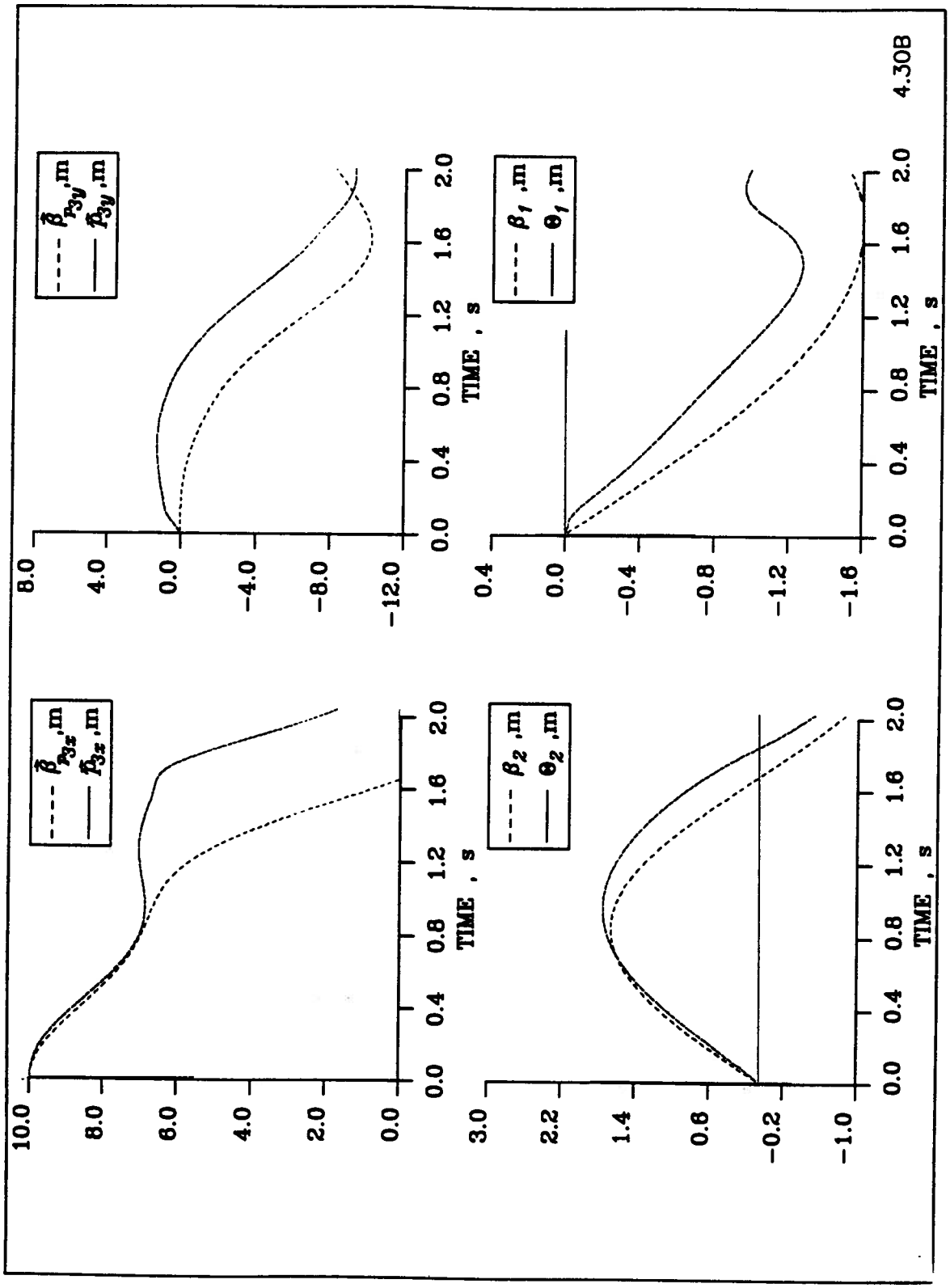

Figure 4.30: (B) Graphs of (from top left figure clockwise) $\beta_{p_{3x}}$ & p_{3x}, $\beta_{p_{3y}}$ & p_{3y}, β_1 & θ_1, β_2 & θ_2, VS time [seconds] for the stationary flexible 2 link manipulator under PD control

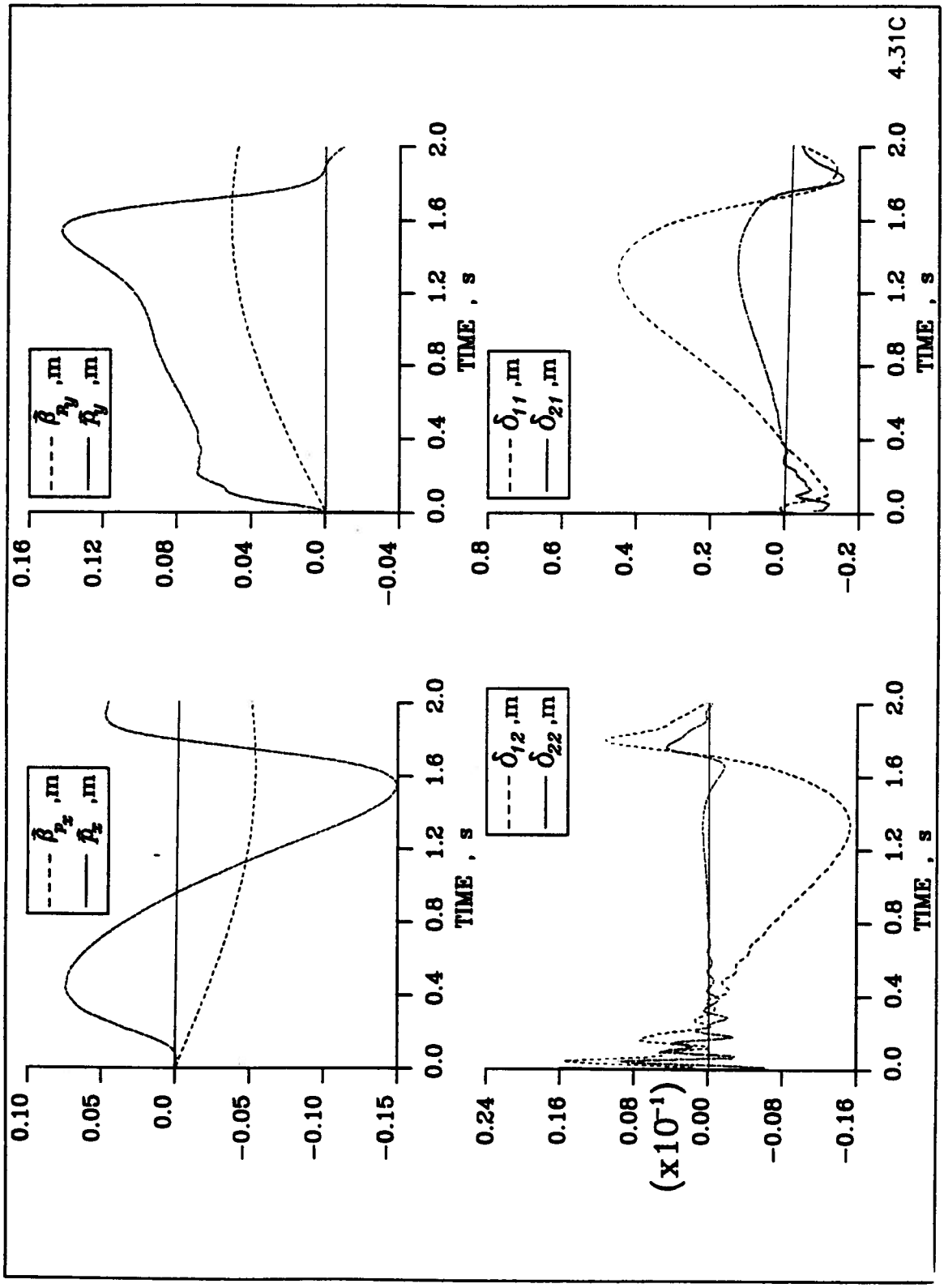

Figure 4.31: (C) Graphs of (from top left figure clockwise) β_{p_x} & p_x, β_{p_y} & p_y, δ_{11} & δ_{21}, δ_{12} & δ_{22}, VS time [seconds] for the stationary flexible 2 link manipulator under PD control

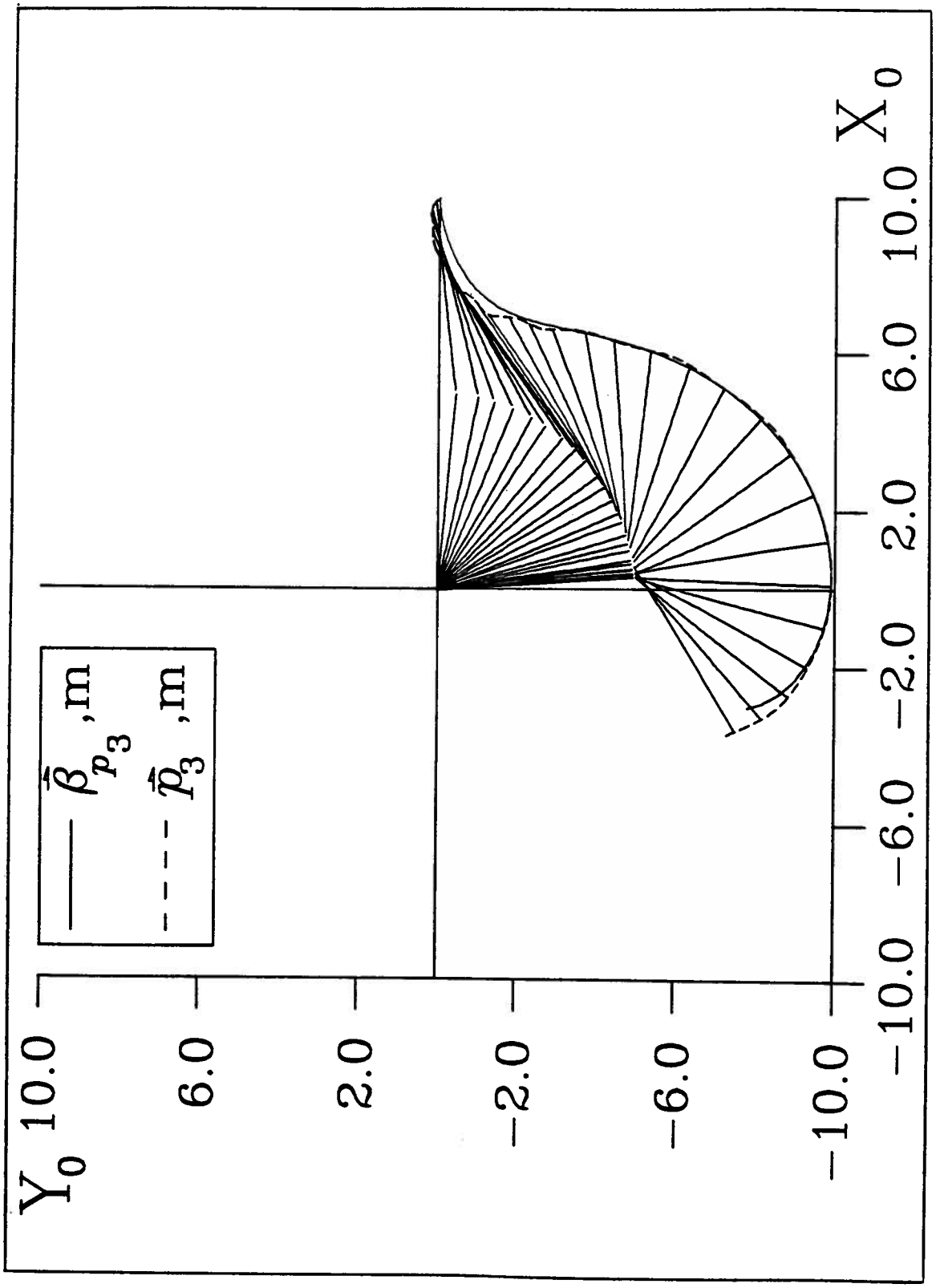

Figure 4.32: (A) Time history response of the manipulator showing the tip and the link positions in the presence of FLT control with the base held fixed

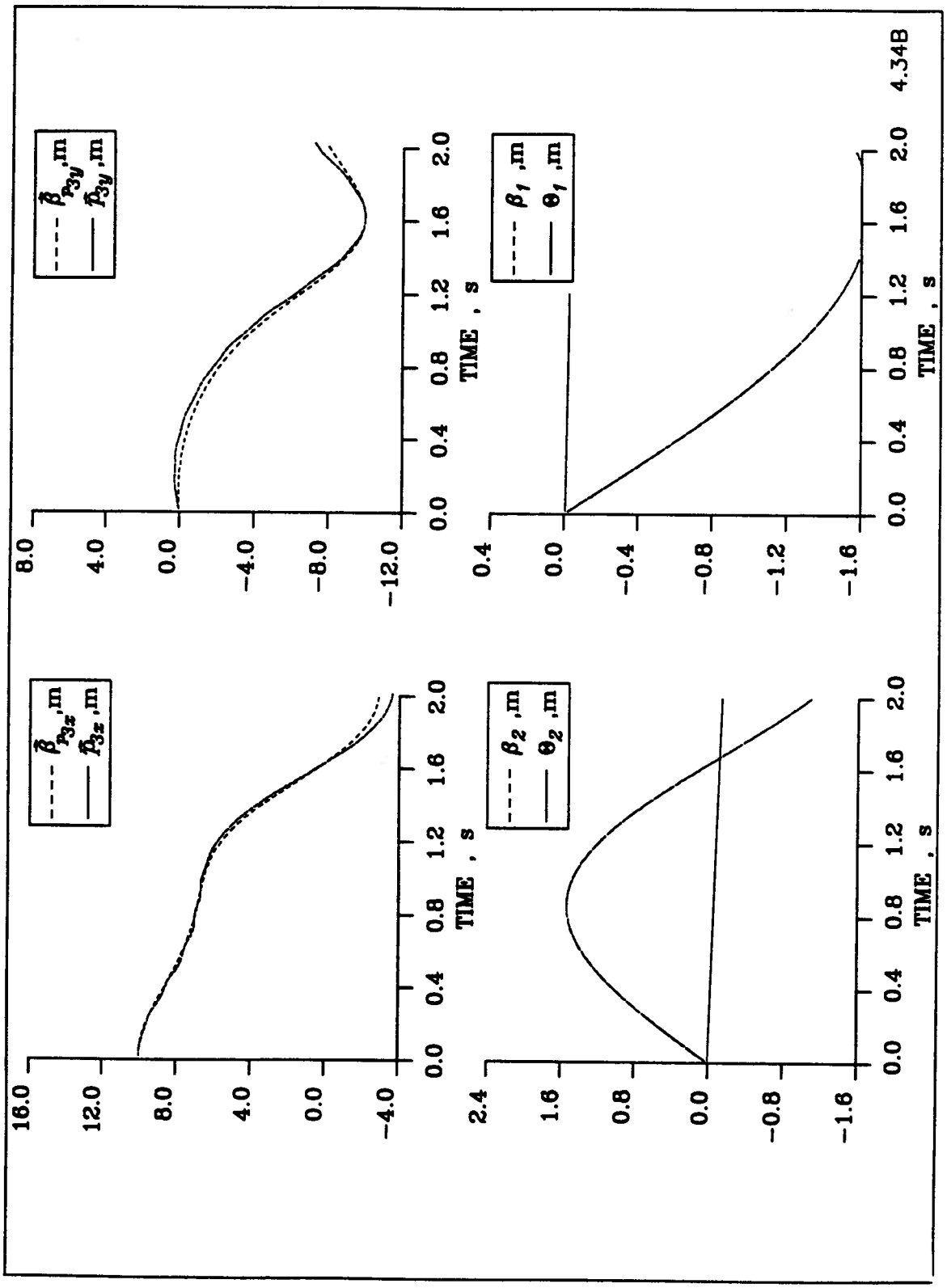

Figure 4.33: (B) Graphs of (from top left figure clockwise) $\beta_{p_{3x}}$ & p_{3x}, $\beta_{p_{3y}}$ & p_{3y}, β_1 & θ_1, β_2 & θ_2, VS time [seconds] for the stationary flexible 2 link manipulator under FLT control

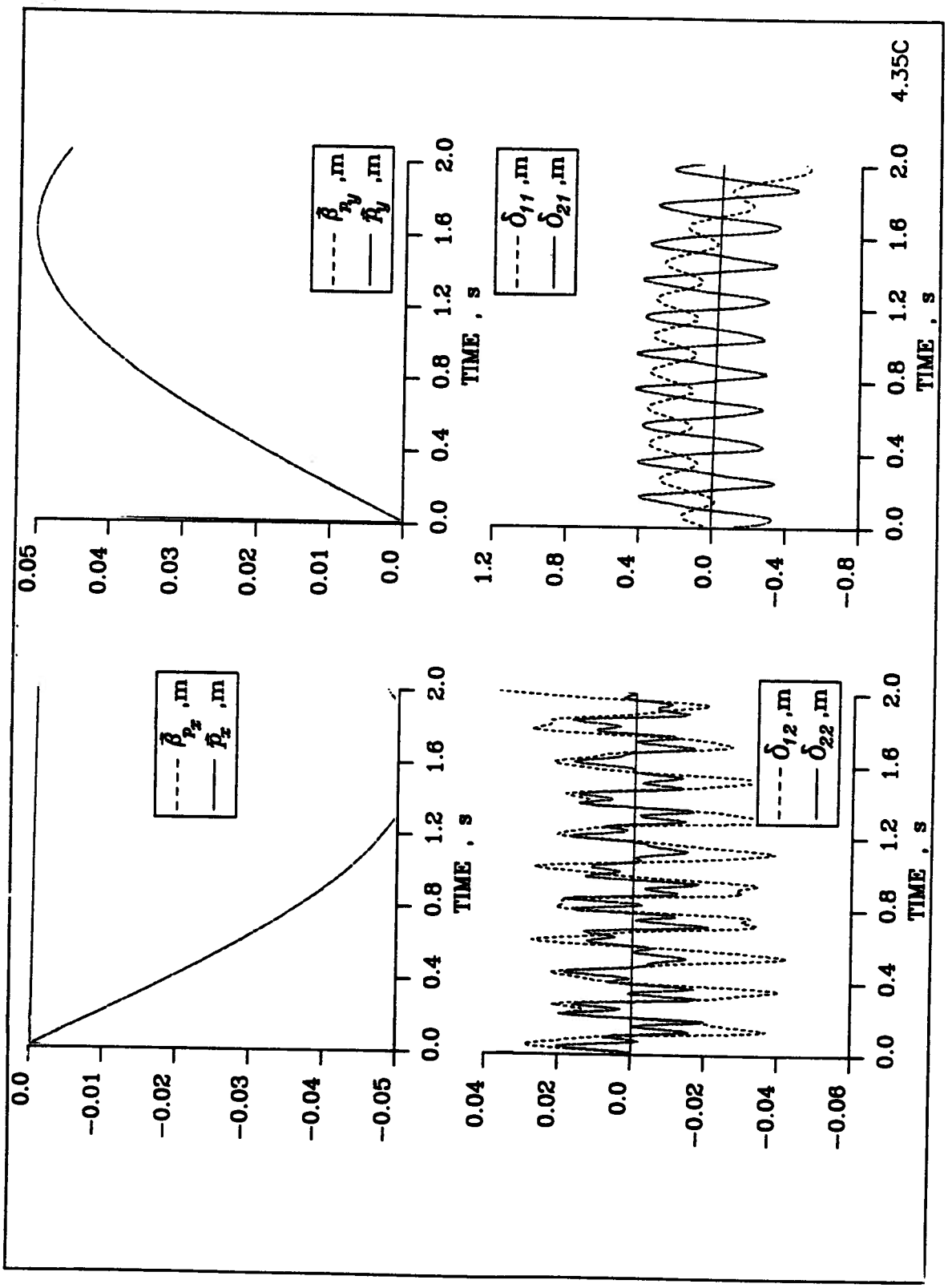

Figure 4.34: (C) Graphs of (from top left figure clockwise) β_{p_x} & p_x, β_{p_y} & p_y, δ_{11} & δ_{21}, δ_{12} & δ_{22}, VS time [seconds] for the stationary flexible 2 link manipulator under FLT control

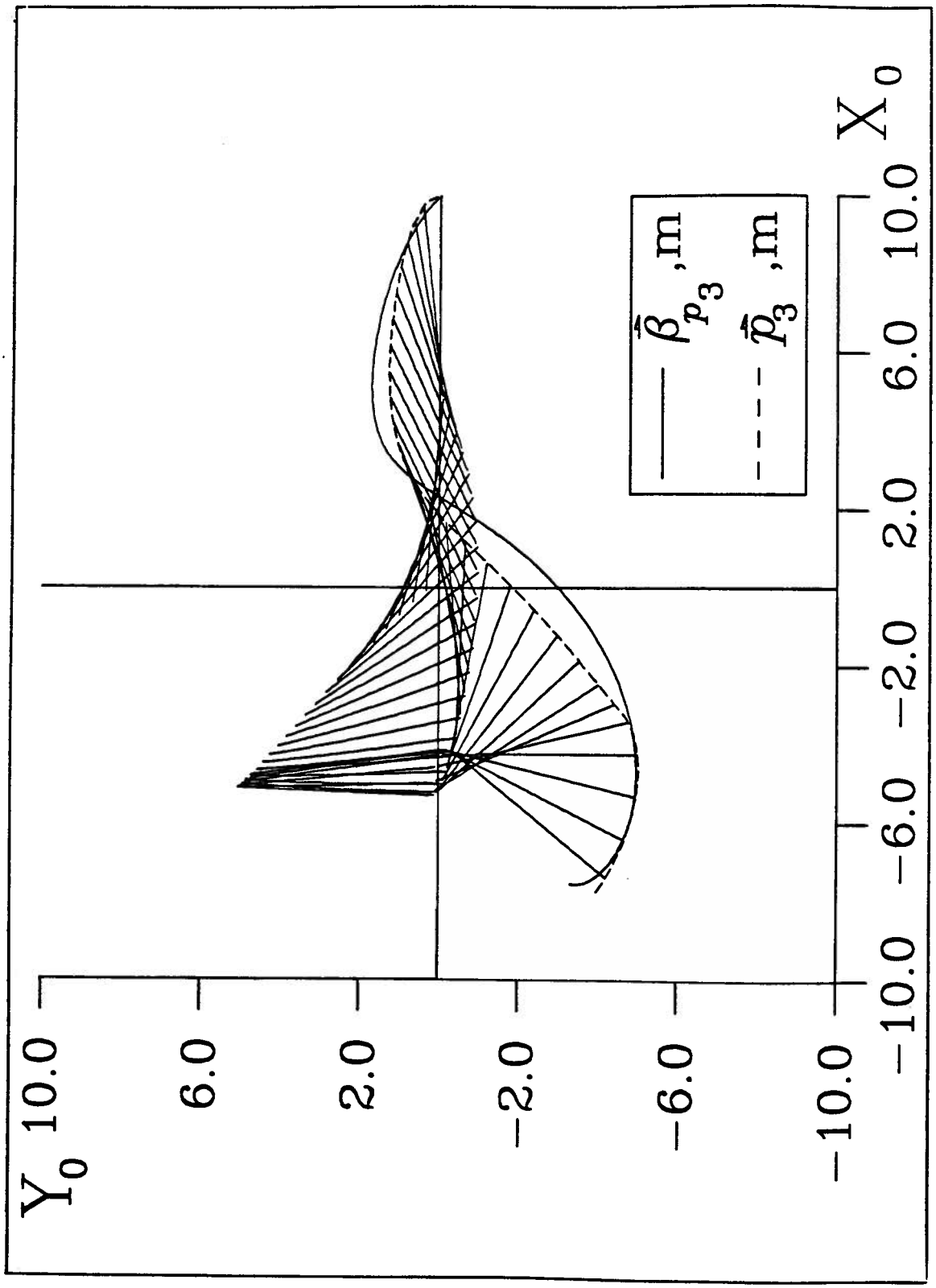

Figure 4.35: (A) Time history response of the manipulator showing the tip and the link positions in the presence of PD control with the base translating as shown.

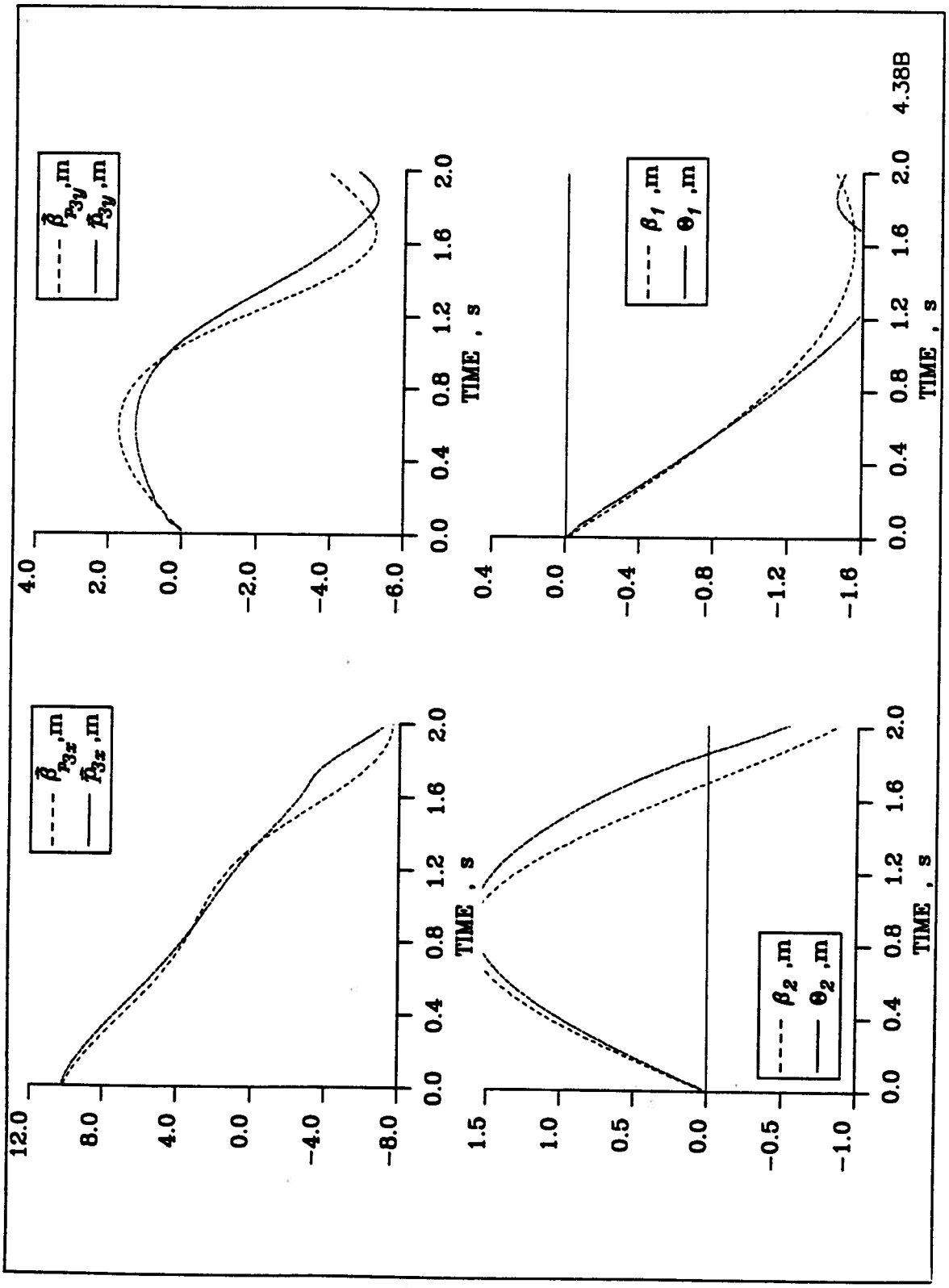

Figure 4.36: (B) Graphs of (from top left figure clockwise) $\beta_{p_{3x}}$ & p_{3x}, $\beta_{p_{3y}}$ & p_{3y}, β_1 & θ_1, β_2 & θ_2, VS time [seconds] for the moving flexible 2 link manipulator under PD control

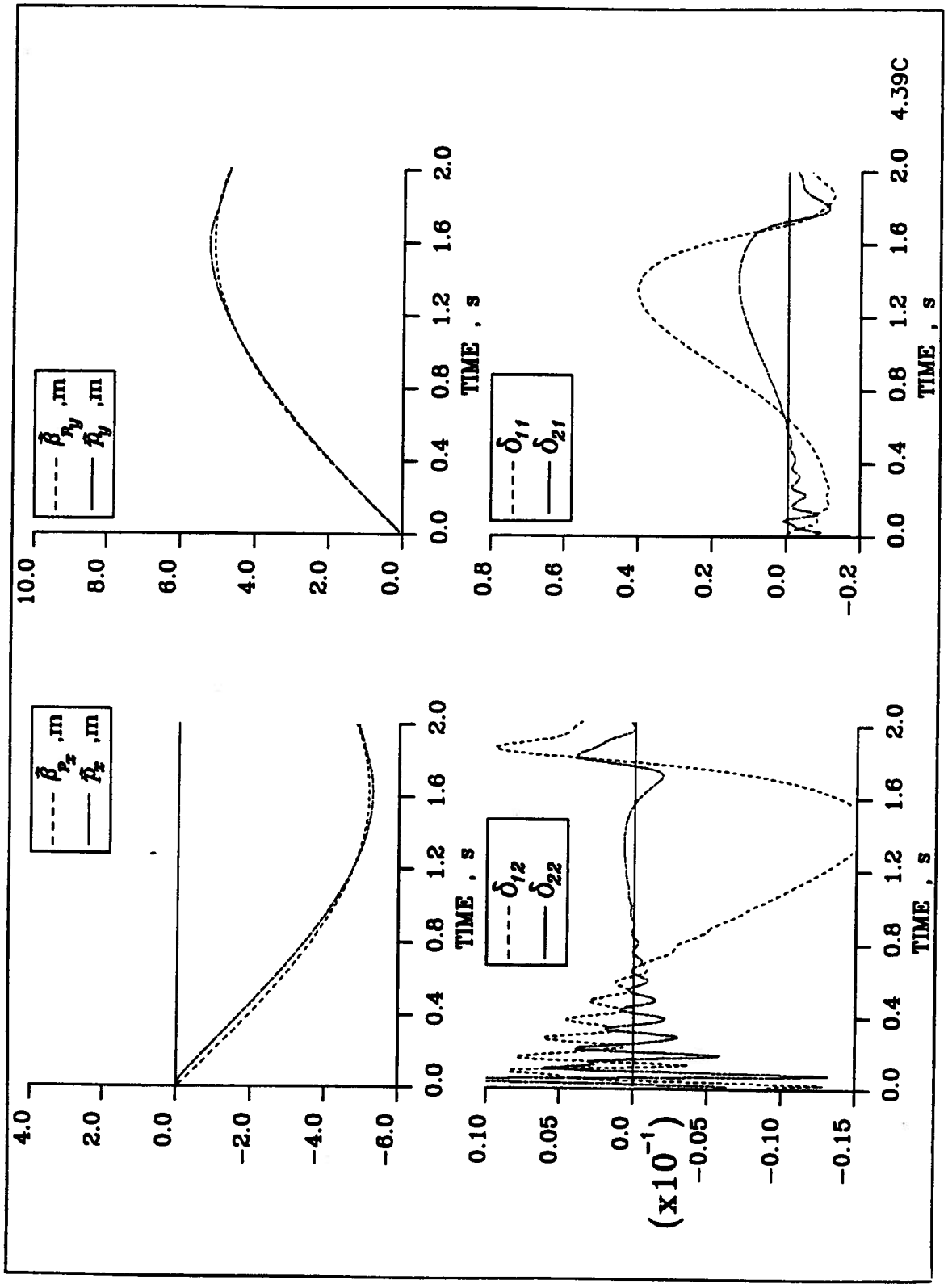

Figure 4.37: (C) Graphs of (from top left figure clockwise) β_{p_x} & p_x, β_{p_y} & p_y, δ_{11} & δ_{21}, δ_{12} & δ_{22}, VS time [seconds] for the moving flexible 2 link manipulator under PD control

As before, considerable improvement in the tracking efficiency of the manipulator is apparent. The rigid degrees of freedom have virtually no detectable tracking error as observed earlier. One point of interest is the vibrational characteristics of the first two flexible degrees of freedom of the modal coordinates. Comparing Figures 4.31, 4.37 with Figures 4.34, 4.40, considerable difference in the frequency content of the waveforms is noticeable. With the PD control the high frequency oscillations of the first and second modal coordinates fade rapidly leaving only the deflection brought about by the nominal motions. On the other hand, with the FLT control, the high frequency contributions dominate the response. This situation would be greatly improved by structural damping.

The set of Figures 4.41, 4.42, and 4.43 as well as Figures 4.44, 4.45, and 4.46 show response of the system as it performs a full three quadrant slewing maneuver. The intent here is to explore a different maneuver profile while keeping the system parameters unchanged. The desired trajectories are chosen to best observe the effects of a constant gravitational field as well as the inclusion of a payload at the tip of the manipulator, as described in the following section.

Figure 4.41 shows the inadequacy of the simple PD controller in the presentce of relatively low joint stiffnesses. However, the FLT controller proves its superiority even though the spring and damping constants are left unchanged (Figure 4.44). Note that the tip follows the required trajectory quite closely save for the deviations that occur due to the link vibrations, which cannot be directly controlled. Furthermore, a large torque required for the maneuver through three quadrants completed in 2s adds to the discrepancy.

Again the slow damping oscillatory motion of the first and second cantilever modes is noted in Figure 4.46, which appears to be assosciated with the FLT control. Consider the fundamental cantilever mode of both the links. Since the coefficient of stiffness and the mass per unit length are equal for both links, the natural frequencies are also equal. As a result both links are locked into synchronous oscillation but out of phase by 180 deg. This effect appears to be independent of the manipulator configuration but remains superimposed on the deflection created by the

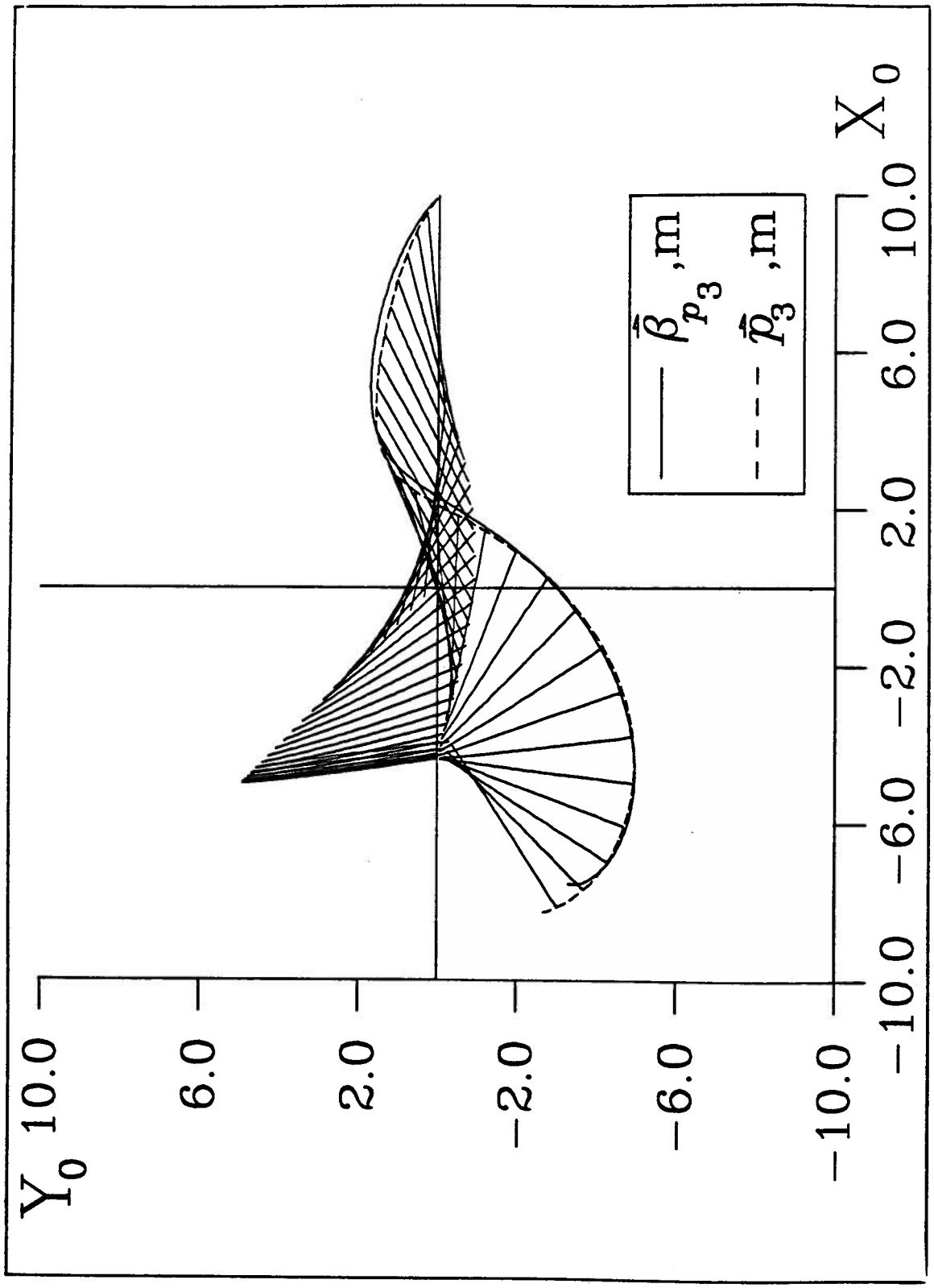

Figure 4.38: (A) Time history response of the manipulator showing the tip and the link postions in the presence of FLT control with the base translating as shown

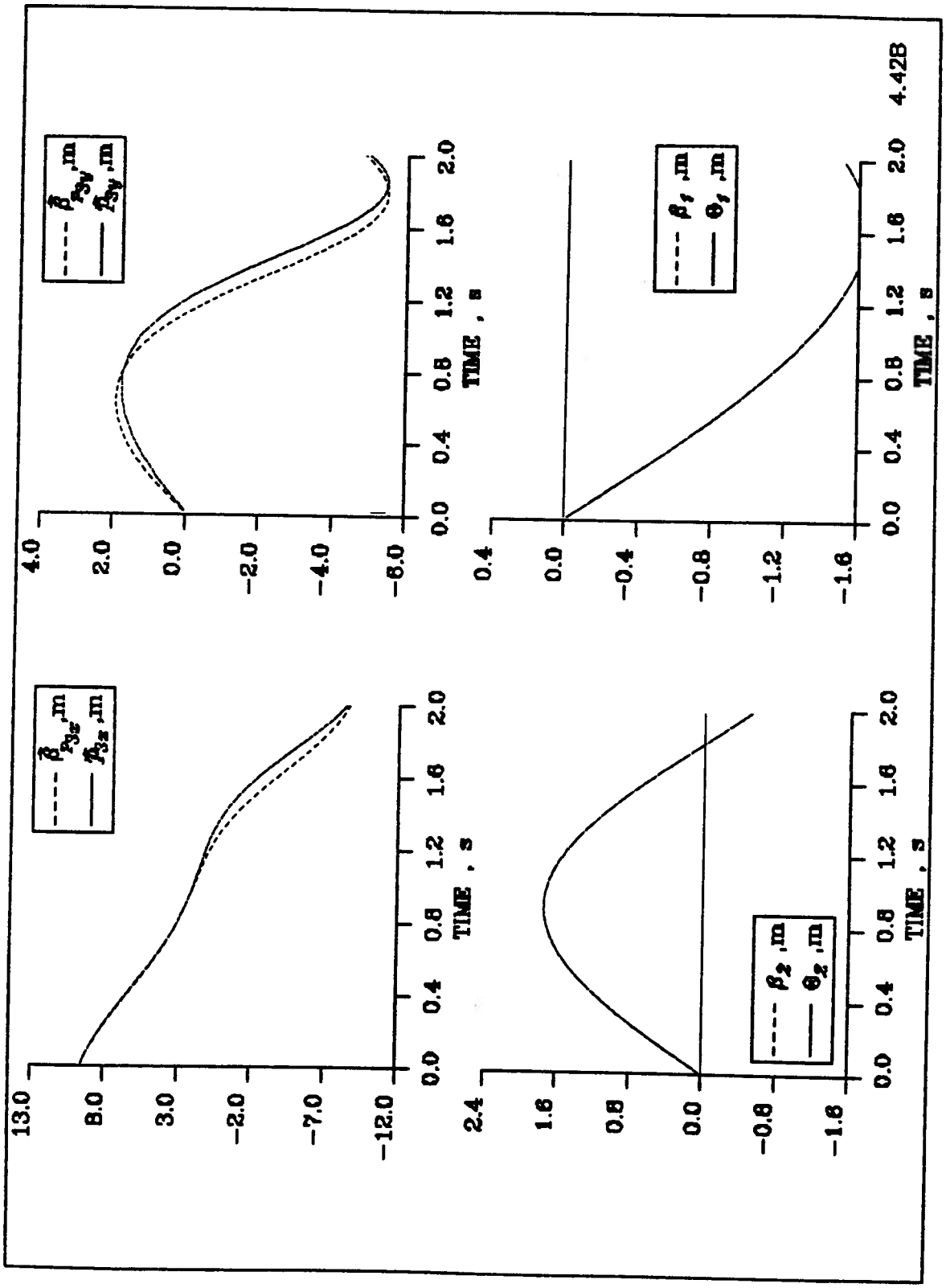

Figure 4.39: (B) Graphs of (from top left figure clockwise) $\beta_{p_{3x}}$ & p_{3x}, $\beta_{p_{3y}}$ & p_{3y}, β_1 & θ_1, β_2 & θ_2, VS time [seconds] for the moving flexible 2 link manipulator under FLT control

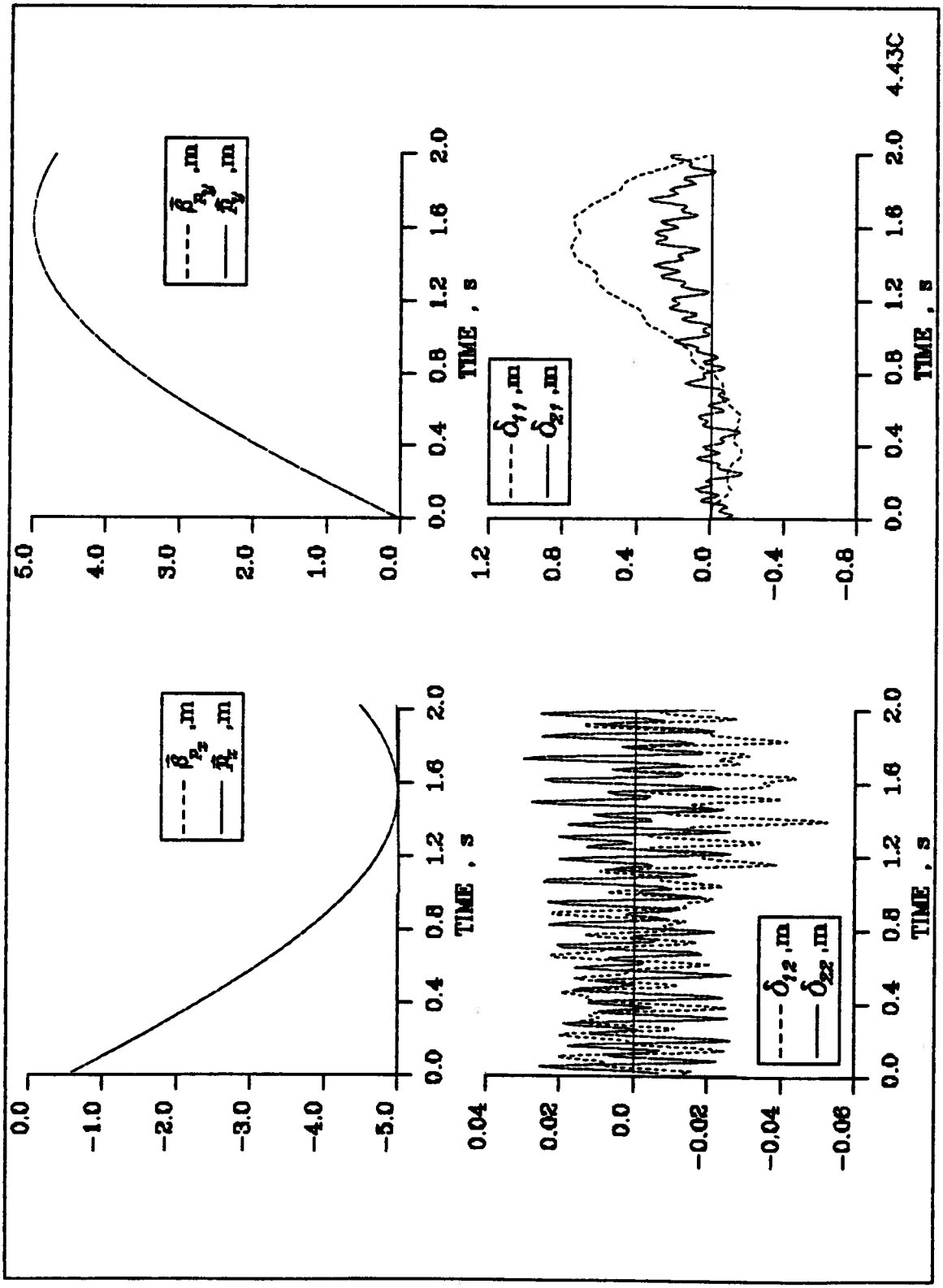

Figure 4.40: (C) Graphs of (from top left figure clockwise) β_{p_x} & p_x, β_{p_y} & p_y, δ_{11} & δ_{21}, δ_{12} & δ_{22}, VS time [seconds] for the moving flexible 2 link manipulator under FLT control

motions of the rigid degrees of freedom. These oscillations are a consequence of the fundamental mode coupling between the links. Second mode effects are not observed because they are small, at least by an order of magnitude. This suggests that to minimize modal response of the links, they should be designed to avoid the frequency coupling. This can be achieved quite readily by selecting the flexural stiffness appropriately.

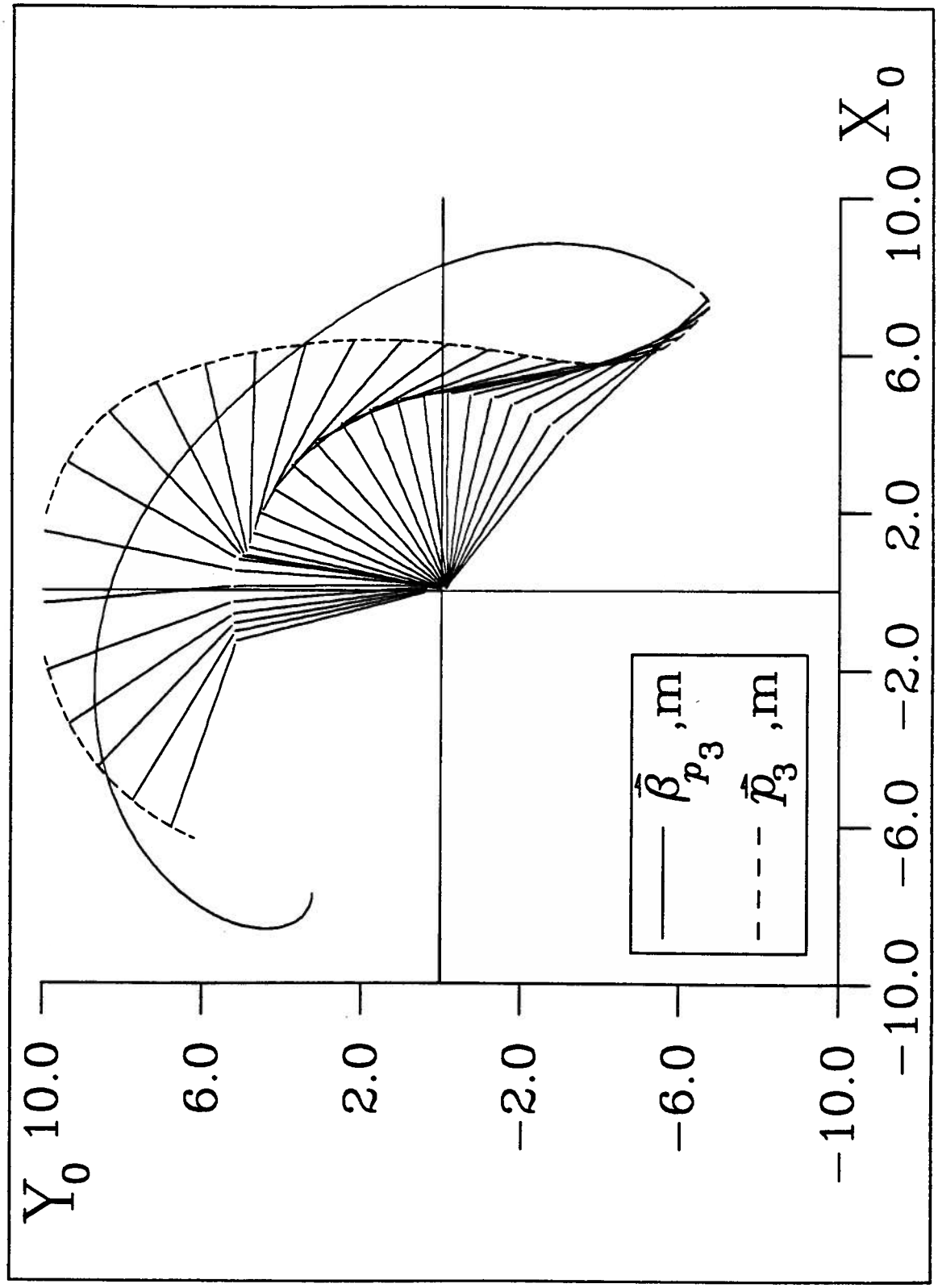

Figure 4.41: (A) Time history response of the manipulator showing the tip and the link positions in the presence of PD control with the base held fixed doing a full three quadrant slewing maneuver

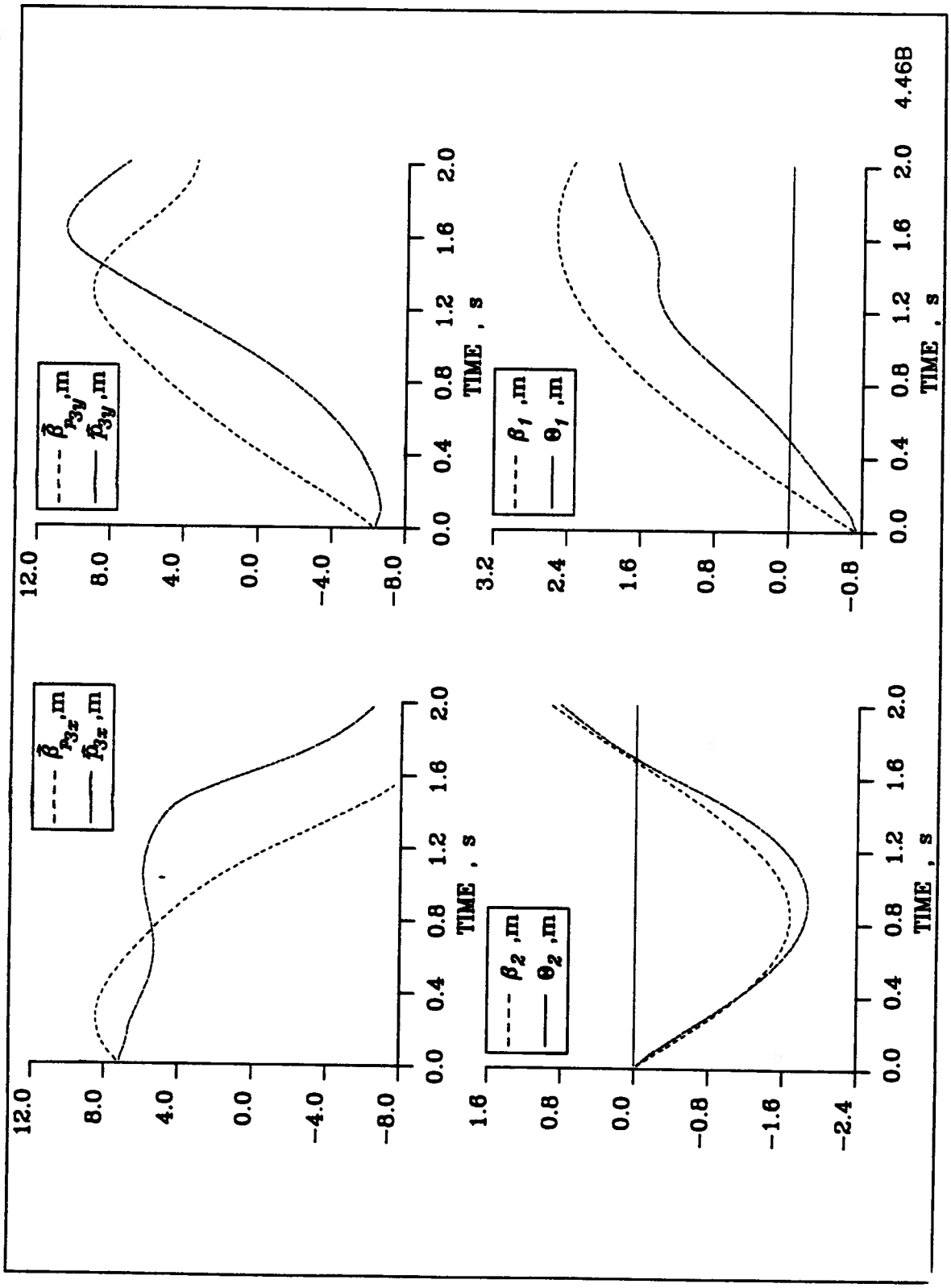

Figure 4.42: (B) Graphs of (from top left figure clockwise) $\beta_{p_{3x}}$ & p_{3x}, $\beta_{p_{3y}}$ & p_{3y}, β_1 & θ_1, β_2 & θ_2, VS time [seconds] for the stationary flexible 2 link manipulator under PD control during a three quadrant slewing maneuver

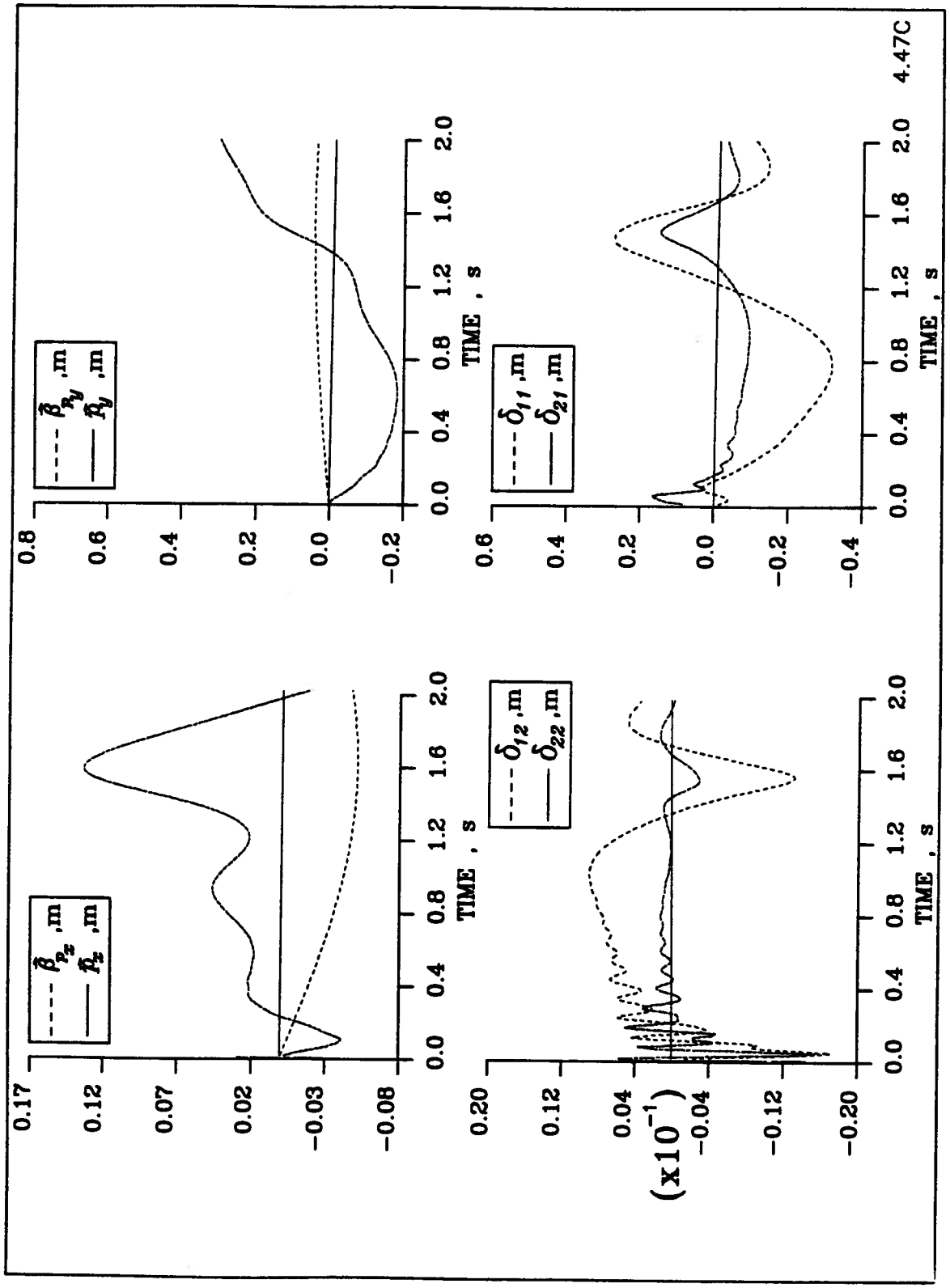

Figure 4.43: (C) Graphs of (from top left figure clockwise) β_{p_x} & p_x, β_{p_y} & p_y, δ_{11} & δ_{21}, δ_{12} & δ_{22}, VS time [seconds] for the stationary flexible 2 link manipulator under PD control during a three quadrant slewing maneuver

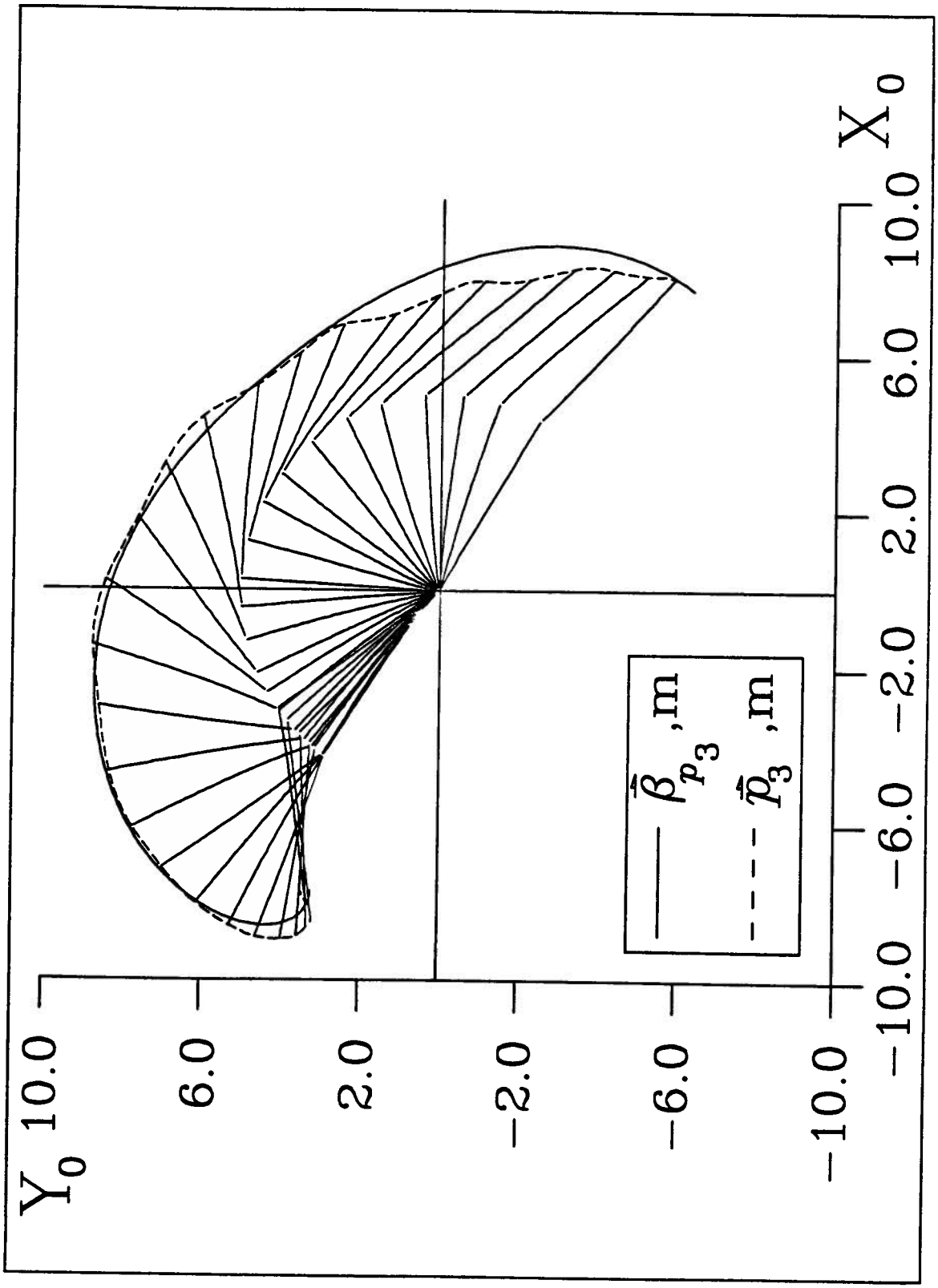

Figure 4.44: (A) Time history response of the manipulator showing the tip and the link positions in the presence of FLT control with the base held fixed doing a full three quadrant slewing maneuver

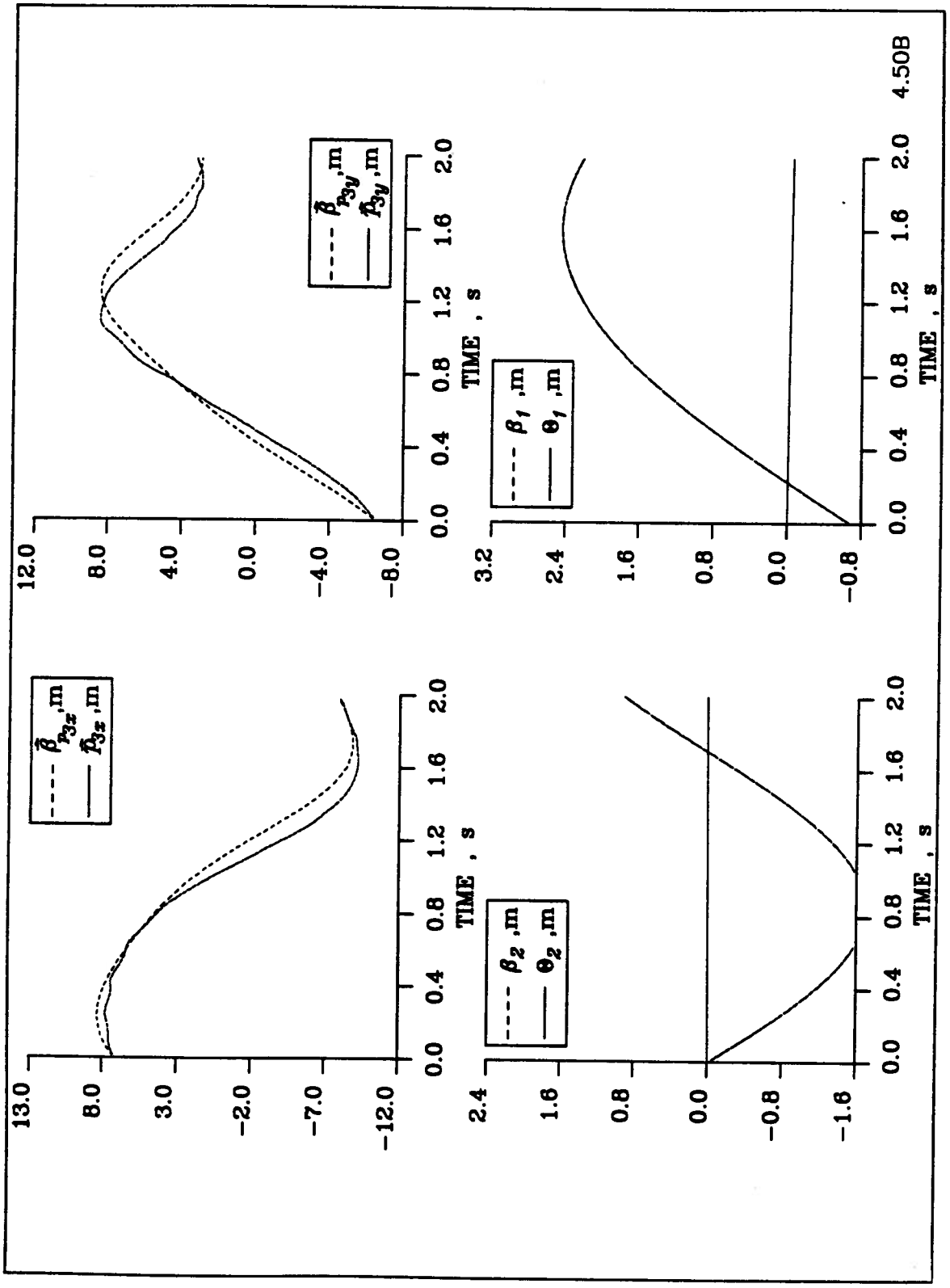

Figure 4.45: (B) Graphs of (from top left figure clockwise) $\beta_{p_{3x}}$ & p_{3x}, $\beta_{p_{3y}}$ & p_{3y}, β_1 & θ_1, β_2 & θ_2, VS time [seconds] for the stationary flexible 2 link manipulator under FLT control during a three quadrant slewing maneuver

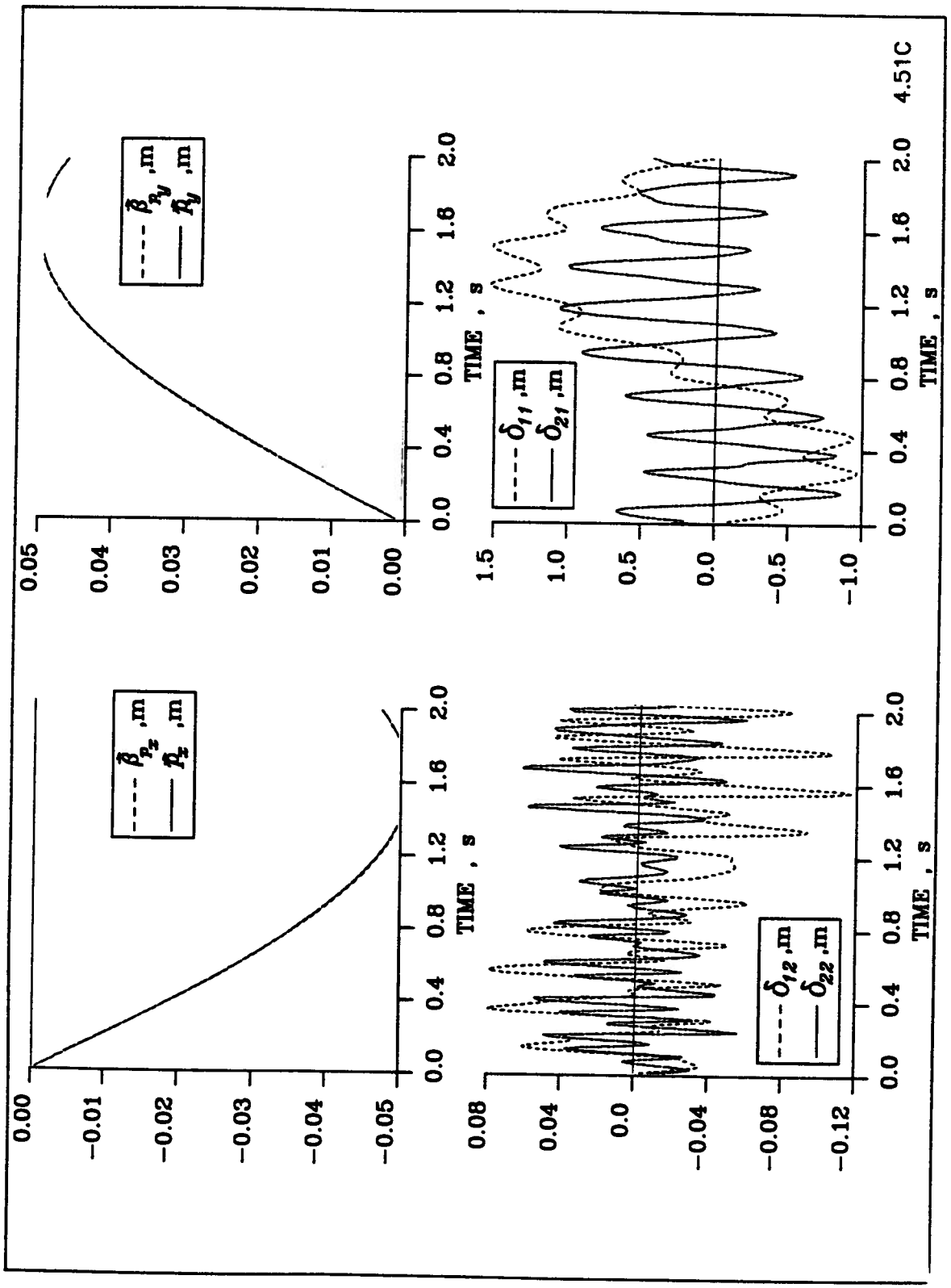

Figure 4.46: (C) Graphs of (from top left figure clockwise) β_{p_x} & p_x, β_{p_y} & p_y, δ_{11} & δ_{21}, δ_{12} & δ_{22}, VS time [seconds] for the stationary flexible 2 link manipulator under FLT control during a three quadrant slewing maneuver

4.4.3 Stationary Manipulator in Non-Zero Gravity Field Without Payload

Figures 4.47, 4.48, and 4.49 show the response of the stationary manipulator using PD control and under the influence of a gravitational acceleration of $9.8m/s^2$. The results may be directly compared with those shown in Figures 4.41, 4.42, and 4.43. It is evident that the joint stiffnesses are insufficient to carry the two links through the full maneuver range when gravity is present (Figure 4.47). Note, in Figures 4.47 and 4.49, the effect of gravity offsets the base and the entire manipulator down as far as 0.3 meters below the origin. The effect is better seen in Figures 4.41 and 4.43.

Next, the FLT control is applied in the same situation as above. Figures 4.50, 4.51, and 4.52 show, as before, that the rigid degrees of freedom are instantly brought into line with the desired trajectories. Of course, this happens since we have full knowledge of all the structural parameters as well as all of the degrees of freedoms. The base deflection is no longer a dominant factor in the manipulator tip deviation from the desired trajectory due to gravity. The major contribution comes from the flexible degrees of freedom. The plots of the flexible coordinates δ_{11} and δ_{21} in Figure 4.52 indicate the level of the contribution. Note, where the initial peak deflections occur, they combine in such a manner as to create the greatest deviation from the desired trajectory. It may be pointed out that the overshoot at the end of the slewing maneuver was absent when the gravitational acceleration was neglected.

4.4.4 Mobile Manipulator in Non-Zero Gravity Field Without Payload

Keeping all the parameters the same as in the previous sections, the effect of a moving base is observed in a nonzero gravity field. Figures 4.53, 4.54, and 4.55 illustrate effectiveness of the PD control as the mobile manipulator undergoes the previous slew maneuver. Corresponding results for the FLT control are presented in Figures 4.56, 4.57, and 4.58. The payload in both the cases is absent.

Note, the base motion is almost enough to carry the two links over the top dead centre during the PD control. Also, the acceleration of the base delays the tip and stretches out the track

path which is further away from the desired trajectory then in the previous simulation (Figure 4.47). Comparison of the mobile manipulator response results with those for the stationary case in the previous section show favourable agreement. The exceptions are the modal coordinates. They tend to exhibit greater excursions for the mobile manipulator case. This trend is also observed in the FLT control data.

4.4.5 Mobile Manipulator in the Gravity Field With Payload

Finally, the attention is turned to the most general case that accounts for the mobile character of the manipulator, operating in the gravitational field, and carrying a payload (Figures 4.56, 4.57, and 4.58). The gravity field is taken as 9.8 m/s^2; the FLT control is active; the base starts in the fourth quadrant and is moving in the direction as shown in Figure 4.59. The payload is 3.0 kg.

The response is basically as expected. In Figure 4.61 the response plots of δ_{11} and δ_{21} show a measure of damping effect on the fundamental mode. The higher order vibrations are suppressed somewhat (compared to those observed in Figure 4.58), although the peak deviation from the desired trajectory is slightly higher in the presence of a payload. As well, the frequency of the vibration of the first mode of link 2 has decreased by about a factor of 1.5 while the vibration frequency in link 1 has gone up by about the same amount. A larger overshoot is noted for this case, at the end of the slewing maneuver, then with any other simulation results obtained so far (Figure 4.59).

The response of the second modal coordinate for both the links is somewhat surprising (δ_{12} and δ_{22} in Figures 4.58 and 4.61). Firstly, the frequency of vibration of link 2 is slightly higher than that of link 1. Secondly, the maximum deviation is less than that observed in the previous section where the payload was zero.

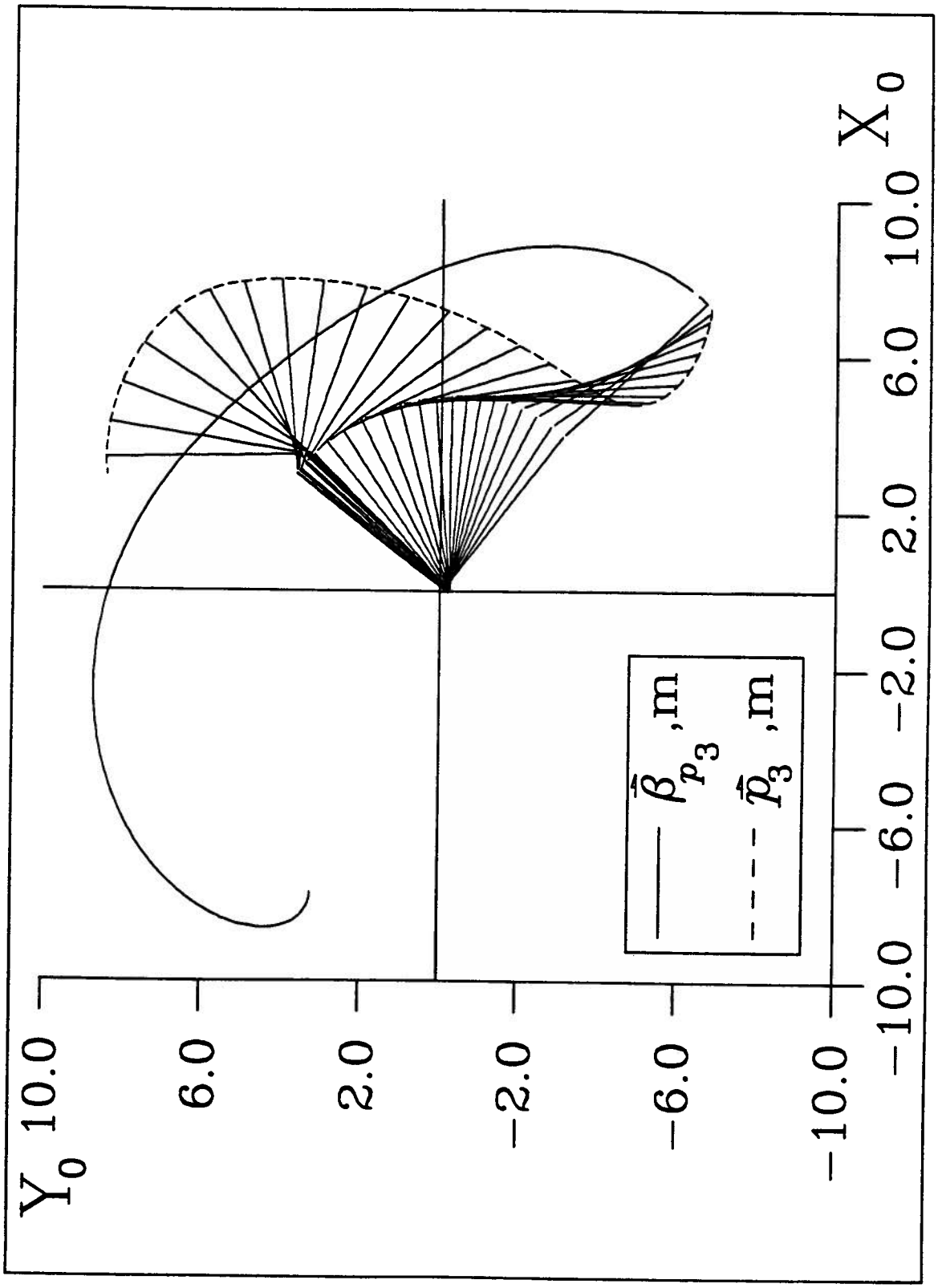

Figure 4.47: (A) Time history response of the manipulator showing the tip and the link positions in the presence of PD control with the base held fixed doing a full three quadrant slewing maneuver in a nonzero gravity field

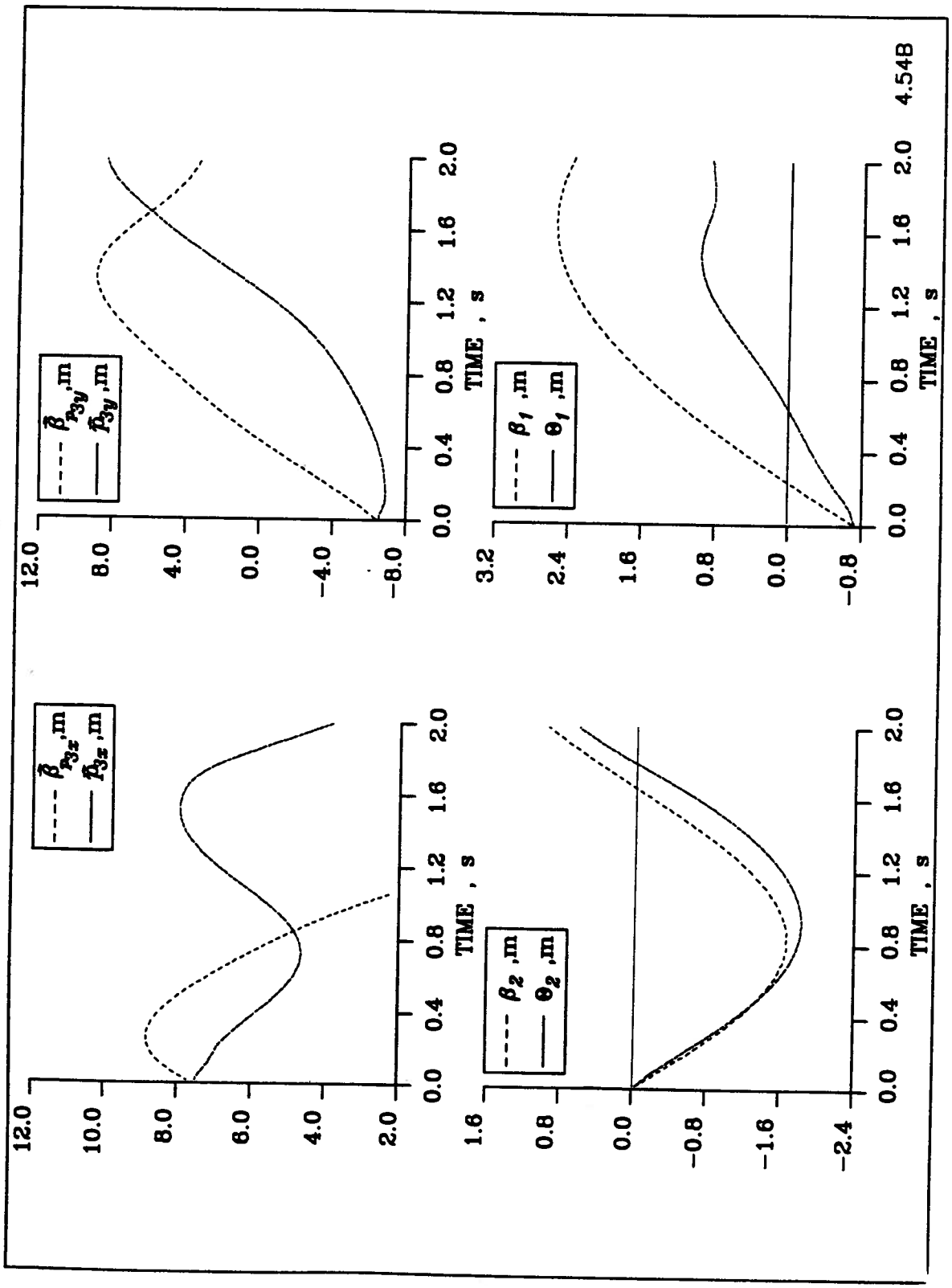

Figure 4.48: (B) Graphs of (from top left figure clockwise) $\beta_{p_{3x}}$ & p_{3x}, $\beta_{p_{3y}}$ & p_{3y}, β_1 & θ_1, β_2 & θ_2, VS time [seconds] for the stationary flexible 2 link manipulator under PD control in nonzero gravity field.

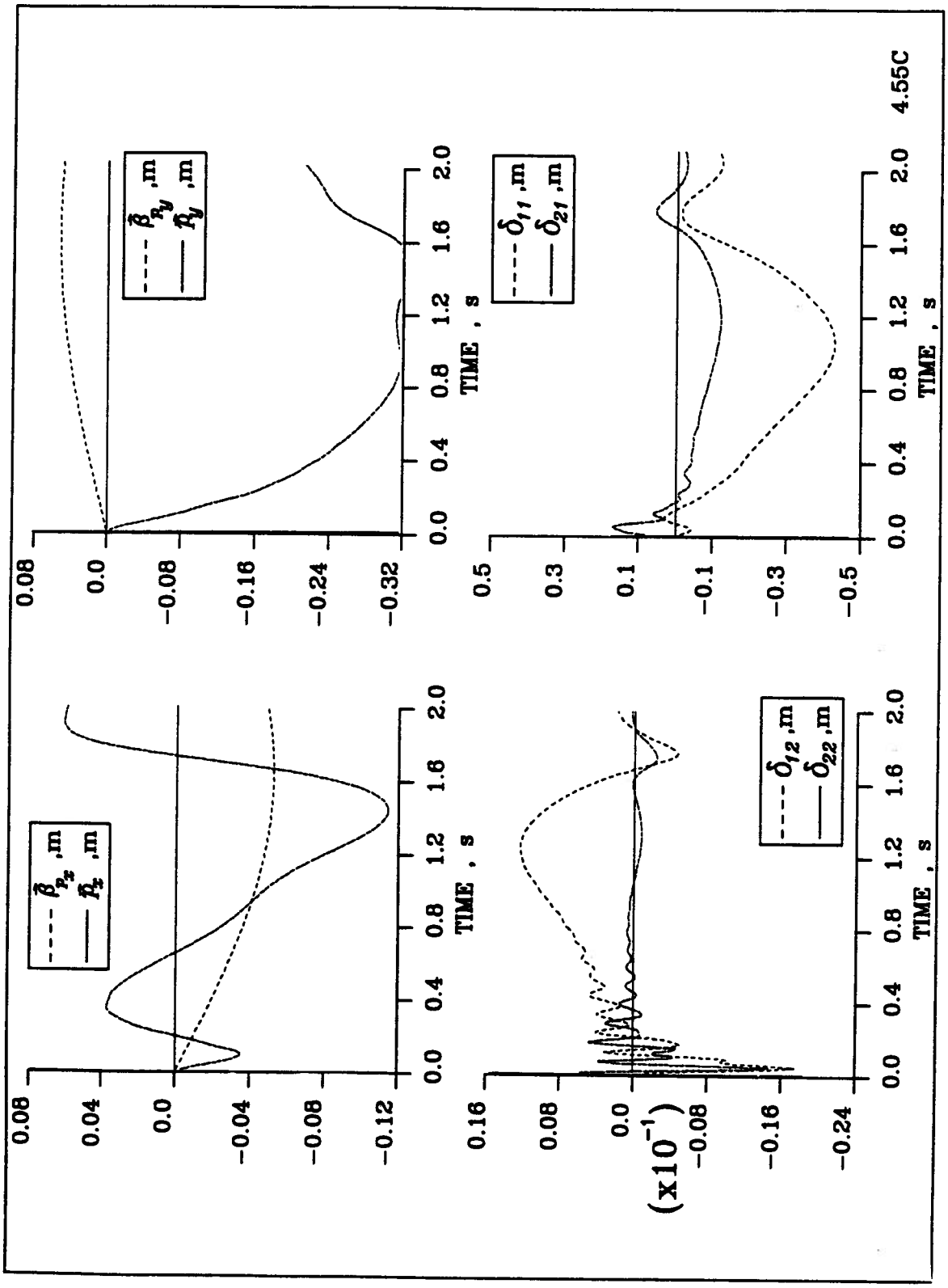

Figure 4.49: (C) Graphs of (from top left figure clockwise) β_{p_x} & p_x, β_{p_y} & p_y, δ_{11} & δ_{21}, δ_{12} & δ_{22}, VS time [seconds] for the stationary flexible 2 Link manipulator under PD control in nonzero gravity field.

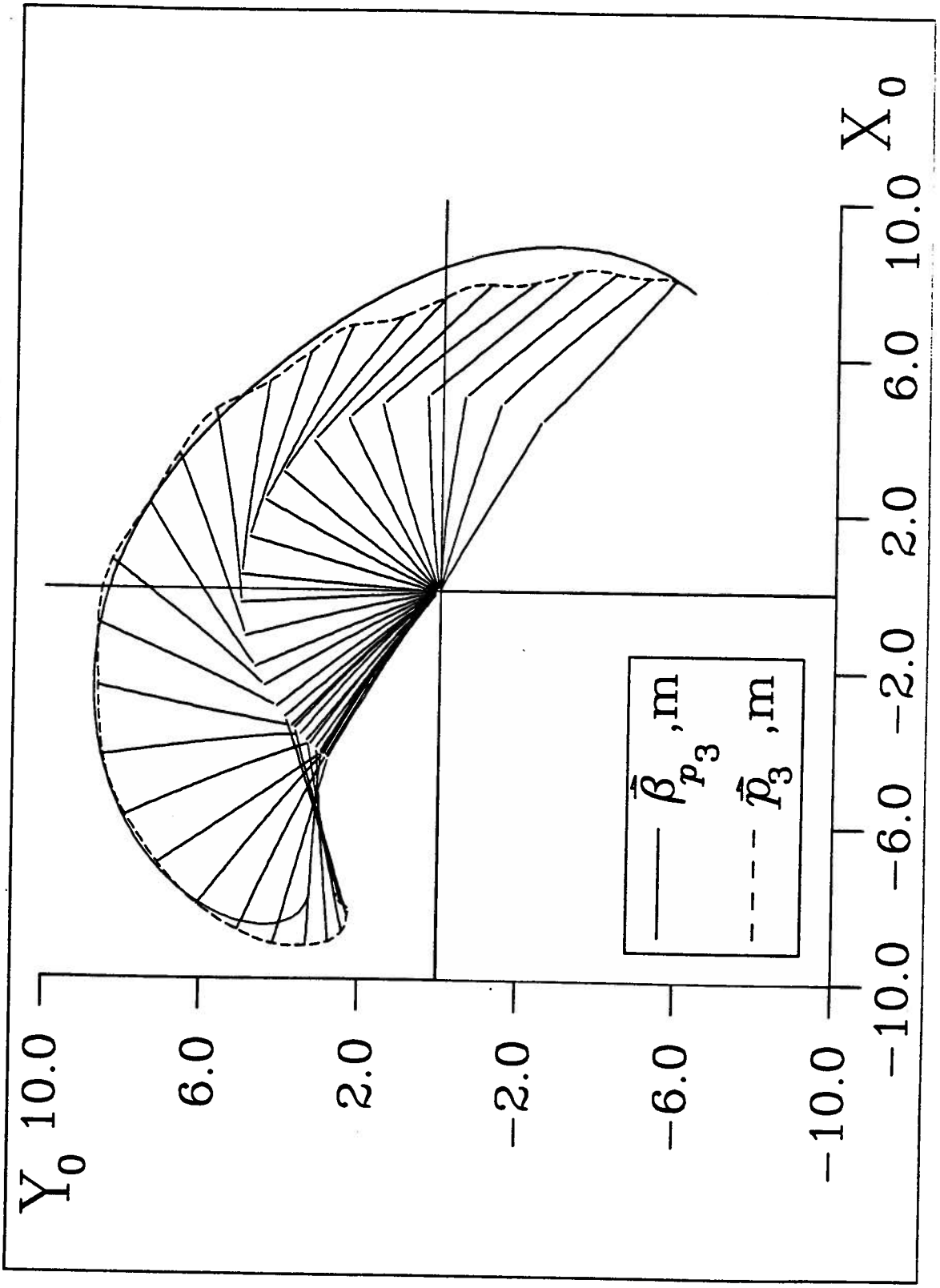

Figure 4.50: (A) Time history response of the manipulator showing the tip and the link positions in the presence of FLT control with the base held fixed doing a full three quadrant slewing maneuver in a nonzero gravity field

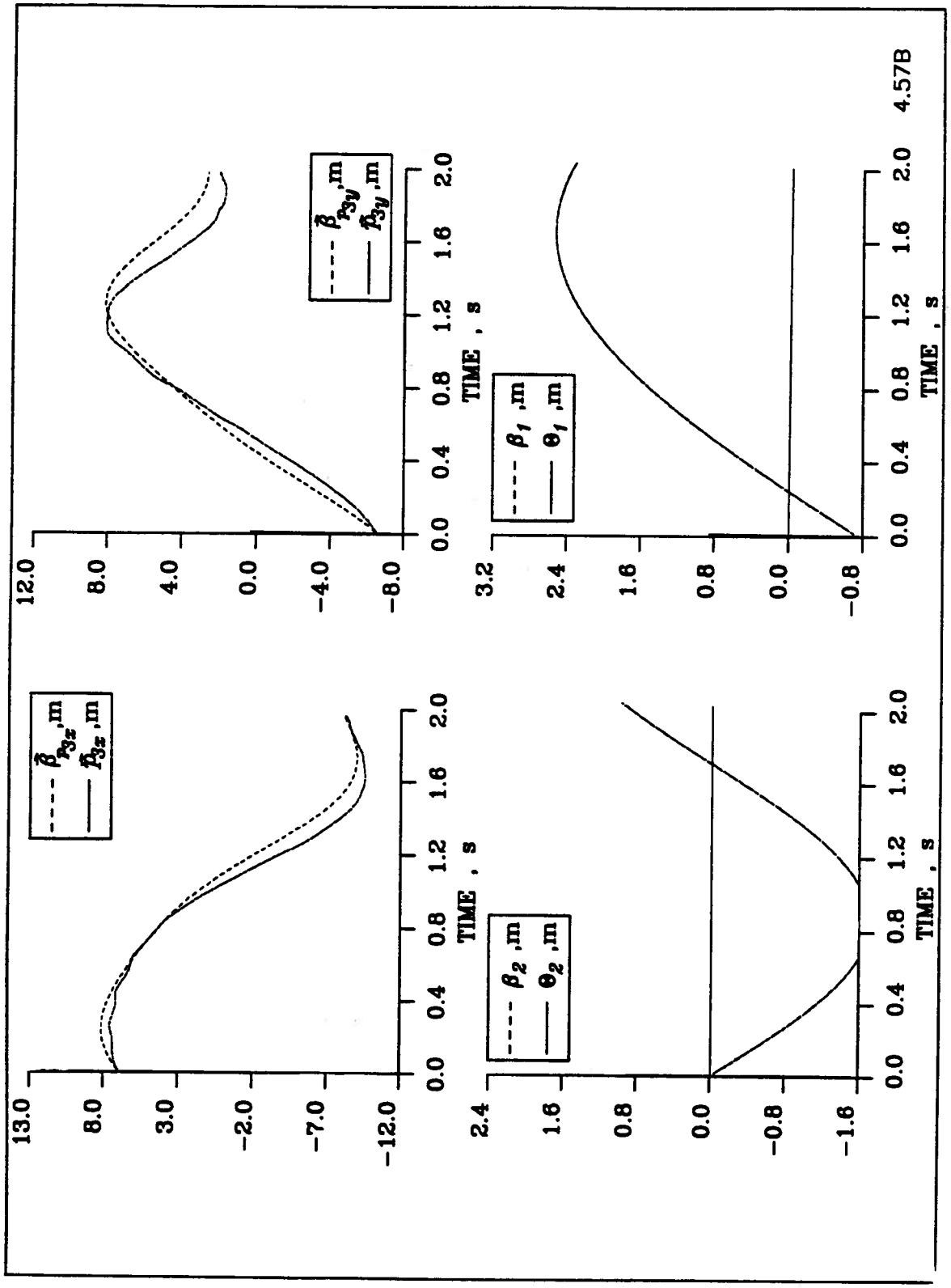

Figure 4.51: (B) Graphs of (from top left figure clockwise) $\beta_{p_{3x}}$ & p_{3x}, $\beta_{p_{3y}}$ & p_{3y}, β_1 & θ_1, β_2 & θ_2, VS time [seconds] for the stationary flexible 2 link manipulator under FLT control in nonzero gravity field.

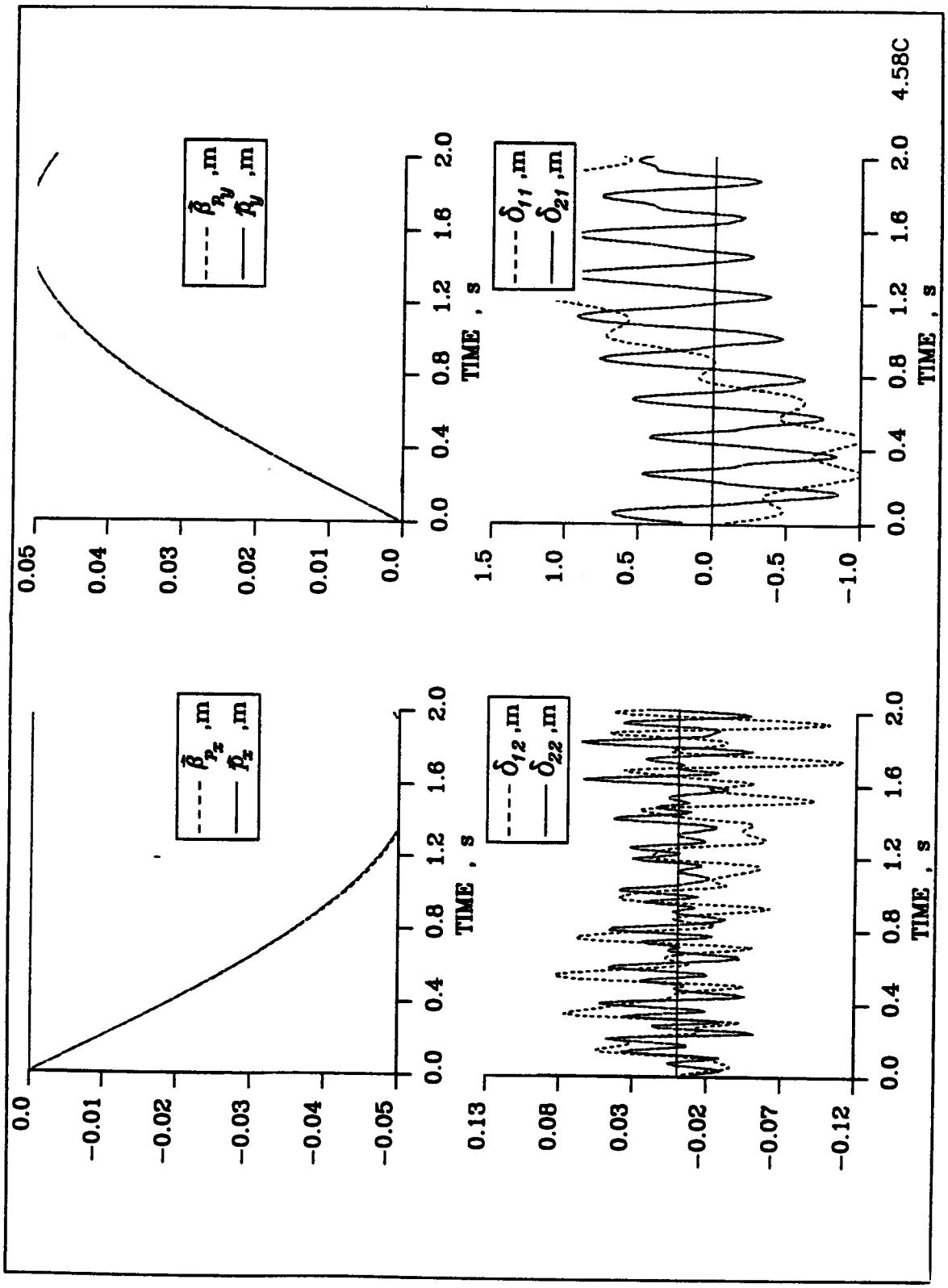

Figure 4.52: (C) Graphs of (from top left figure clockwise) β_{p_x} & p_x, β_{p_y} & p_y, δ_{11} & δ_{21}, δ_{12} & δ_{22}, VS time [seconds] for the stationary flexible 2 link manipulator under FLT control in nonzero gravity field.

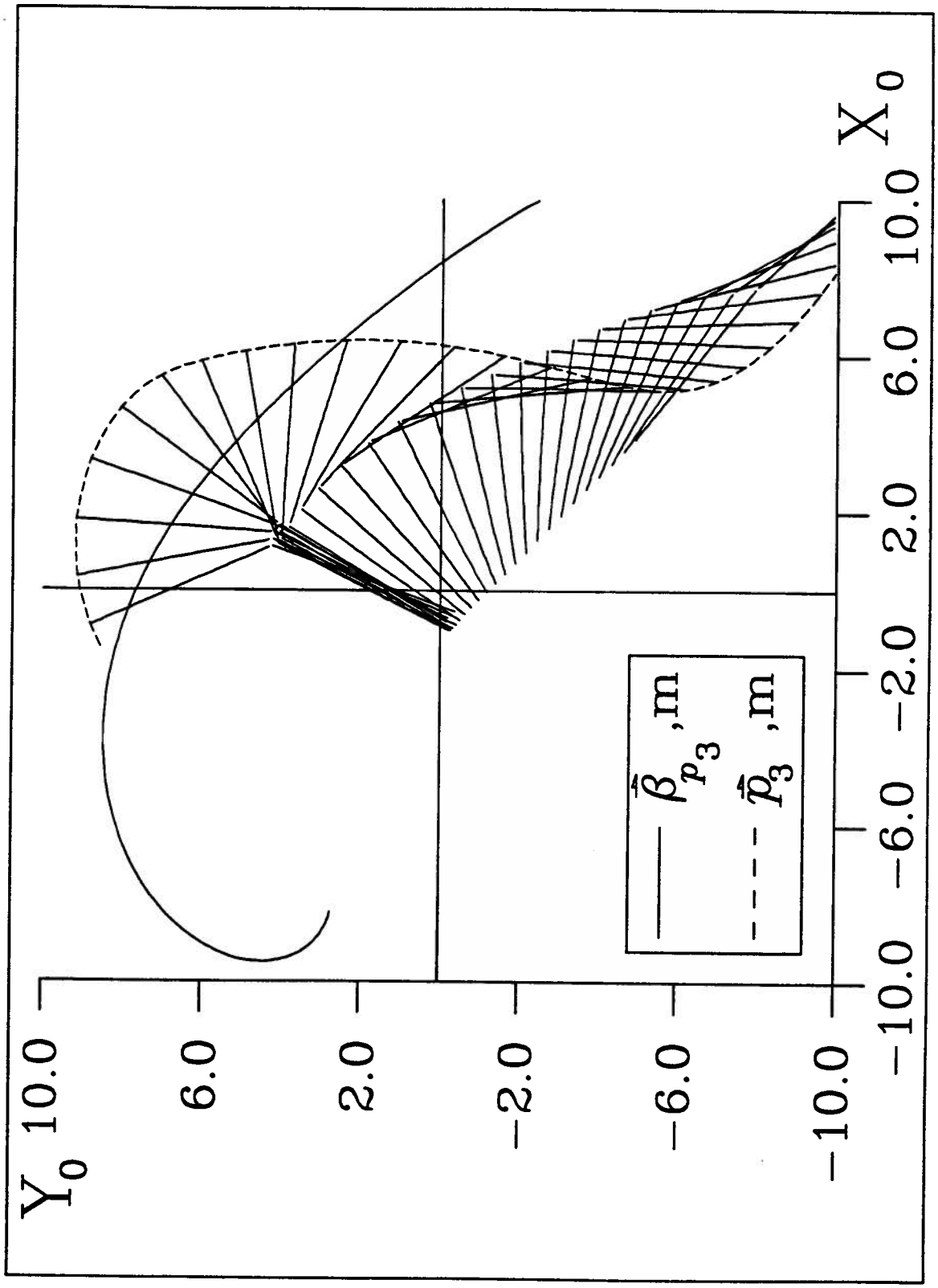

Figure 4.53: (A) Time history response of the manipulator showing the tip and the link positions in the presence of PD control with the base translating as shown doing a full three quadrant slewing maneuver in a nonzero gravity field

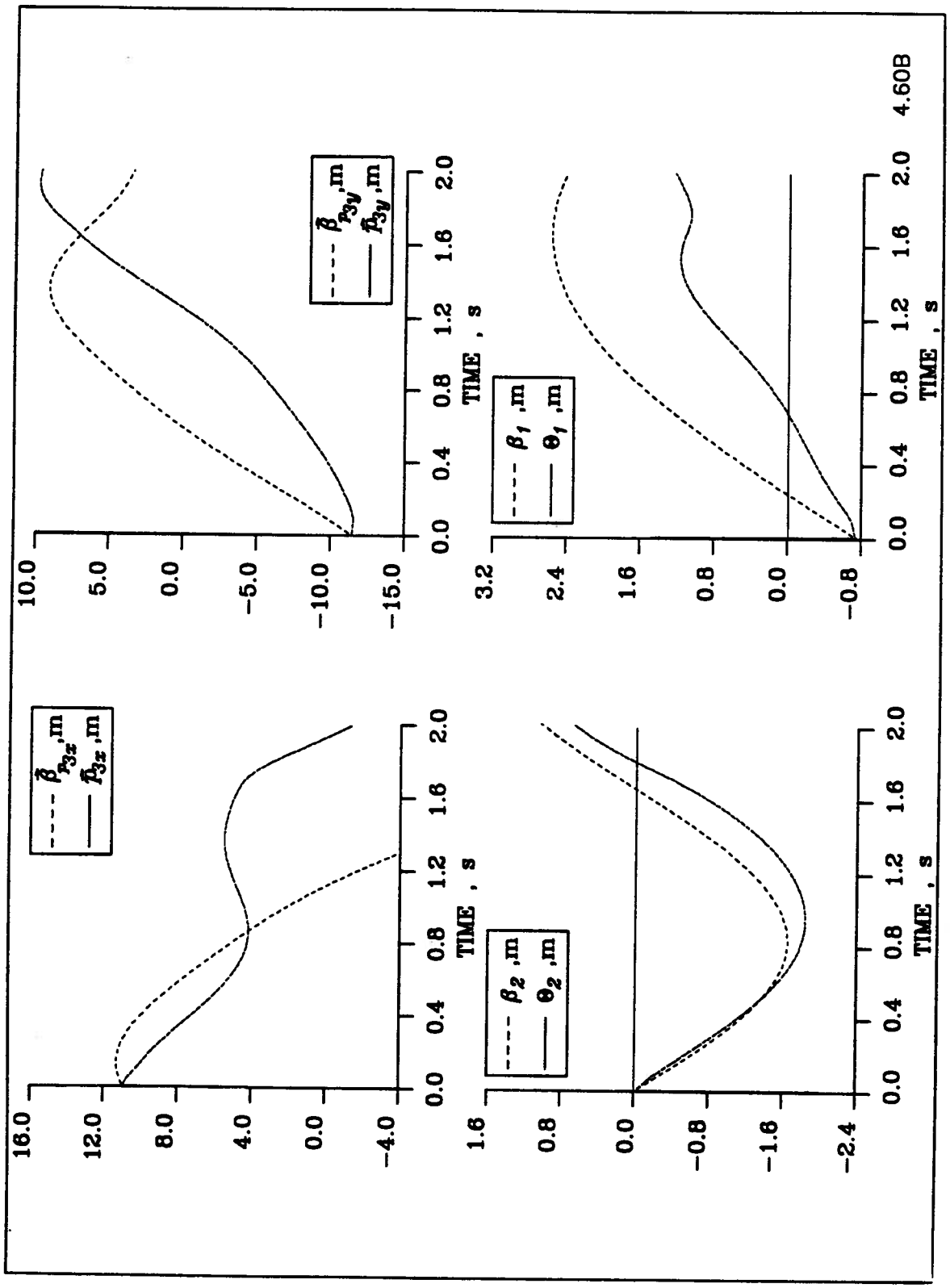

Figure 4.54: (B) Graphs of (from top left figure clockwise) $\beta_{p_{3x}}$ & p_{3x}, $\beta_{p_{3y}}$ & p_{3y}, β_1 & θ_1, β_2 & θ_2, VS time [seconds] for the moving flexible 2 link manipulator under PD control in nonzero gravity field.

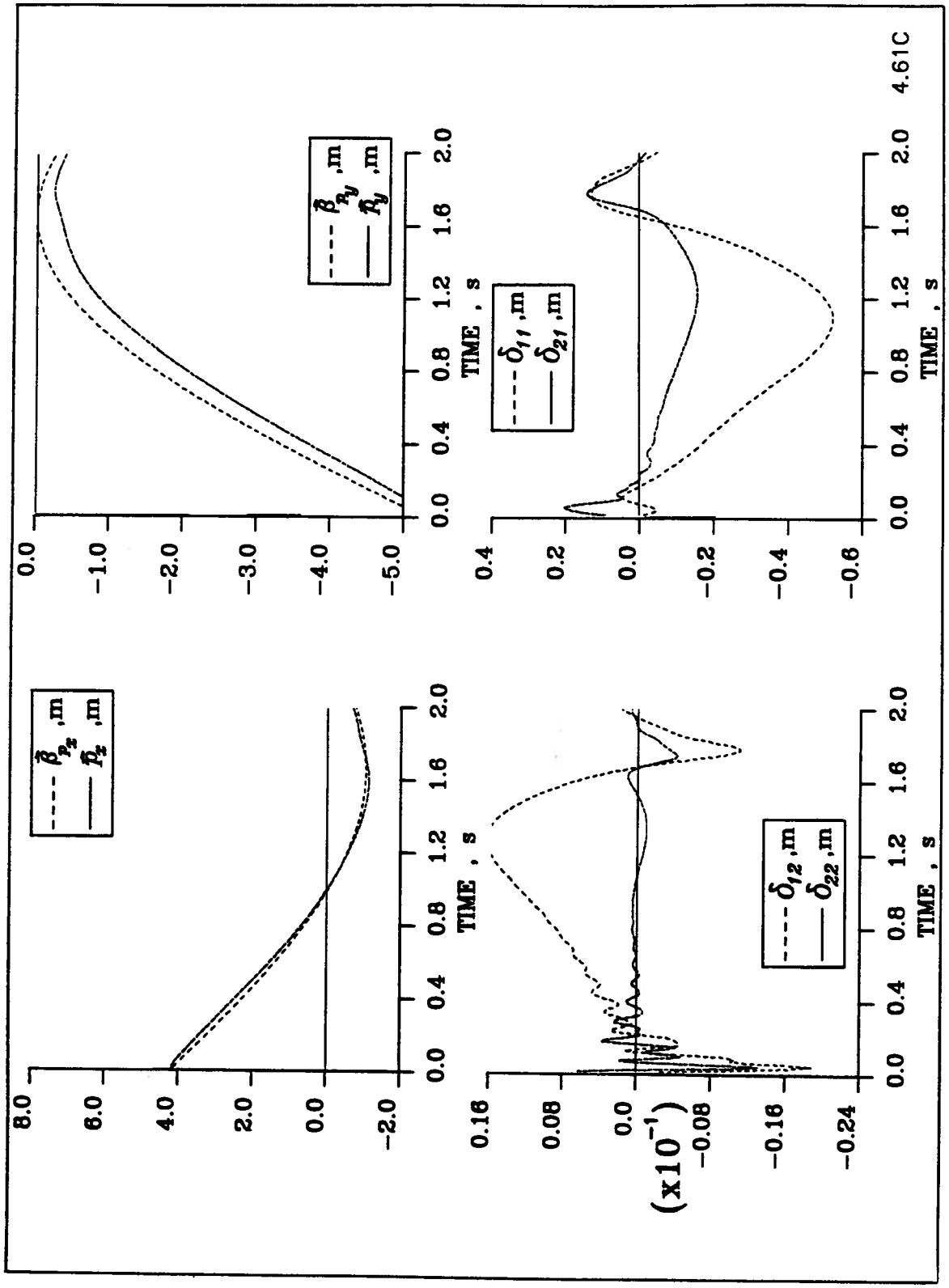

Figure 4.55: (C) Graphs of (from top left figure clockwise) β_{p_x} & p_x, β_{p_y} & p_y, δ_{11} & δ_{21}, δ_{12} & δ_{22}, VS time [seconds] for the moving flexible 2 link manipulator under PD control in nonzero gravity field.

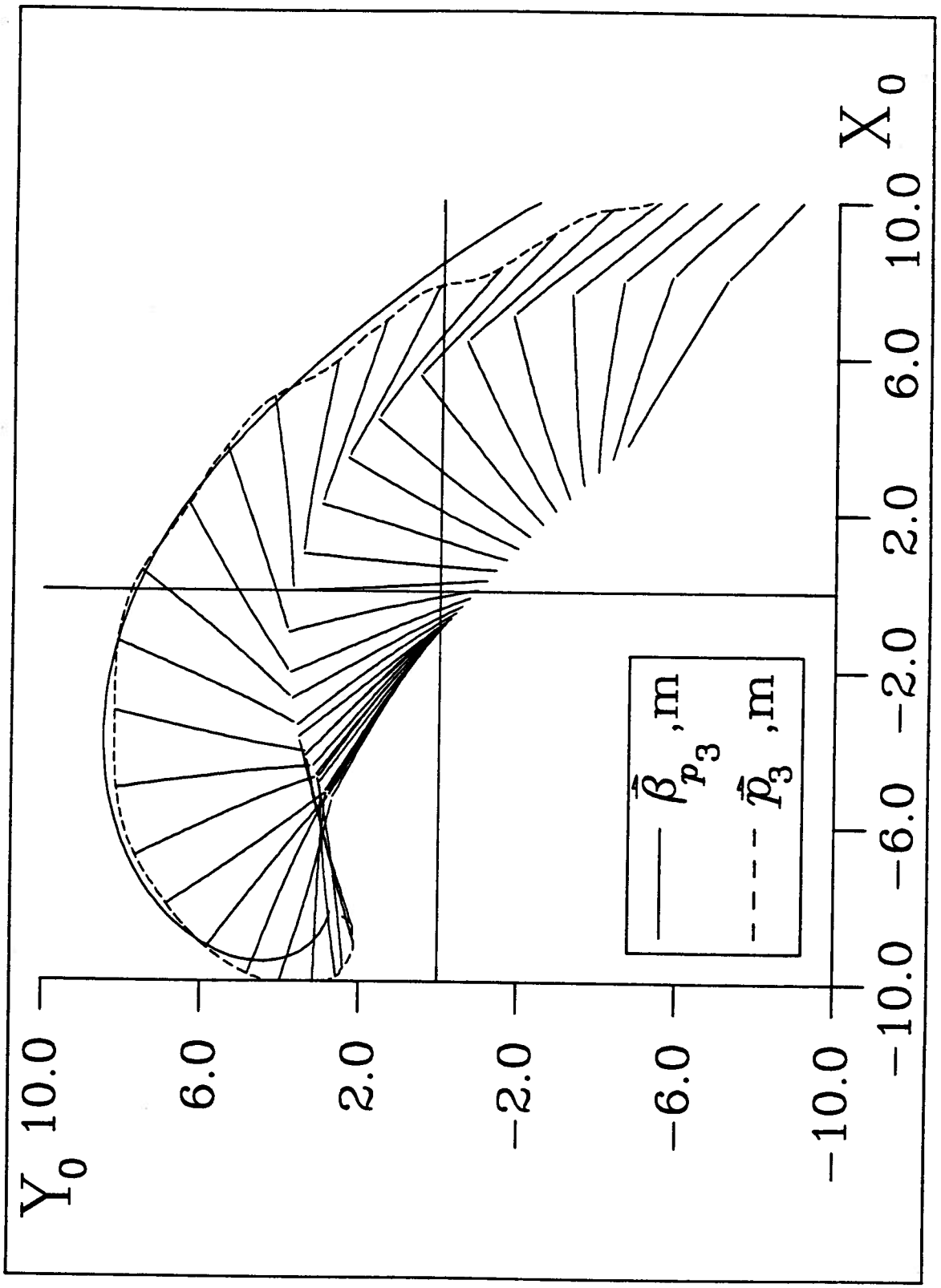

Figure 4.56: (A) Time history response of the manipulator showing the tip and the link positions in the presence of FLT control with the base translating as shown doing a full three quadrant slewing maneuver in a nonzero gravity field

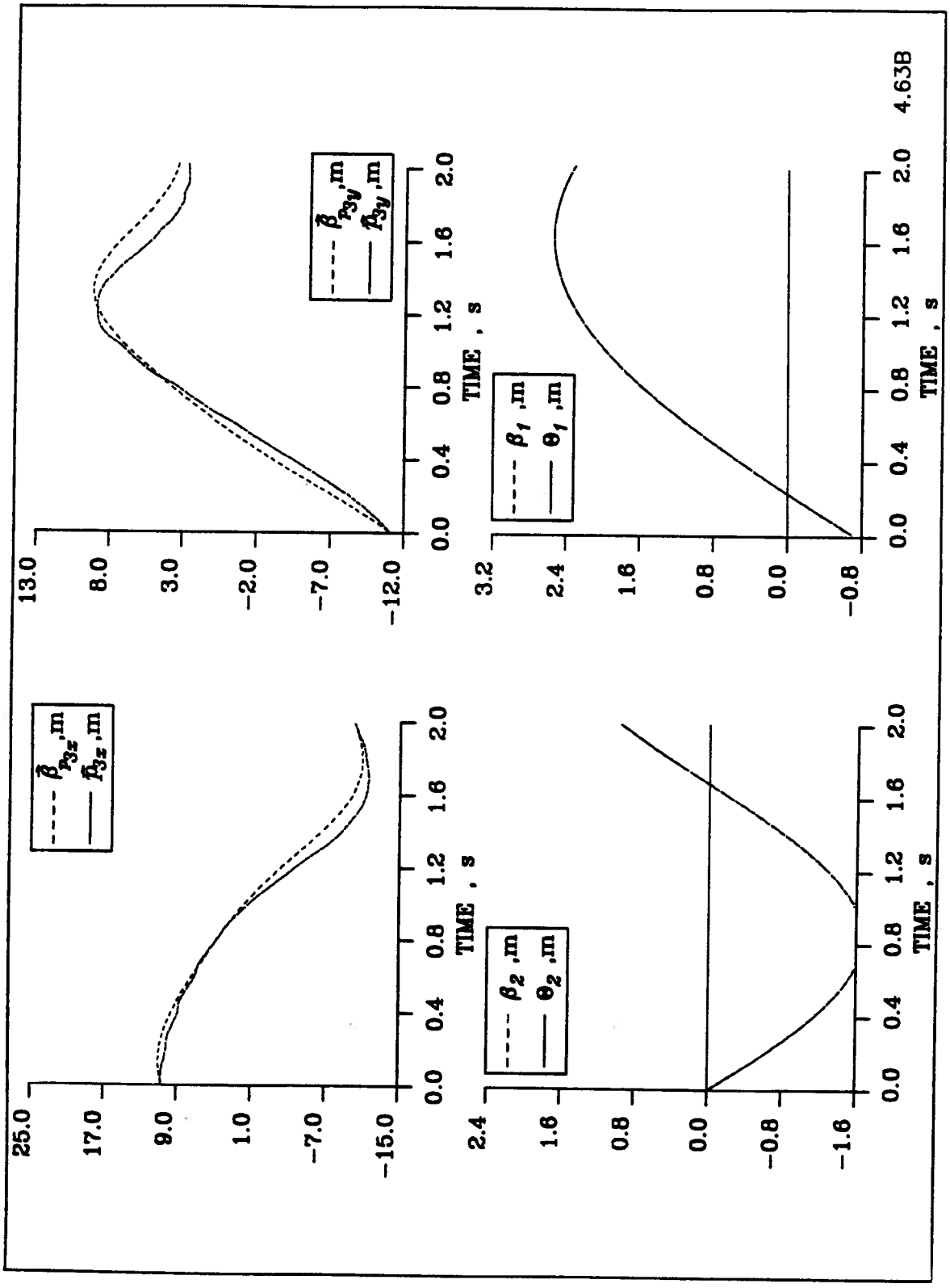

Figure 4.57: (B) Graphs of (from top left figure clockwise) $\beta_{p_{3x}}$ & p_{3x}, $\beta_{p_{3y}}$ & p_{3y}, β_1 & θ_1, β_2 & θ_2, VS time [seconds] for the moving flexible 2 link manipulator under FLT control in nonzero gravity field.

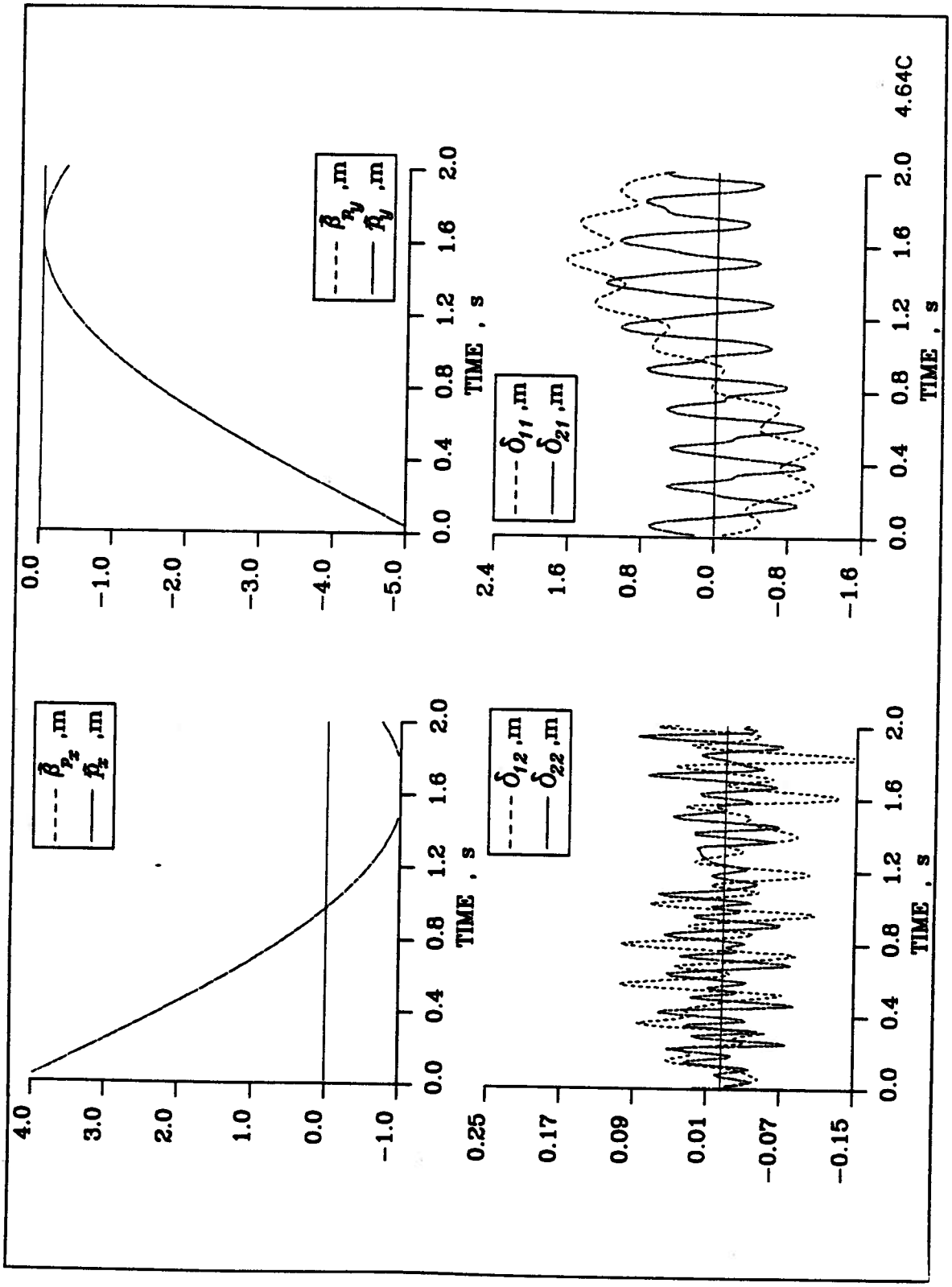

Figure 4.58: (C) Graphs of (from top left figure clockwise) β_{p_x} & p_x, β_{p_y} & p_y, δ_{11} & δ_{21}, δ_{12} & δ_{22}, VS time [seconds] for the moving flexible 2 link manipulator under FLT control in nonzero gravity field.

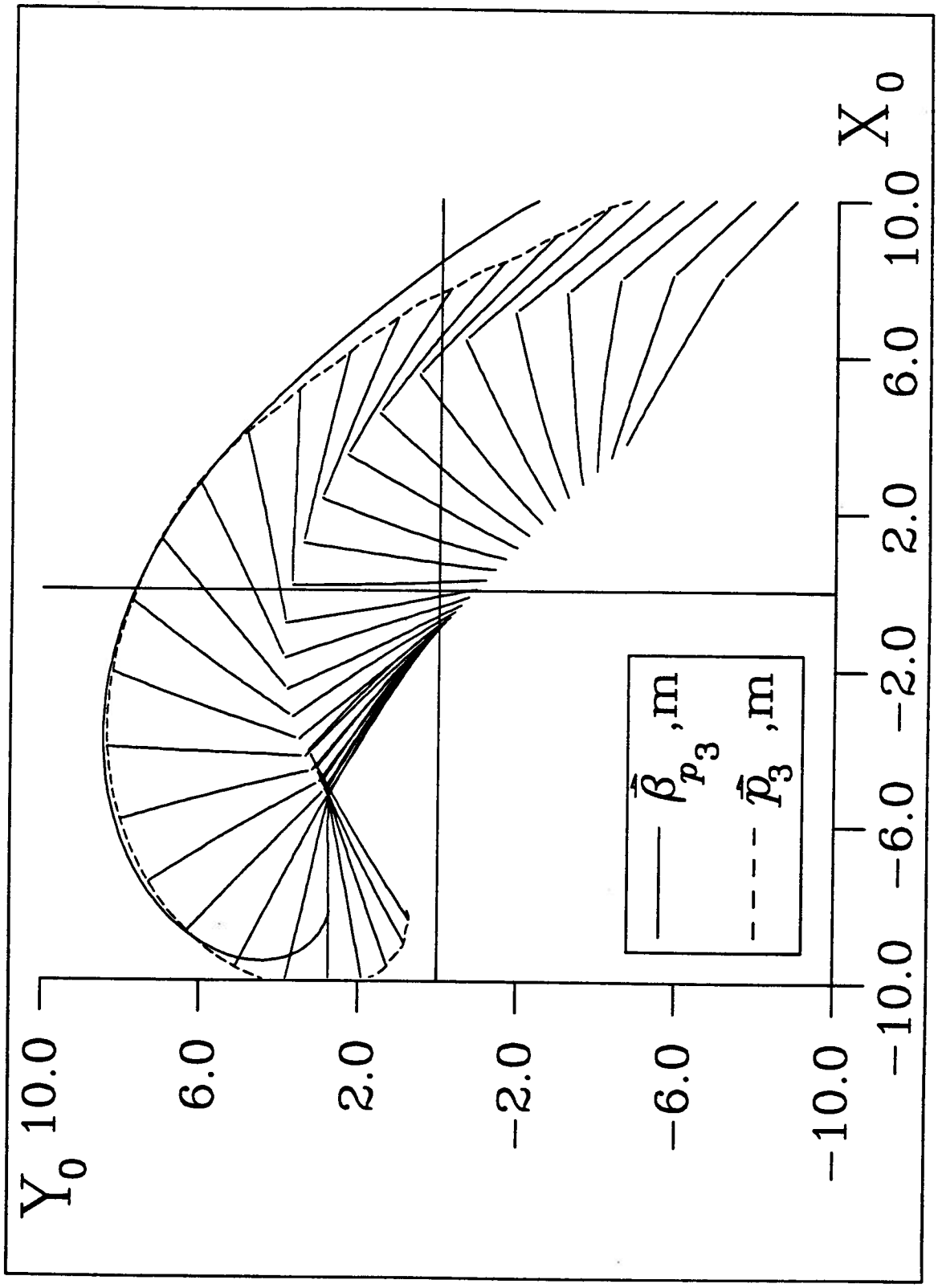

Figure 4.59: (A) Time history response of the manipulator showing the tip and the link positions in the presence of FLT control with the base translating as shown doing a full three quadrant slewing maneuver in a nonzero gravity field with payload

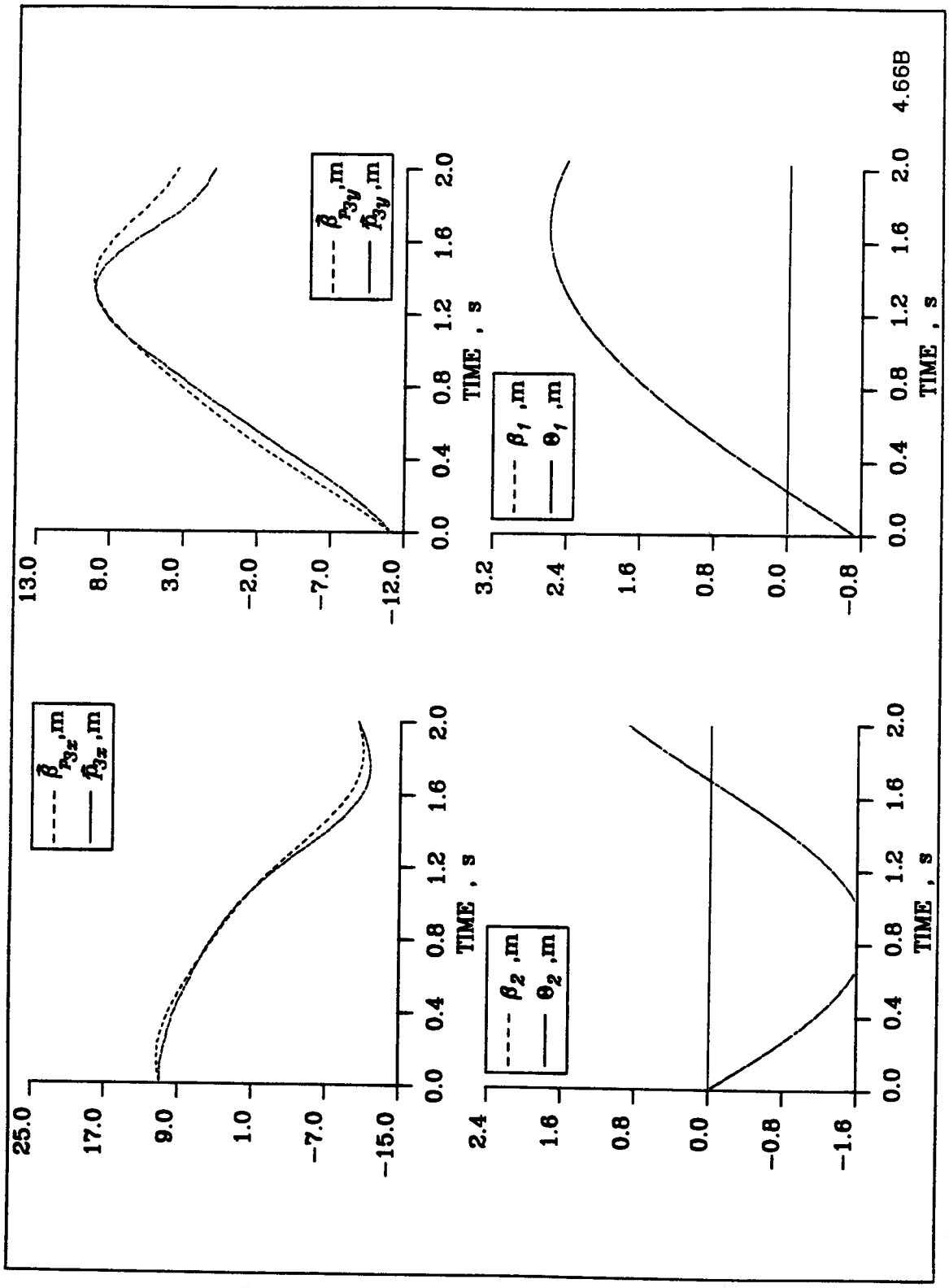

Figure 4.60: (B) Graphs of (from top left figure clockwise) $\beta_{p_{3x}}$ & p_{3x}, $\beta_{p_{3y}}$ & p_{3y}, β_1 & θ_1, β_2 & θ_2, VS time [seconds] for the moving flexible 2 link manipulator under FLT control in nonzero gravity field with payload.

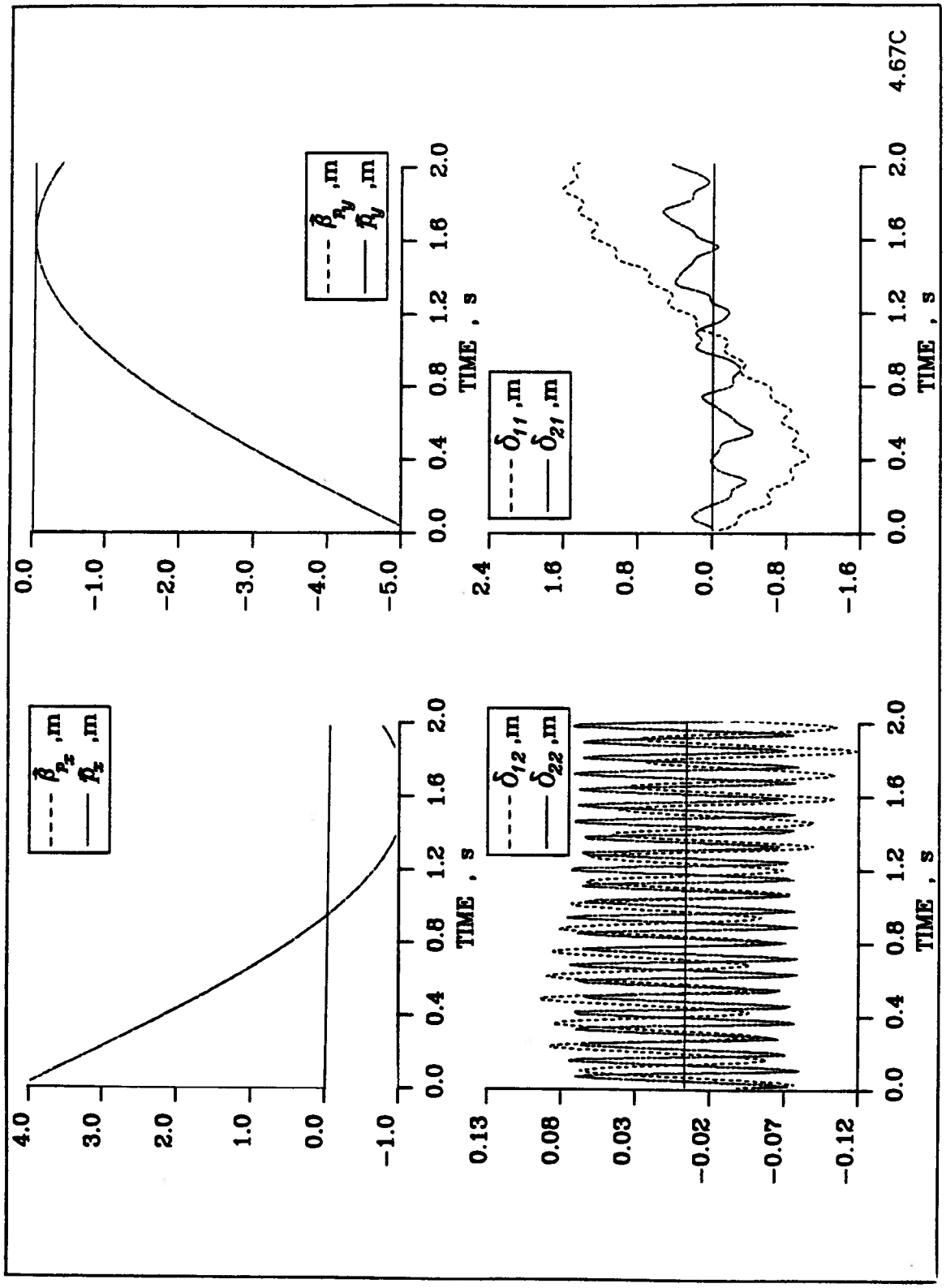

Figure 4.61: (C) Graphs of (from top left figure clockwise) β_{p_x} & p_x, β_{p_y} & p_y, δ_{11} & δ_{21}, δ_{12} & δ_{22}, VS time [seconds] for the moving flexible 2 link manipulator under FLT control in nonzero gravity field with payload.

Chapter 5

CONCLUDING REMARKS

5.1 Summary of Results and Conclusions

Developed in this thesis is a general formulation for investigating planar dynamics and control of a ground based mobile flexible two-link manipulator. This formulation is also applicable to the space station based systems involving flexible slewing appendages that can be modelled as cantilever beams. Two methods were considered for the development of the dynamical equations of motion. The first approach uses homogeneous transformations while the second employs vector analysis to arrive at the kinematic relations for the manipulator, and then the kinetic and potential energies of the system. The use of homogeneous transformations resulted in considerably less effort and proved to be efficient. A computer code is developed for integration of the highly nonlinear, nonautonomous and coupled equations of motion representing a stiff system. Validity of the formulation and the program was assessed through analysis of simple cases. This involved graphical representations of the manipulator in stick figure form showing the configuration and location of the manipulator at discrete time intervals. Although the amount of information that can be obtained through a systematic parametric study is enormous, the focus is on results that may help in establishing trends. In general, the approach is to select a set of realistic parameters representing a highly flexible physical system and subject it to various slew maneuvers and control strategies. The objecctive was to gain some insight into the effectiveness of the control procedures.

During the simulation, it became evident that the system can become unstable with certain parameter values and manipulator configurations. This was also affected by the damping of the rigid degrees of freedom. Of course, to avoid numerical instability it was essential to set the

error tolerance below the critical value (10^{-3} in the present study). The system stiffness also proved to be an important parameter in governing its stability. Under certain combinations of joint and structural flexibilties and slew maneuvers the tip trajectory error was found to be excessive even in the presence of the FLT control. The manipulator flexibility influences the end tip payload position by superimposing a high frequency component over the rigid response.

A major influence on the response of the manipulator is the time history of the slew maneuver. Maneuvers involving high acceleration rates led to greater vibration of the flexible degrees of freedom. This effect was more pronounced due to abrupt changes in velocity at the beginning or the end of a slew maneuver. However, the effect was greatly minimized through introduction of a smooth sinusoidal maneuver profile. The choice of two modes was found to be adequate in representing the tip dynamics. As expected, the presence of payload tended to reduce the vibratory response in the flexible degrees of freedom.

A promising new approach in the nonlinear control of systems is the Feedback Linearization Technique (FLT). The method is straightforeward and the control algorithm in its basic form is simple. For control of a highly nonlinear system such as the mobile flexible manipulator considered here, this approach looks very promising. If all of the state variables are known and used in the control algorithm (Quasi-Closed Loop Control (QOLC)), the rigid degrees of freedom, which are colocally controlled, can be made to follow the desired trajectory with considerable accuracy. The effect of the FLT is to decouple the rigid degrees of freedom from one another and from the flexible ones such that the coupling effects on the rigid body dynamics are eliminated. The converse, of course, is not true since we cannot directly control the flexible degrees of freedom. The flexible body dynamics is thus susceptible to dynamic influence from the rigid degrees of freedom. Hence, the manipulator tip tracking error is strictly due to the combined stuctural flexibility of the links. This fact implies that we require a secondary level of control to deal with the flexible modes.

There are certain aspects which need attention for implementation of the FLT in a practical situation. Demand on computational power is the major one. Fortunately, the computer

technology has made over years, and continues to make, spectacular advances. With parallel processing architecture, real time implementation of control, even for a complex system, may be within reach. Control of the rigid degrees of freedom requires precise knowledge of the correct structural parameters of the manipulator so that an accurate model may be derived for the controller. Furthermore, sensor information for the flexible degrees of freedom must be obtained for the controller. This would require additional filter circuits and other additional hardware. One way to circumvent this problem is to use Quasi-Open Loop Control (QOLC) which utilizes sensor feedback information of the rigid degrees of freedom and calculates the predicted flexible degrees of freedom to be used by the main controller algorithm. This, however, would require additional computational power. Thus success of the FLT is largely dependent on the advances in the computer and software technologies.

5.2 Comments About the Numerical Simulation

There are a number features regarding the simulation program that are worth commenting on, particularly for its future use in studying dynamics and control of mobile flexible manipulators with payload and operating in the gravity field enviornment:

- The program can be used to simulate the links with as many as six modes. Additional modes can be accomodated simply by making the appropriate changes in the relevant subroutines. Only two modes were used in the present study because it offered desireable trade off between the simulation speed and faithful representation of the flexible system dynamics. The mode numbers used can be changed through the PARAMETER statements, using the global ALTER editor command, as described at the beginning of the MAIN routine.

- The program can be used in any system envoirnment that supports the ANSI standard FORTRAN77 assembler language. For use in the UBC-MTSG enviornment, just issue

the commands stated at the start of the MAIN routine, but first be sure to CREATE the required files as stated. To run in the UBC-UNIXG enviornment, the basic assembler and link commands must be modified.

- The program can be joined with the dynamical models of other systems and then simulated simultaneously as one single unified system. The dynamic model of the manipulator, contained in the subroutine FCN and used by the MTSG's integration subroutine GEARB (or IMSL's DIVPAG), may be easily modified by adding the extra terms to the mass matrix **D**, the forcing vector $\vec{F}$ and the over all system state vector $\vec{V}$. Subsequently, the manipulator must be dynamically synthesized with the connecting system via the generalized force vector $\vec{Q}$.

- A useful feature for a highly flexible systems under the influence of externally induced steady state force fields (such as the gravitational field), which has the effect of preloading the system to assume a state of 'deflected' static equilibrium, is the MTSG subroutine HYBRID1 (or the IMSL library subroutine DNEQNF). In general, its purpose is to find the zero of a system in N variables by a modification of the Powell Hybrid Method. Objective here is to evaluate the initial conditions of all the generalized coordinates of the system in static equilibrium under the influence of the gravity. The reason for this is to start the slewing maneuver of the manipulator from a 'true' static equilibrium condition. In other words, now the velocity and acceleration of the generalized coordinates, both flexible and rigid, are zero. Note, however, that the IMSL subroutine DNEQNF works flawlesly with this program. On the other hand, HYBRID1 has not been shown to work properly with this code and requires a certain amount of debugging before use. As a result it has been COMMENTED out and deactivated. This, however, does not seriously effect the results because the stiffness coefficients are relatively high and the slew maneuvers are fast and therefore the generalized forces are high enough to dominate any effects of nonzero initial conditions.

- In the subroutine FCN, which contains the dynamical equations of motion of the manipulator, the forcing vector $\vec{\mathbf{F}}$ is segmented into its basic contributing components and then summed at the end. This greatly facilitates studying the effects of each of the components on the dynamical response of the manipulator simply by blanking certain terms or combinations of terms. Amongst other things, one may study what effect inaccurate modelling will have on the stability and robustness of the FLT control of the manipulator.

5.3 Recommendations for Future Work

The intention of this thesis is to present a relatively general formulation, based on a model of contemporary interest, which will provide some insight into the dynamics and control of the complex and highly nonlinear ground based, mobile, flexible, twolink manipultor. The tip tracking of moving flexible manipulators have yet to be studied in sufficient detail, especially under the FLT control. This is a new area of research which promises robust, efficient, control of highly nonlinear systems. To investigate this as well as other areas of interest a few suggestions are listed below:

- Extension of the model to three dimension would improve its verstility through application to a large class of systems. Inplane and out-of-plane degrees of freedom, including torsion of the manipulator links, would enhance the usefulness of the model significantly. The FLT control of such systems would represent an important advance in the field.

- The problem of computational time and cost is a major consideration when performing dynamical simulations of complicated nonlinear systems with large numbers of degrees of freedom. Development of a parallel processing enviornment would go a long way in increasing the speed and the real time implementation of the FLT.

- Robust control of the rigid degrees of freedom is strongly dependent on the accuracy of the model. There is considerable scope for parametric studies in this area. As mentioned earlier, the model subroutine FCN is structured to facilitate the investigation of the effects

of incorrect modelling of the manipulator being controlled. The effect of inaccurate model on the tip trajectory is an important avenue for future study.

- There is a considerable scope for detailed parametric study to assess the influence of;
  - structural properties;
  - differential equation solver parameters;
  - time histories of slew trajectories;
  - FLT control parameters;
  - payload mass;
  - gravitational acceleration.
- In order to minimize vibration of the flexible links, it is suggested that a secondary controller be built into the base and the joints. Its purpose would be to superimpose, on the main controller action, a secondary damping action to improve tracking of the manipulator's tip trajectory. This approach can be easily tested using the existing program.
- In the problem formulation chapter. two methods of deriving the dynamical equations of motion were suggested. One employed the use of homogeneous transformation, a more direct method. The other relies on the vector approach, an appearantly more general, less direct and more labour intensive method. It would be useful to investigate the pros and cons of these two, as well as other approaches. The comparison may be in terms of efficiency of derivation and compatibility with commercially available softwares, to expedite as well as synthesize derivation and simulation processes.
- End effector compliance and force control during pick/place operations of industrial robots is a very important area in robotic design [38], particularly if high speed, delicate and precise operations are involved. This would involve introducing constraint relations. Such studies, though challenging, should prove to be equally satisfying.

Bibliography

[1] Rivin, E.I., *Mechanical Design of Robots*, McGraw Hill Book Company, 1988.

[2] Andeen, G.B., *Robot Design Handbook*, McGraw Hill Book Company, 1988.

[3] Millar, R.K.A., Graham, W.R., and Vigneron, F.R., "Simulation of the Motion of a Shuttle Attached Flexible Manipulator Arm", *Proceedings of the 10th World Congress on System Simulation and Scientific Computation*, Montreal, Canada, August 1982, Editor: W.F. Ames, Published by Association for Mathematics and Computers in Simulation, pp. 225-277.

[4] Modi, V.J., "Attitude Dynamics of Satellites with Flexible Appendages - A Brief Review", *Journal of Spacecraft and Rocket*, Vol.II, No.II, November 1974, pp. 743-751.

[5] Chan, J.K., *Dynamics and Control of an Oriting Space Platform Based Mobile Flexible Manipulator*, M.A.Sc. Thesis, University of British Columbia, 1990.

[6] Mah, H., *On the Nonlinear Dynamics of a Space Platform Based Mobile Flexible* Manipulator, Ph.D. Thesis, University of British Columbia, 1992.

[7] Cannon Jr., R.H., and Schmitz E., "Initial Experiments on the End-Point Control of a Flexible One-Link Robot", *The International Journal of Robotics Research*, Vol. 3, No. 3, Fall 1984, pp. 62-75.

[8] Cannon Jr., R.H., and Rovner, D.M., "Experiments Toward On-Line Identification and Control of A Very Flexible One-Link Manipulator", *The International Journal of Robotics Research*, Vol. 6, No. 4, Winter 1987, pp. 3-19.

[9] Binford, T.O., and Cannon Jr. R.H., *First Annual Report on End Point Control of Flexible Robots*, Prepared for Air Force Wright Aeronautical Laboratories, Stanford University, Report No. 13389-01-00, 1983.

[10] DeCarlo, R.A., Zak, S.H., and Matthews, G.P., "Variable Structure Control of Nonlinear Multivariable Systems", *Proceedings of the IEEE*, Vol. 76, No. 3, March 1988, pp.212-232.

[11] Balestrino, A., De Maria, G., and Sciavicco, "An Adaptive Model Following Control for Robotic Manipulators", *Journal of Dynamic Systems, Measurements, and Control*, Vol. 105, September 1983, pp. 143-151.

[12] Leininger, G.G., and Wang, S., "Pole Placement Self-Tuning Control of Manipulators", *IFAC Symposium on Comuter Aided Design of Multi-Variable Technological Systems*, September 15-17, 1982, G. Leininger Symp. Editor, West Lafayette, IN.

[13] Rovner, D.M., and Franklin, G.F., "Experiments in Load-adaptive Control of a Very Flexible One-link Manipulator", *Automatica*, Vol. 24, No. 4, 1988, pp.541-548.

[14] Spong, M.W., "Modeling and Control of Elastic Joint Robots", *Journal of Dynamic Systems, Measurements, and Control*, Vol. 109, December 1987, pp.310-319.

[15] Meirovitch, L., *Elements of Vibration Ananlysis*, Mac Graw Hill Book Company, 1986.

[16] Meirovitch, L., "Analytical Methods in Vibration", The MacMillan Co., 1967.

[17] Thomson, W.T., *Theory of Vibration with Applications*, Prentice Hall Incorporated, 1972.

[18] Paul, R.P., *Robot Manipulators: Mathematics Programming and Control*, The MIT Press, 1981.

[19] Fu K.S., Gonzalez R.C., Lee C.S.G., *Robotics: Control, Sensing, Vision and Intelligence*, McGraw Hill Book Co., 1987.

[20] Goldstein, H., *Classical Mechanics*, Addison-Wesley Publishing Company, 1965.

[21] Meriam, J.L., *Dynamics*, John Wiley and Sons Inc., 1975.

[22] Wolfram, S., "Mathematica: A System for Doing Mathematics by computer", 2nd Edition, Addison-Wesley Publishing Company, 1991.

[23] Slotine, J.E. and Sastry, S.S., "Tracking Control Non-linear Systems using Sliding Surfaces with Application to Robot Manipulators", *International Journal of Control*, Vol. 38, No. 2, 1983, pp. 465-492.

[24] Slotine, J.E., "Sliding Controller Design for Non-linear Systems", *International Journal of Control*, Vol. 40, No. 2, 1984, pp. 421-434.

[25] Slotine, J.E., "The Robust Control of Robot Manipulators", *International Journal of Robotic Research*, Vol. 4, No. 2, 1985, pp. 49-64.

[26] Slotine, J.E., and Li, W., "On the Adaptive Control of Robotic Manipulators", *International Journal of Robotics Research*, Vol. 6, No. 3, 1987, pp. 49-59.

[27] Freund, E., "The structure of Decoupled Nonlinear Systems", *International Journal of Control*, Vol. 21, No. 3, 1975, pp. 443-450.

[28] Freund, E., "Fast Nonlinear Control with Arbitrary Pole-Placement for Industrial Robots and Manipulators", *The International Journal of Robotics Research*, Vol. 1, No. 1, 1982, pp. 65-78.

[29] Spong, M.W., "Modeling and Control of Elastic Joint Robots", *Journal of Dynamic Systems, Measurements, and Control*, Vol. 109, December 1987, pp.310-319.

[30] Beijczy, A.K., *Robot Arm Dynamics and Control*, JPL TM 33-669, California Institute of Technology, Pasadena, California, 1974.

[31] Singh, S.N., and Schy, A.A., "Invertibility and Robust Nonlinear Control of Robotic System", *Proceedings of 23rd Conference on Decision and Control*, Las Vegas, Nevada, December 1984, pp. 1058-1063.

[32] Spong, M.W., and Vidyasagar, M., "Robust Linear Compensator Design for Nonlinear Robotic Control", *Proceedings of IEEE Conference on Robotics and Automation*, St. Louis. Missouri, March 1985, pp. 954-959.

[33] Spong, M.W., and Vidyasagar, M., "Robust Nonlinear Control of Robot Manipulator", *Proceedings of the 24th IEEE Conference on Decision and Control*, Fort Lauderdale. Florida, December 1985, pp. 1767-1772.

[34] Karray, F., Modi, V.J., and Chan, J.K., "Inverse control of Flexible Orbiting Manipulators", *Proceedings of the American Control Conference*, Boston, Mass., June 1991, Editor: A.G. Ulsoy, pp. 1909-1912.

[35] Modi, V.J., Karray, F., and Chan, J.K., "On the Control of a Class of Flexible Manipulators Using Feedback Linearization Approach", *42nd Congress of the International Astronautical Federation*, October, 1991, Montreal, Canada, Paper No. IAF-91-324.

[36] Gear, C.W., *Numerical Initital Value Problems in Ordinary Differential Equations*, Prentice Hall Inc., Englewood Cliffs, NJ, 1971.

[37] Rice, J.R., *Numerical Methods, Software, and Analysis: IMSL Reference Edition*, McGraw Hill Book Company, 1983.

[38] Latournell, D.J., Cherchas, D.B., "Force and Motion Control of a Single Flexible Link Manipulator Link", *CAMROL, Dept. of Mechanical Engineering*, University of B.C., Oct.1990.

[39] Lee, C.S.G., "On the Control of Robot Manipulators", *Dept. of Electrical and Computer Engineering*, University of Michigan, 1984.

[40] Ogata, K., *Discrete-Time Control Systems*, Prentice-Hall Incorporated, 1987.

Appendix A

KINETIC ENERGY EQUATIONS

Following are the total kinetic energy expressions for the earth based flexible manipulator links 1 and 2 in terms of their physical parameters and generalized coordinates:

LINK 1

$$
\begin{aligned}
T_1 &= \frac{1}{2}\int_{M_1} v_1^2 dm_1 \\
&= \frac{m_1 l_1^2}{6}\dot{\theta}_1^2 + \dot{\theta}_1 \sum_{j=1}^{m} \Phi_{X1j}\dot{\delta}_{1j} \\
&\quad + \frac{1}{2}\dot{\theta}_1^2 \sum_{j=1}^{m} \Phi_{S1j}\delta_{1j}^2 + \frac{1}{2}\sum_{j=1}^{m} \Phi_{S1j}\dot{\delta}_{1j}^2 \\
&\quad - \dot{\theta}_1 \left(S_1\dot{p}_y + C_1\dot{p}_x\right)\sum_{j=1}^{m} \Phi_{1j}\delta_{1j} \\
&\quad - \left(S_1\dot{p}_x - C_1\dot{p}_y\right)\left(\dot{\theta}_1\frac{m_1 l_1}{2} + \sum_{j=1}^{m} \Phi_{1j}\dot{\delta}_{1j}\right) \\
&\quad + \frac{1}{2}m_1\left(\dot{p}_x^2 + \dot{p}_y^2\right).
\end{aligned}
$$

LINK 2

$$
\begin{aligned}
T_1 &= \frac{1}{2}\int_{M_2} v_2^2 dm_2 \\
&= \frac{1}{2}\dot{\alpha}_{12}^2\frac{m_2 l_2^2}{3} + \dot{\alpha}_{12}\sum_{j=1}^{m} \Phi_{X2j}\dot{\delta}_{2j} + \frac{1}{2}\sum_{j=1}^{m} \Phi_{S2j}\dot{\delta}_{2j} \\
&\quad + \frac{1}{2}\dot{\alpha}_{12}^2 \sum_{j=1}^{m} \Phi_{S1j}\delta_{1j}^2 \\
&\quad + \frac{1}{2}m_2\left(\left(l_1\dot{\theta}_1 + \dot{y}_{l_1}\right)^2 + \dot{y}_{l_1}^2\dot{\theta}_1^2 + \dot{p}_x^2 + \dot{p}_y^2\right) \\
&\quad + \left(\dot{\alpha}_{12}\dot{\theta}_1 y_{l_1}\sum_{j=1}^{m} \Phi_{2j}\delta_{2j} + \left(\frac{m_2 l_2}{2}\dot{\alpha}_{12} + \sum_{j=1}^{m} \Phi_{2j}\dot{\delta}_{2j}\right)\left(l_1\dot{\theta}_1 + \dot{y}_{l_1}\right)\right) C_2
\end{aligned}
$$

$$
\begin{aligned}
&+\left(\left(\frac{m_2 l_2}{2}\dot{\alpha}_{12}+\sum_{j=1}^{m}\Phi_{2j}\dot{\delta}_{2j}\right)y_{l_1}\dot{\theta}_1-\dot{\alpha}_{12}\left(l_1\dot{\theta}_1+\dot{y}_{l_1}\right)\sum_{j=1}^{m}\Phi_{2j}\delta_{2j}\right)S_2\\
&-\left(\frac{m_2 l_2}{2}\dot{\alpha}_{12}+\sum_{j=1}^{m}\Phi_{2j}\dot{\delta}_{2j}\right)\left(S_{12}\dot{p}_x-C_{12}\dot{p}_y\right)\\
&-\dot{\alpha}_{12}\sum_{j=1}^{m}\Phi_{2j}\delta_{2j}\left(S_{12}\dot{p}_y+C_{12}\dot{p}_x\right)\\
&-m_2\left(l_1\dot{\theta}_1+\dot{y}_{l_1}\right)\left(S_1\dot{p}_x-C_1\dot{p}_y\right)\\
&-m_2 y_{l_1}\dot{\theta}_1\left(S_1\dot{p}_y+C_1\dot{p}_x\right).
\end{aligned}
$$

Total kinetic energy of the system is given by

$$T = T_1 + T_2.$$

The contribution of payload mass m_P and of the mobile base m_B are included, in the simulation code, by adding the effect of the point mass to the inertia terms for link 2 and for the base. The joint mass is assumed negligible with respect to the mass of the links.

Appendix B

POTENTIAL ENERGY

The total potential energy expressions for the two-link manipulator can be written as:

LINK 1

$$U_1 = \sum_{j=1}^{m} \Phi_{D1j} \delta_{1j}^2 + \frac{m_1 l_1}{2} g S_1 + g C_1 \sum_{j=1}^{m} \Phi_{1j} \delta_{1j} + g m_1 p_y .$$

LINK 2

$$U_2 = \sum_{j=1}^{m} \Phi_{D2j} \delta_{2j}^2 + g m_2 (l_1 S_1 + y_{l_1} C_1) + g m_2 p_y + \frac{1}{2} g m_2 l_2 S_{12} + g C_{12} \sum_{j=1}^{m} \Phi_{2j} \delta_{2j} .$$

where

$$U = U_1 + U_2$$

$$= \text{Total flexural and gravitational potential energy of the system .}$$

Appendix C

EQUATIONS OF MOTION

The various contributions to the governing differential equations from the inertia, gyroscopic, centripetal, coriolis and other forces as well as their coupling effects are summarized below:

$$
\begin{aligned}
f_{TD_1 p_x} &= -\dot{\theta}_1^2 \left(\frac{m_1 l_1}{2} C_1 - S_1 \sum_{j=1}^{m} \Phi_{1j} \delta_{1j} \right) - 2\dot{\theta}_1 C_1 \sum_{j=1}^{m} \Phi_{1j} \dot{\delta}_{1j}; \\
f_{TD_1 p_y} &= -\dot{\theta}_1^2 \left(\frac{m_1 l_1}{2} S_1 + C_1 \sum_{j=1}^{m} \Phi_{1j} \delta_{1j} \right) - 2\dot{\theta}_1 S_1 \sum_{j=1}^{m} \Phi_{1j} \dot{\delta}_{1j}; \\
f_{TD_1 \theta_1} &= \dot{\theta}_1 \left(2 \sum_{j=1}^{m} \Phi_{S1j} \delta_{1j} \dot{\delta}_{1j} + (S_1 \dot{p}_x - C_1 \dot{p}_y) \sum_{j=1}^{m} \Phi_{1j} \delta_{1j} \right) \\
&\quad - (S_1 \dot{p}_y + C_1 \dot{p}_x) \left(\frac{m_1 l_1}{2} \dot{\theta}_1 - \sum_{j=1}^{m} \Phi_{1j} \dot{\delta}_{1j} \right); \\
f_{TD_1 \delta_{1k}} &= -\dot{\theta}_1 (S_1 \dot{p}_y + C_1 \dot{p}_x) \Phi_{1k}; \\
f_{TD_1 \theta_2} &= 0; \\
f_{TD_1 \delta_{2k}} &= 0; \\
f_{TD_2 p_x} &= -\left(\frac{m_2 l_2}{2} \dot{\alpha}_{12} + \sum_{j=1}^{m} \Phi_{2j} \dot{\delta}_{2j} \right) \dot{\alpha}_{12} C_{12} \\
&\quad + \dot{\alpha}_{12} \left(\dot{\alpha}_{12} S_{12} \sum_{j=1}^{m} \Phi_{2j} \delta_{2j} - C_{12} \sum_{j=1}^{m} \Phi_{2j} \dot{\delta}_{2j} \right) \\
&\quad - m_2 \left(\dot{\theta}_1 C_1 \left(l_1 \dot{\theta}_1 + \dot{y}_{l_1} \right) - y_{l_1} \dot{\theta}_1^2 S_1 \right); \\
f_{TD_2 p_y} &= -\left(\frac{m_2 l_2}{2} \dot{\alpha}_{12} + \sum_{j=1}^{m} \Phi_{2j} \dot{\delta}_{2j} \right) \dot{\alpha}_{12} S_{12} \\
&\quad - \dot{\alpha}_{12} \left(\dot{\alpha}_{12} C_{12} \sum_{j=1}^{m} \Phi_{2j} \delta_{2j} + S_{12} \sum_{j=1}^{m} \Phi_{2j} \dot{\delta}_{2j} \right) \\
&\quad - m_2 \left(\dot{\theta}_1 S_1 \left(\left(l_1 \dot{\theta}_1 + \dot{y}_{l_1} \right) + \dot{y}_{l_1} \right) + y_{l_1} \dot{\theta}_1^2 C_1 \right);
\end{aligned}
$$

$$
\begin{aligned}
f_{TD_2\theta_1} &= \left(2\dot{\alpha}_{12}\sum_{j=1}^{m}\Phi_{S2j}\delta_{2j}\dot{\delta}_{2j}\right) - 2m_2 y_{l_1}\dot{y}_{l_1}\dot{\theta}_1 - \left(l_1\dot{\theta}_1 + \dot{y}_{l_1}\right)\frac{m_2 l_2}{2}\dot{\alpha}_2 S_2 \\
&+\dot{\theta}_1\frac{m_2 l_2}{2}\left(\dot{y}_{l_1}S_2 + y_{l_1}\dot{\alpha}_2 C_2\right) \\
&+\left(2\dot{\theta}_1 + \dot{\alpha}_2\right)\left(C_2\left(\dot{y}_{l_1}\sum_{j=1}^{m}\Phi_{2j}\delta_{2j} + y_{l_1}\sum_{j=1}^{m}\Phi_{2j}\dot{\delta}_{2j}\right) - y_{l_1}\dot{\alpha}_2 S_2\sum_{j=1}^{m}\Phi_{2j}\delta_{2j}\right) \\
&+\left(\frac{m_2 l_2}{2}\dot{\alpha}_{12} + \sum_{j=1}^{m}\Phi_{2j}\dot{\delta}_{2j}\right)\left(-l_1\dot{\alpha}_2 S_2 + \left(\dot{y}_{l_1}S_2 + y_{l_1}\dot{\alpha}_2 C_2\right)\right) \\
&-\left(l_1\dot{\theta}_1 + \dot{y}_{l_1} + \dot{\alpha}_{12}l_1\right)\left(\dot{\alpha}_2 C_2\sum_{j=1}^{m}\Phi_{2j}\delta_{2j} + S_2\sum_{j=1}^{m}\Phi_{2j}\dot{\delta}_{2j}\right) \\
&-\left(\frac{m_2 l_2}{2}\dot{\alpha}_{12} + \sum_{j=1}^{m}\Phi_{2j}\dot{\delta}_{2j}\right)\left(S_{12}\dot{p}_y + C_{12}\dot{p}_x\right) \\
&+\dot{\alpha}_{12}\sum_{j=1}^{m}\Phi_{2j}\delta_{2j}\left(S_{12}\dot{p}_x - C_{12}\dot{p}_y\right) \\
&-m_2\left(\left(l_1\dot{\theta}_1 + \dot{y}_{l_1}\right)\left(S_1\dot{p}_y + C_1\dot{p}_x\right) - y_{l_1}\dot{\theta}_1\left(S_1\dot{p}_x - C_1\dot{p}_y\right)\right); \\
f_{TD_2\delta_{1k}} &= \left(2\dot{\alpha}_{12}\sum_{j=1}^{m}\Phi_{S2j}\delta_{2j}\dot{\delta}_{2j}\right)\phi'_{l_1k} + \dot{\theta}_1 C_2\left(\dot{y}_{l_1}\sum_{j=1}^{m}\Phi_{2j}\delta_{2j} + y_{l_1}\sum_{j=1}^{m}\Phi_{2j}\dot{\delta}_{2j}\right) \\
&+\phi'_{l_1k}\dot{\theta}_1\dot{\alpha}_2 y_{l_1}\left(\frac{m_2 l_2}{2}C_2 - S_2\sum_{j=1}^{m}\Phi_{2j}\delta_{2j}\right) \\
&+\phi'_{l_1k}\frac{m_2 l_2}{2}S_2\left(\dot{y}_{l_1}\dot{\theta}_1 - \dot{\alpha}_2\left(l_1\dot{\theta}_1 + \dot{y}_{l_1}\right)\right) \\
&-\phi_{l_1k}\dot{\alpha}_2 S_2\left(\frac{m_2 l_2}{2}\dot{\alpha}_{12} + \sum_{j=1}^{m}\Phi_{2j}\dot{\delta}_{2j}\right) \\
&-\left(\phi'_{l_1k}\left(l_1\dot{\theta}_1 + \dot{y}_{l_1}\right) + \dot{\alpha}_{12}\phi_{l_1k}\right)\left(\dot{\alpha}_2 C_2\sum_{j=1}^{m}\Phi_{2j}\delta_{2j} + S_2\sum_{j=1}^{m}\Phi_{2j}\dot{\delta}_{2j}\right) \\
&-\phi'_{l_1k}\left(S_{12}\dot{p}_y + C_{12}\dot{p}_x\right)\left(\frac{m_2 l_2}{2}\dot{\alpha}_{12} + \sum_{j=1}^{m}\Phi_{2j}\dot{\delta}_{2j}\right) \\
&+\phi'_{l_1k}\dot{\alpha}_{12}\sum_{j=1}^{m}\Phi_{2j}\delta_{2j}\left(S_{12}\dot{p}_x - C_{12}\dot{p}_y\right) \\
&-\phi_{l_1k}\dot{\theta}_1 m_2\left(S_1\dot{p}_y + C_1\dot{p}_x\right);
\end{aligned}
$$

$$
\begin{aligned}
f_{TD_2\theta_2} &= \left(2\dot{\alpha}_{12}\sum_{j=1}^{m}\Phi_{S2j}\delta_{2j}\dot{\delta}_{2j}\right)+\left(\dot{y}_{l_1}\sum_{j=1}^{m}\Phi_{2j}\delta_{2j}+y_{l_1}\sum_{j=1}^{m}\Phi_{2j}\dot{\delta}_{2j}\right)\dot{\theta}_1 C_2 \\
&\quad +y_{l_1}\dot{\theta}_1\dot{\alpha}_2\left(\frac{m_2 l_2}{2}C_2-S_2\sum_{j=1}^{m}\Phi_{2j}\delta_{2j}\right) \\
&\quad -\left(l_1\dot{\theta}_1+\dot{y}_{l_1}\right)\left(\dot{\alpha}_2 C_2\sum_{j=1}^{m}\Phi_{2j}\delta_{2j}+S_2\sum_{j=1}^{m}\Phi_{2j}\dot{\delta}_{2j}\right) \\
&\quad +\frac{m_2 l_2}{2}S_2\left(\dot{y}_{l_1}\dot{\theta}_1-\dot{\alpha}_2\left(l_1\dot{\theta}_1+\dot{y}_{l_1}\right)\right) \\
&\quad -\left(S_{12}\dot{p}_y+C_{12}\dot{p}_x\right)\left(\frac{m_2 l_2}{2}\dot{\alpha}_{12}+\sum_{j=1}^{m}\Phi_{2j}\dot{\delta}_{2j}\right) \\
&\quad +\dot{\alpha}_{12}\sum_{j=1}^{m}\Phi_{2j}\delta_{2j}\left(S_{12}\dot{p}_x-C_{12}\dot{p}_y\right); \\
f_{TD_2\delta_{2k}} &= \Phi_{2k}\left(\dot{\theta}_1\left(\dot{y}_{l_1}S_2+y_{l_1}\dot{\alpha}_2 C_2\right)-\dot{\alpha}_2 S_2\left(l_1\dot{\theta}_1+\dot{y}_{l_1}\right)-\dot{\alpha}_{12}\left(S_{12}\dot{p}_y+C_{12}\dot{p}_x\right)\right);
\end{aligned}
$$

$$
\begin{aligned}
f_{T_1 p_x} &= 0; \\
f_{T_1 p_y} &= 0; \\
f_{T_1\theta_1} &= \dot{\theta}_1\left(S_1\dot{p}_x-C_1\dot{p}_y\right)\sum_{j=1}^{m}\Phi_{1j}\delta_{1j}-\left(S_1\dot{p}_y+C_1\dot{p}_x\right)\left(\frac{m_1 l_1}{2}\dot{\theta}_1+\sum_{j=1}^{m}\Phi_{1j}\dot{\delta}_{1j}\right); \\
f_{T_1\delta_{1k}} &= \dot{\theta}_1^2\Phi_{S1k}\delta_{1k}-\dot{\theta}_1\left(S_1\dot{p}_y+C_1\dot{p}_x\right)\Phi_{1k}; \\
f_{T_1\theta_2} &= 0; \\
f_{T_1\delta_{2k}} &= 0; \\
f_{T_2 p_x} &= 0; \\
f_{T_2 p_y} &= 0; \\
f_{T_2\theta_1} &= -\left(S_{12}\dot{p}_y+C_{12}\dot{p}_x\right)\left(\frac{m_2 l_2}{2}\dot{\alpha}_{12}+\sum_{j=1}^{m}\Phi_{2j}\dot{\delta}_{2j}\right) \\
&\quad +\left(S_{12}\dot{p}_x-C_{12}\dot{p}_y\right)\dot{\alpha}_{12}\sum_{j=1}^{m}\Phi_{2j}\delta_{2j} \\
&\quad -\left(S_1\dot{p}_y+C_1\dot{p}_x\right)\left(l_1\dot{\theta}_1+\dot{y}_{l_1}\right)m_2
\end{aligned}
$$

$$
\begin{aligned}
& + (S_1\dot{p}_x - C_1\dot{p}_y)\, m_2 y_{l_1}\dot{\theta}_1; \\
f_{T_2\delta_{1k}} &= \phi_{l_1k}\dot{\theta}_1 m_2 \left(y_{l_1}\dot{\theta}_1 - (S_1\dot{p}_y + C_1\dot{p}_x)\right) \\
& + \dot{\alpha}_{12}\sum_{j=1}^{m}\Phi_{2j}\delta_{2j}\left(\phi_{l_1k}\dot{\theta}_1 C_2 - \phi'_{l_1k}\left(S_2\dot{\theta}_1 y_{l_1} + \left(l_1\dot{\theta}_1 + \dot{y}_{l_1}\right)C_2 + (S_{12}\dot{p}_x - C_{12}\dot{p}_y)\right)\right) \\
& + \left(\frac{m_2 l_2}{2}\dot{\alpha}_{12} + \sum_{j=1}^{m}\Phi_{2j}\dot{\delta}_{2j}\right)\cdot \\
& \left(\phi'_{l_1k}\left(C_2 y_{l_1}\dot{\theta}_1 - (S_{12}\dot{p}_y + C_{12}\dot{p}_x) - S_2\left(l_1\dot{\theta}_1 + \dot{y}_{l_1}\right)\right) + \phi_{l_1k}\dot{\theta}_1 S_2\right); \\
f_{T_2\theta_2} &= \left(\frac{m_2 l_2}{2}\dot{\alpha}_{12} + \sum_{j=1}^{m}\Phi_{2j}\dot{\delta}_{2j}\right)\cdot\left(C_2 y_{l_1}\dot{\theta}_1 - S_2\left(l_1\dot{\theta}_1 + \dot{y}_{l_1}\right) - (S_{12}\dot{p}_y + C_{12}\dot{p}_x)\right) \\
& - \dot{\alpha}_{12}\sum_{j=1}^{m}\Phi_{2j}\delta_{2j}\left(S_2\dot{\theta}_1 y_{l_1} + C_2\left(l_1\dot{\theta}_1 + \dot{y}_{l_1}\right) + (S_{12}\dot{p}_x - C_{12}\dot{p}_y)\right); \\
f_{T_2\delta_{2k}} &= \dot{\alpha}_{12}^2\Phi_{S2k}\delta_{2k} \\
& + \dot{\alpha}_{12}\Phi_{2k}\left(\dot{\theta}_1 y_{l_1}C_2 - S_2\left(l_1\dot{\theta}_1 + \dot{y}_{l_1}\right) - (S_{12}\dot{p}_y + C_{12}\dot{p}_x)\right);
\end{aligned}
$$

$$
\begin{aligned}
f_{U_1p_x} &= 0; \\
f_{U_1p_y} &= gm_1; \\
f_{U_1\theta_1} &= g\left(\frac{m_1 l_1}{2}C_1 - S_1\sum_{j=1}^{m}\Phi_{1j}\delta_{1j}\right); \\
f_{U_1\delta_{1k}} &= 2\Phi_{D1k}\delta_{1k} + gC_1\Phi_{1k}; \\
f_{U_1\theta_2} &= 0; \\
f_{U_1\delta_{2k}} &= 0; \\
f_{U_2p_x} &= 0; \\
f_{U_2p_y} &= gm_2; \\
f_{U_2\theta_1} &= g\left(\left(\frac{m_2 l_2}{2}C_{12} - S_{12}\sum_{j=1}^{m}\Phi_{2j}\delta_{2j}\right) + m_2\left(l_1C_1 - y_{l_1}S_1\right)\right); \\
f_{U_2\delta_{1k}} &= g\left(\phi'_{l_1k}\left(\frac{m_2 l_2}{2}C_{12} - S_{12}\sum_{j=1}^{m}\Phi_{2j}\delta_{2j}\right) + \phi_{l_1k}m_2C_1\right); \\
f_{U_2\theta_2} &= g\left(\frac{m_2 l_2}{2}C_{12} - S_{12}\sum_{j=1}^{m}\Phi_{2j}\delta_{2j}\right);
\end{aligned}
$$

$$f_{U_2\delta_{2k}} = gC_{12}\Phi_{2k} + 2\Phi_{D2k}\delta_{2k}.$$

The various time dependent terms of the system mass matrix can be deconvoluted from the acceleration/force expressions summarized below:

$$\begin{aligned}
f_{D_2p_x} &= +\ddot{p}_x(m_2) \\
&\quad +\ddot{p}_y(0) \\
&\quad +\ddot{\theta}_1\left(\left(\frac{m_2l_2}{2}S_{12} + C_{12}\sum_{j=1}^{m}\Phi_{2j}\delta_{2j}\right) - m_2(l_1S_1 + y_{l_1}C_1)\right) \\
&\quad +\ddot{\delta}_{1r}\left(-\phi_{l_1r}m_2S_1\left(\frac{m_2l_2}{2}S_{12} + C_{12}\sum_{j=1}^{m}\Phi_{2j}\delta_{2j}\right)\right) \\
&\quad +\ddot{\theta}_2\left(-\left(\frac{m_2l_2}{2}S_{12} + C_{12}\sum_{j=1}^{m}\Phi_{2j}\delta_{2j}\right)\right); \\
f_{D_2p_y} &= +\ddot{p}_x(0) \\
&\quad +\ddot{p}_y(m_2) \\
&\quad +\ddot{\theta}_1\left(\left(\frac{m_2l_2}{2}C_{12} - S_{12}\sum_{j=1}^{m}\Phi_{2j}\delta_{2j}\right) + m_2(l_1C_1 - y_{l_1}S_1)\right) \\
&\quad +\ddot{\delta}_{1r}\left(\phi'_{l_1r}\left(\frac{m_2l_2}{2}C_{12} - S_{12}\sum_{j=1}^{m}\Phi_{2j}\delta_{2j}\right) + \phi_{l_1r}m_2C_1\right) \\
&\quad +\ddot{\theta}_2\left(\frac{m_2l_2}{2}C_{12} - S_{12}\sum_{j=1}^{m}\Phi_{2j}\delta_{2j}\right) \\
&\quad +\ddot{\delta}_{2r}(C_{12}\Phi_{2r}); \\
f_{D_2\theta_1} &= +\ddot{p}_x\left(-\left(\frac{m_2l_2}{2}S_{12} + C_{12}\sum_{j=1}^{m}\Phi_{2j}\delta_{2j}\right) - m_2(l_1S_1 + y_{l_1}C_1)\right) \\
&\quad +\ddot{p}_y\left(\left(\frac{m_2l_2}{2}C_{12} - S_{12}\sum_{j=1}^{m}\Phi_{2j}\delta_{2j}\right) + m_2(l_1C_1 - y_{l_1}S_1)\right) \\
&\quad +\ddot{\theta}_1\left(\left(\frac{m_2l_2^2}{3} + \sum_{j=1}^{m}\Phi_{S2j}\delta_{2j}^2\right) + 2\frac{m_2l_2}{2}(l_1C_2 + y_{l_1}S_2)\right) \\
&\quad +\ddot{\theta}_1\left(m_2\left(y_{l_1}^2 + l_1^2\right) - 2\sum_{j=1}^{m}\Phi_{2j}\delta_{2j}(l_1S_2 - y_{l_1}C_2)\right)
\end{aligned}$$

$$
\begin{aligned}
&+\ddot{\delta}_{1r}\left(\phi'_{l_1r}\left(\left(\frac{m_2l_2^2}{3}+\sum_{j=1}^{m}\Phi_{S2j}\delta_{2j}^2\right)+\frac{m_2l_2}{2}\left(l_1C_2+y_{l_1}S_2\right)-\sum_{j=1}^{m}\Phi_{2j}\delta_{2j}\left(l_1S_2-y_{l_1}C_2\right)\right)\right)\\
&+\ddot{\delta}_{1r}\left(\phi_{l_1r}\left(m_2l_1+\left(\frac{m_2l_2}{2}C_2-S_2\sum_{j=1}^{m}\Phi_{2j}\delta_{2j}\right)\right)\right)\\
&+\ddot{\theta}_2\left(\left(\frac{m_2l_2^2}{3}+\sum_{j=1}^{m}\Phi_{S2j}\delta_{2j}^2\right)+\frac{m_2l_2}{2}\left(l_1C_2+y_{l_1}S_2\right)-\sum_{j=1}^{m}\Phi_{2j}\delta_{2j}\left(l_1S_2-y_{l_1}C_2\right)\right)\\
&+\ddot{\delta}_{2r}\left(\Phi_{X2r}+\Phi_{2r}\left(l_1C_2+y_{l_1}S_2\right)\right);\\
f_{D_2\delta_{1k}} \;=\; &+\ddot{p}_x\left(-\phi'_{l_1k}\left(\frac{m_2l_2}{2}S_{12}+C_{12}\sum_{j=1}^{m}\Phi_{2j}\delta_{2j}\right)-\phi_{l_1k}S_1m_2\right)\\
&+\ddot{p}_y\left(+\phi'_{l_1k}\left(\frac{m_2l_2}{2}C_{12}-S_{12}\sum_{j=1}^{m}\Phi_{2j}\delta_{2j}\right)+\phi_{l_1k}C_1m_2\right)\\
&+\ddot{\theta}_1\left(\phi_{l_1k}\left(\frac{m_2l_2}{2}C_2-S_2\sum_{j=1}^{m}\Phi_{2j}\delta_{2j}\right)\right)\\
&+\ddot{\theta}_1\left(\phi'_{l_1k}\left(\left(\frac{m_2l_2^2}{3}+\sum_{j=1}^{m}\Phi_{S2j}\delta_{2j}^2\right)-\sum_{j=1}^{m}\Phi_{2j}\delta_{2j}\left(l_1S_2-y_{l_1}C_2\right)+\frac{m_2l_2}{2}\left(l_1C_2+y_{l_1}S_2\right)\right)\right)\\
&+\ddot{\delta}_{1r}\left(\phi'_{l_1r}\left(\phi'_{l_1k}\left(\frac{m_2l_2^2}{3}+\sum_{j=1}^{m}\Phi_{S2j}\delta_{2j}^2\right)+\phi_{l_1k}\left(\frac{m_2l_2}{2}C_2-S_2\sum_{j=1}^{m}\Phi_{2j}\delta_{2j}\right)\right)\right)\\
&+\ddot{\delta}_{1r}\left(\phi_{l_1r}\left(\phi_{l_1k}m_2+\phi'_{l_1k}\left(\frac{m_2l_2}{2}C_2-S_2\sum_{j=1}^{m}\Phi_{2j}\delta_{2j}\right)\right)\right)\\
&+\ddot{\theta}_2\left(\phi'_{l_1k}\left(\frac{m_2l_2^2}{3}+\sum_{j=1}^{m}\Phi_{S2j}\delta_{2j}^2\right)+\phi_{l_1k}\left(\frac{m_2l_2}{2}C_2-S_2\sum_{j=1}^{m}\Phi_{2j}\delta_{2j}\right)\right)\\
&+\ddot{\delta}_{2r}\left(\phi'_{l_1k}\Phi_{X2r}+\phi_{l_1k}\Phi_{2r}C_2\right);\\
f_{D_2\theta_2} \;=\; &+\ddot{p}_x\left(-\left(\frac{m_2l_2}{2}S_{12}+C_{12}\sum_{j=1}^{m}\Phi_{2j}\delta_{2j}\right)\right)\\
&+\ddot{p}_y\left(+\left(\frac{m_2l_2}{2}C_{12}-S_{12}\sum_{j=1}^{m}\Phi_{2j}\delta_{2j}\right)\right)\\
&+\ddot{\theta}_1\left(\left(\frac{m_2l_2^2}{3}+\sum_{j=1}^{m}\Phi_{S2j}\delta_{2j}^2\right)+\frac{m_2l_2}{2}\left(l_1C_2+y_{l_1}S_2\right)-\sum_{j=1}^{m}\Phi_{2j}\delta_{2j}\left(l_1S_2-y_{l_1}C_2\right)\right)\\
&+\ddot{\delta}_{1r}\left(\phi'_{l_1r}\left(\frac{m_2l_2^2}{3}+\sum_{j=1}^{m}\Phi_{S2j}\delta_{2j}^2\right)+\phi_{l_1r}\left(\frac{m_2l_2}{2}C_2-S_2\sum_{j=1}^{m}\Phi_{2j}\delta_{2j}\right)\right)
\end{aligned}
$$

$$
\begin{aligned}
& +\ddot{\theta}_2 \left(\frac{m_2 l_2^2}{3} + \sum_{j=1}^{m} \Phi_{S2j} \delta_{2j}^2 \right) \\
& +\ddot{\delta}_{2r} \left(\Phi_{X2r} \right); \\
f_{D_2 \delta_{2k}} \;=\; & +\ddot{p}_x \left(-\Phi_{2k} S_{12} \right) \\
& +\ddot{p}_y \left(+\Phi_{2k} C_{12} \right) \\
& +\ddot{\theta}_1 \left(+\Phi_{X2k} + \Phi_{2k} \left(l_1 C_2 + y_{l_1} S_2 \right) \right) \\
& +\ddot{\delta}_{1r} \left(\Phi_{2k} \phi_{l_1 r} C_2 + \phi'_{l_1 r} \Phi_{X2k} \right) \\
& +\ddot{\theta}_2 \left(\Phi_{X2k} \right) \\
& +\ddot{\delta}_{2r} \left(\Phi_{S2k} \right);
\end{aligned}
$$

These separate terms are then combined to form a complete set of differential equations as follows:

$$
\begin{aligned}
f_{D_1 p_x} + f_{D_2 p_x} + f_{TD_1 p_x} + f_{TD_2 p_x} - f_{T_1 p_x} - f_{T_2 p_x} + f_{U_1 p_x} + f_{U_2 p_x} &= Q_{p_x}; \\
f_{D_1 p_y} + f_{D_2 p_y} + f_{TD_1 p_y} + f_{TD_2 p_y} - f_{T_1 p_y} - f_{T_2 p_y} + f_{U_1 p_y} + f_{U_2 p_y} &= Q_{p_y}; \\
f_{D_1 \theta_1} + f_{D_2 \theta_1} + f_{TD_1 \theta_1} + f_{TD_2 \theta_1} - f_{T_1 \theta_1} - f_{T_2 \theta_1} + f_{U_1 \theta_1} + f_{U_2 \theta_1} &= Q_{\theta_1}; \\
f_{D_1 \delta_{1k}} + f_{D_2 \delta_{1k}} + f_{TD_1 \delta_{1k}} + f_{TD_2 \delta_{1k}} - f_{T_1 \delta_{1k}} - f_{T_2 \delta_{1k}} + f_{U_1 \delta_{1k}} + f_{U_2 \delta_{1k}} &= Q_{\delta_{1k}}; \\
f_{D_1 \theta_2} + f_{D_2 \theta_2} + f_{TD_1 \theta_2} + f_{TD_2 \theta_2} - f_{T_1 \theta_2} - f_{T_2 \theta_2} + f_{U_1 \theta_2} + f_{U_2 \theta_2} &= Q_{\theta_2}; \\
f_{D_1 \delta_{2k}} + f_{D_2 \delta_{2k}} + f_{TD_1 \delta_{2k}} + f_{TD_2 \delta_{2k}} - f_{T_1 \delta_{2k}} - f_{T_2 \delta_{2k}} + f_{U_1 \delta_{2k}} + f_{U_2 \delta_{2k}} &= Q_{\delta_{2k}};
\end{aligned}
$$

The above equations can be represented in a compact form using the vector notation as

$$
\begin{aligned}
\vec{f}_D + \vec{f}_{TD} - \vec{f}_T + \vec{f}_U &= \vec{Q}, \\
\text{i.e.} \quad \mathbf{D}\ddot{\vec{q}} + \vec{\mathrm{f}}_{\mathrm{TD}} - \vec{\mathrm{f}}_{\mathrm{T}} + \vec{\mathrm{f}}_{\mathrm{U}} &= \vec{Q}, \\
\text{or} \qquad \mathbf{D}\ddot{\vec{q}} + \vec{\mathbf{f}} &= \vec{Q}.
\end{aligned}
$$

This equation can be rewritten in the following form and solved numerically using a state space based integration algorithm:

$$
\ddot{\vec{q}} \;=\; \mathbf{D}^{-1} \left(\vec{Q} - \vec{\mathbf{f}} \right).
$$